Ytterbium-Doped Femtosecond Solid-State Lasers

Dissertation

zur Erlangung des akademischen Grades
doctor rerum naturalium (Dr. rer. nat.)

vorgelegt dem Rat der Physikalisch-Astronomischen Fakultät
der Friedrich-Schiller-Universität Jena

von Diplom-Physikerin Gabriela Paunescu
geboren am 26. September 1972 in Amărăştii de Jos, Rumänien

Gutachter

1. Prof. Dr. R. Sauerbrey

2. Prof. Dr. R. Menzel

3. Prof. Dr. W.L. Bohn

Tag der öffentlichen Verteidigung: 20.04.2006

Contents

Introduction

Ultrafast lasers allow for extremely short temporal resolution, very fast repetition rate, broad optical spectra and high peak optical intensities. Therefore they are finding application in a variety of fields. Femtosecond pulses are currently used in many diverse areas of science and medicine, as well as in information technology and communications [1, 2]. In science, ultrashort optical pulses are a useful tool to investigate fast processes with very short temporal resolution. Some examples would include the molecular dynamics [3], chemical reactions dynamics [4], carriers relaxation in semiconductors [5] and structural changes in solid state materials [6].
Apart from their shortness, the femtosecond pulses open the possibility for extremely high energy density that can even induce relativistic effects [7]. Amplification of such pulses leads to peak powers of $10^{12}W$ and above. Currently, there are several laser-development programs worldwide aiming to generate pulses with petawatt peak powers ($1PW = 10^{15}W$) and focus them to an intensity of about $10^{22}W/cm^2$.
The goal of POLARIS - a laser project in progress at the University of Jena - is the design and build-up of an all-diode-pumped, high-peak-power femtosecond laser system reaching the petawatt level. The laser amplifiers are based on Yb^{3+}-doped fluoride phosphate glass. This glass can be produced with high quality at sizes of several tens of cm^3. The pump system consists of stacked laser-diode bars at 940 nm wavelength focused tightly to the glass.
For this kind of high-power laser systems, stable, maintenance-free seed laser oscillators are required. The goal of this work was to develop a diode-pumped Yb-based mode-locked laser oscillator for the POLARIS front end. In order to be suitable to seed the POLARIS amplifier chain, the laser should deliver 100-fs pulses with an

energy above 1-nJ and a center wavelength in the range of 1027-1040 nm.

The first assignment of the work was to find an appropriate laser design to fulfill these requirements. Different Yb-doped materials were tested as gain medium. Mode-locking experiments were performed using Yb-doped fluoride-phosphate glass and two recently developed Yb-doped crystals, Yb:KGW and Yb:KYW which are very promising for ultrashort pulse generation.

The passive mode-locking was achieved using semiconductor saturable absorber mirrors, so-called SESAMs. The laser performances concerning the pulse duration and the output power are strongly influenced by a number of parameters of the saturable absorber, such as modulation depth, saturation fluence, recovery time and nonsaturable losses. In order to optimize the laser, different SESAMs were tested. It was found that the pulse duration and output power are quit different using different SESAMs. To explain these experimental results, the parameters of the SESAMs must be known. Therefore the second part of this work focuses on the optical characterization of this devices. Because in a classical pump-probe setup the intracavity conditions can not be reproduced without amplified femtosecond pulses, a novel method to characterize the SESAMs was developed. Using this new technique, the absorber parameters, in particular the modulation depth and the dynamic response, have been measured under the exact laser operation conditions.

The text is organized as follows. The Chapter 1 gives a short review of the basic principles of mode-locking. It briefly introduces the mathematical formalism used to describe the passive mode-locking with saturable absorbers. The theoretical predictions concerning the mode-locking stability against Q-switching and against the onset of multiple pulsing are shown. The design of the passive mode-locked lasers is treated in the Chapter 2. It includes the resonator stability calculations, the pumping system description, the optical and spectroscopic properties of the Yb-doped materials, as well as the SESAMs structure and the dispersion management. The laser experiments are presented in Chapter 3. The results obtained using different Yb-based gain media are shown. The Chapter 4 treats the optical characterization of the saturable absorbers used for passive mode-locking. The new developed experimental method is explained and the obtained results are presented.

Chapter 1

Basics of Passive Mode-Locking

1.1 General considerations

The principle of ultrashort pulse generation within a mode-locked laser was treated in many books and review articles [8–10].

In general, a laser transition has a finite linewidth over which it can provide optical gain and so laser emission has a finite spectral bandwidth $\Delta\nu$. In a laser cavity, the radiation is confined to discrete frequencies or modes ν_m, which are separated by $\delta\nu = 1/T_{RT} = c/2L$, where T_{RT} is the cavity round trip time, c the speed of light and L the optical length of the cavity. This is schematically illustrated in figure 1.1.

When no attempt is made to control the laser spectrum, the free-running modes oscillate independently with random phases. The resulting laser output is noisy and incoherent, with no regular temporal structure.

If all the laser modes can be made to oscillate in phase, i.e. they can be locked together, the output intensity of the laser becomes temporally well defined, with a period equal to the time needed to complete a cavity round-trip, as shown in figure 1.2.

The temporal profile is the Fourier transform of the spectral profile and so, the duration of the pulses, t_p is related to the full gain linewidth by the relation:

$$\Delta\nu \times t_p \geq k \tag{1.1}$$

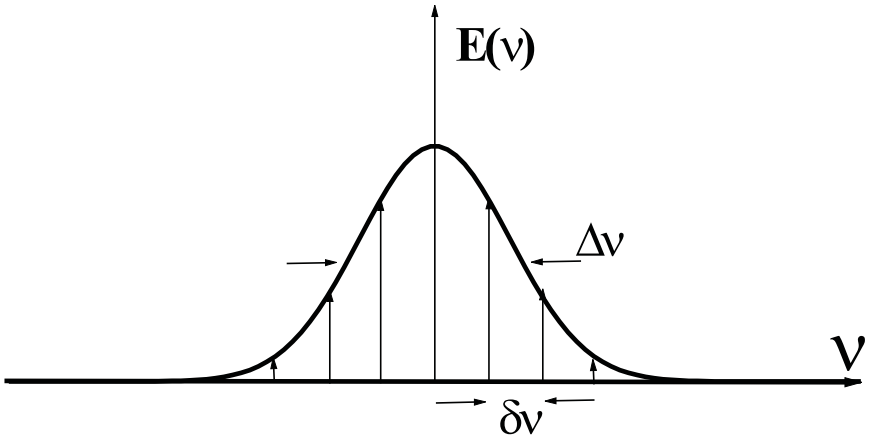

Figure 1.1: The cavity modes for laser radiation with a finite spectral bandwidth $\Delta\nu$.

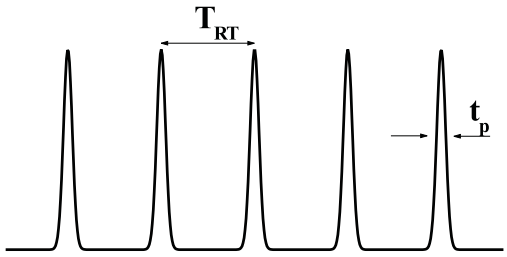

Figure 1.2: The laser output if the modes are locked together. T_{RT} is the cavity round trip time.

where k is a constant which depends only on the shape of the pulses.

To force the modes to have equal phases an additional mechanism called mode-locking is required.

The mode-locking techniques developed so far fall into two broad categories: active mode-locking and passive mode-locking.

In the first approach, the radiation in the laser cavity is modulated by a signal derived from an external clock source which is matched to the cavity round trip time. This is of the order of ns for most bulk lasers which implies that modulators operating at frequencies of the order of hundreds of MHz are required. Such high frequency

modulation can be provided by the output of other mode-locked lasers (through gain modulation), or directly by intracavity acousto-optic or electro-optic devices (cavity loss modulation.

In the case of passive mode-locking, the laser radiation itself generates a modulation through the action of a non-linear device in the laser cavity. This modulation is thus automatically synchronized to the cavity round trip time frequency and requires no external clock signal.

The passive mode-locking is produced by the insertion of an element with saturable absorption in the laser cavity. Different saturable absorbers, such as organic dyes, color filter glasses, semiconductor materials, dye or rare earth doped crystals have been used. An other possibility is to convert a so-called reactive nonlinear effect into an effective saturable absorber. Reactive effects influence the phase of the light only, but not its intensity profile. This self-phase modulation induces a delay between the high and low intensities. This mechanism can be very fast, with a response time of less than 1 fs. To create an effective saturable absorber, a phase-to-amplitude convertor is needed. Several techniques have been proposed. One of them is the additive-pulse mode-locking, in which the self-phase modulator is placed in a second cavity coupled to the gain cavity. This acts as a nonlinear mirror, providing high reflectivity for the high intensity center part of the pulse and low reflectivity everywhere else. Another method is Kerr-lens mode locking technique, where the transverse Kerr nonlinearity of the amplifying medium is translated into an effective absorber by suitable arrangement of intracavity apertures. The focused high intensity light experiences lower losses at these apertures and the short pulse regime is preferred.

1.2 Saturable absorber parameters

Independent of the nature of saturable absorber, there are some key parameters that determine the short pulse generation process. The modulation depth, the linear (nonsaturable) losses, the saturation fluence and the recovery time of the reflectivity/transmission are the macroscopic properties of the saturable absorber that deter-

mine the operation of a passively mode-locked laser.

If the saturable absorber is embedded in a mirror structure, as is the case for semiconductor-based saturable absorbers, the characteristic parameter is the reflectivity. Otherwise the transmission must be taken into account. Relevant for mode-locking are the reflectivity dependence on the incident fluence and the dynamic response, i.e. the temporal evolution of the reflectivity after the saturation.

The modulation depth ΔR is the maximum change in reflectivity between low and high incident fluence. The incident fluence needed to increase the reflectivity to a given fraction - 1/e - from the modulation depth is the saturation fluence. The remaining loss at incident pulse fluences much higher than the saturation fluence are called linear or non-saturable losses.

1.3 Mechanism of passive mode-locking

There are three fundamental models [10] which well explain the passive mode-locking mechanisms: slow saturable absorber mode-locking with dynamic gain saturation [11,12], fast saturable absorber mode-locking [13,14] and soliton mode-locking [15–17]. In the first case (figure 1.3a), a short net-gain window is formed by the combined saturation of absorber and gain. The absorber has to saturate and recover faster than the gain, but the recovery time of the saturable absorber can be much longer than the pulse duration. Dynamic gain saturation consists in a pulse-induced saturation of the gain, followed by a recovery faster than the pulse repetition period. This can not occur in a solid state laser, due to the long upper state lifetime, typically in the microsecond or millisecond range, while the pulse repetition period is typically in the nanosecond range.

In the case of the fast saturable absorber model, no dynamic gain saturation occurs and the short net-gain window is formed only by the fast saturable absorber (figure 1.3b). The first mode-locking technique for solid state lasers based on this model was the additive pulse mode-locking (APM). Because of the required interferometric cavity length stabilization, this method was not suitable for real world applications. The

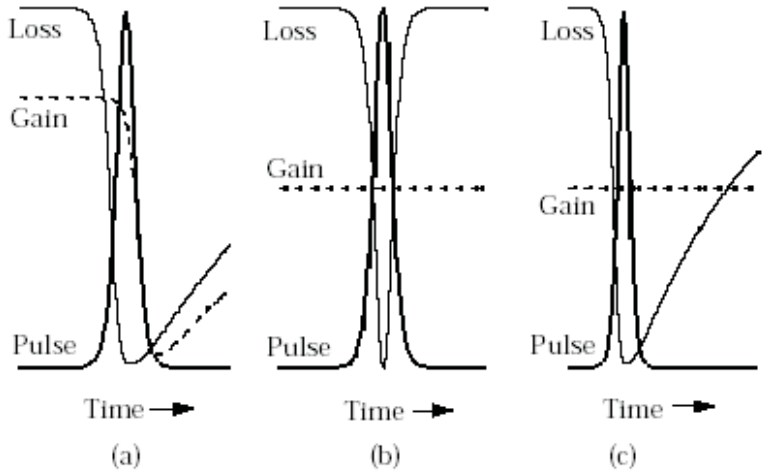

Figure 1.3: The evolution of the gain and loss for slow saturable absorber mode-locking with dynamic gain saturation (a), fast saturable absorber mode-locking (b) and soliton mode-locking (c) according to U. Keller [10].

Kerr-lens mode-locking (KLM) was the first useful demonstration of a fast saturable absorber mode-locking technique for a solid state laser [18]. Pulses shorter than 10 fs have been achieved from a Ti:sapphire laser [19, 20]. Due to the nonresonant nature of the Kerr effect in the crystal, KLM can be used to mode lock lasers from the visible to near infrared without any additional intracavity element. However, KLM has some significant disadvantages. To enhance self-focusing the cavity is typically operated near the end of its stability range. This requires a critical alignment whereby mirrors and laser crystal have to be positioned to a typical accuracy of several hundred microns. Furthermore, very shot pulse lasers based on a fast saturable absorber alone, do not spontaneously start from the CW regime. This is due to the fact that the peak intensity changes by about six orders of magnitude when the laser switches from CW-operation. Self-starting KLM lasers have been demonstrated down to about 50 fs [21, 22] by designing the resonator to minimize the nonlinear mode variations and dynamic loss modulation. Even then, the measured mode-locking build-up time is in the order of several milliseconds. Thus, usually separate starting mechanisms are required.

In soliton mode-locking (figure 1.3c), the pulse is completely shaped by soliton formation, i.e. the interplay between negative group velocity dispersion (GVD) and self-phase modulation (SPM). The absorber dynamics only stabilizes the soliton against the growth of "continuum", as the lost energy is called in soliton perturbation theory [23]. This energy is initially contained in a low-intensity background pulse with a bandwidth much smaller than the bandwidth of the soliton. Therefore this pulse exhibits a higher gain and after a sufficient buildup time can reach the lasing threshold, destabilizing the soliton. The insertion of a saturable absorber in the cavity increases the losses experienced by the low-intensity background and it will decrease in time. In the final stage of pulse formation, it is the solitonlike pulse shaping that locks the modes together. With this method one can generate pulses, which are considerable shorter than the recovery time of the absorber. Therefore, this scheme was called soliton mode-locking stabilized by a slow saturable absorber. It was shown [17, 24] that the net-gain window can remain open more than 10 times longer than the ultrashort pulse, depending on the laser parameters. This is possible because, for the soliton, the nonlinear effects due to SPM and the linear effects owing to the negative GVD are in balance. In contrast, the noise or instabilities that would like to grow are not intense enough to experience the nonlinearity and therefore spread in time. However, when they are spread in time they are even absorbed by a slowly recovering absorber. Then, the instabilities experience less gain per round-trip than the soliton and they decay with time.

1.4 Theoretical model of soliton mode-locking with saturable absorbers

1.4.1 Basic equations

For a large class of laser systems, the pulse-shaping dynamics are well described by the master equation approach [16, 25]. The laser pulse that builds up in the cavity experiences changes over one round-trip due to GVD, SPM, gain, loss, filter action due

to the finite gain, output coupler and mirror bandwidth, a time dependent absorption and phase change due to the absorber. The relevant equation for the motion of the laser pulse averaged over one round-trip is the generalized complex Ginzburg-Landau equation [16] (GCGLE):

$$T_R \frac{\partial A(T,t)}{\partial T} = -iD\frac{\partial^2 A}{\partial t^2} + i\delta|A|^2 A + [g - l + D_{g,f}\frac{\partial^2}{\partial t^2} - q(T,t)]A(T,t). \tag{1.2}$$

A(T,t) is the slowly varying field envelope that describes the pulses on two time scales, the soliton or retarded time t and the slow time T of multiple round trips. T_R is the cavity round-trip time, D the intracavity GVD and l the frequency-independent loss per round trip (output coupler, etc.). $D_{g,f}$ describes the effects of gain and intracavity filter dispersion:

$$D_{g,f} = \frac{g}{\Omega_g^2} + \frac{1}{\Omega_f^2}, \tag{1.3}$$

where Ω_g and Ω_f are the HWHM gain and filter bandwidth, respectively.
The SPM coefficient δ is given by:

$$\delta = \frac{2\pi n_2 l_L}{\lambda_0 A_{eff,L}}, \tag{1.4}$$

where n_2 is the nonlinear refractive index of the laser medium, λ_0 the center wavelength of the pulse and $A_{eff,L}$ and l_L the effective mode area inside the laser medium and length of the light path through the laser medium within one round-trip, respectively.
The pulse energy W is given by:

$$W = \int_{-T_R/2}^{T_R/2} |A(T,t)|^2 dt. \tag{1.5}$$

The saturable gain g is described by the equation:

$$\frac{\partial g}{\partial T} = -\frac{g - g_0}{T_g} - \frac{Wg}{P_g T_g T_R}, \tag{1.6}$$

with g_0 the small signal gain, T_g and P_g the relaxation time and the saturation power of the gain medium.

If we assume a gain medium with a long relaxation time and a large saturation energy, the gain is fixed to its steady-state value:

$$g = \frac{g_0}{1 + \frac{W}{P_g T_R}}. \tag{1.7}$$

The gain is only appreciably saturated by a series of successive pulses travelling through the gain medium, i.e. the dynamic gain saturation during each individual pulse is neglected.

q(T,t) is the response of the saturable absorber to an ultrashort pulse (the time-dependent saturable losses) and it is described by the rate equation:

$$\frac{\partial q(T,t)}{\partial t} = -\frac{q - q_0}{\tau_a} - \frac{|A(T,t)|^2}{E_a} q, \tag{1.8}$$

where τ_a is the relaxation time, q_0 is the maximal change in the reflectivity and E_a the saturation energy of the absorber.

If the free carriers generated in the saturable absorber contribute to the refractive index, a complex saturable absorbtion must be considered in the equation 1.8:

$$q(T,t) \rightarrow q(T,t)(1 + i\alpha). \tag{1.9}$$

The α-parameter is called the linewidth enhancement factor and represents the ratio between the amplitude absorption and the refractive index changes. Because the saturation of the absorption and the refractive index change are related to the ex-

cited carrier density, it was assumed that they are proportional to each other like in semiconductor lasers.

In equation 1.8 the absorber response consists only in a saturable part. However, it has been shown [26–28] that in some semiconductor saturable-absorber structures, two-photon absorption (TPA) and free carrier absorption (FCA) are significant and can affect the mode locking and Q-switching tendency of a laser. This effects increase with the pulse intensity or fluence and therefore induce a so-called inverse saturable absorption in the semiconductor structure. A basic model for a laser that is mode-locked with a saturable absorber including inverse saturable absorption can be found in [29].

Two asymptotic cases for the saturable absorber response can be considered. The first case is the slow saturable absorber, which occurs in the limit $\tau_A \gg \tau$. In this case, the relaxation term in 1.8 is neglected and direct integration leads to:

$$q_{A,slow}(t) = q_{A0} exp[-\frac{W}{E_A}\int_{-\infty}^{t} |f(t')|^2 dt']. \tag{1.10}$$

The second case is the fast saturable absorber, $\tau_A \to 0$, so that the absorber response is instantaneous

$$q_{A,fast}(t) = \frac{q_{A0}}{1 + \frac{|A(t)|^2}{P_A}}, \tag{1.11}$$

where $P_A = E_A/\tau_A$. Here, P_A is the saturation power of the saturable absorber.

Equations 1.10 and 1.11 show that, in the slow case, the absorber saturates as a function of energy and, in the fast case, as a function of peak power.

For the basic equation 1.2 no analytic solutions are known. Without the dissipative terms due to gain and loss in 1.2, one arrives at the nonlinear Schrödinger equation (NLSE), which has the first-order soliton solution in case of negative GVD [16]:

$$A_s(T,t) = A_0 sech[x(T,t)] \exp[i\theta(T,t)] \tag{1.12}$$

where

$$x = \frac{1}{\tau}(t + 2Dp_0T - t_0) \tag{1.13}$$

is a retarded time normalized to the soliton width τ. The total phase is given by

$$\theta = -p_o t - D(\frac{1}{\tau^2 - p_0^2})\frac{T}{T_R} + \theta_0. \tag{1.14}$$

The variables p_0, t_0 and θ_0 were introduced because the collective variables of the soliton are not yet fixed. The pulse energy is

$$W = \int_{-\infty}^{\infty} |A(T,t)|^2 dt = 2A_0^2\tau. \tag{1.15}$$

The pulse width τ is related to the full-width at half maximum (FWHM) of the soliton by $\tau_{FWHM} = 1.76 \times \tau$. The balance between GVD and SPM means that the chirp introduced by GVD is compensated by the nonlinear phase shift due to SPM within each round-trip, which leads to

$$\Phi_0 = \frac{|D|}{\tau^2} = \frac{1}{2}\delta A_0^2 = \frac{\delta W}{4\tau}. \tag{1.16}$$

Therefore, the area theorem defines the relationship between the pulse width and the energy:

$$\tau = \frac{4|D|}{\delta W}. \tag{1.17}$$

To find an approximate solution of the equation 1.2, the soliton perturbation theory can be used.

1.4.2 Q-switching dynamics of mode-locked lasers

The solid-state lasers passively mode-locked with a saturable absorber can show a tendency for Q-switched mode-locked operation (QML). In this regime the laser output consists of mode-locked pulses underneath a stable or unstable Q-switched envelope. These instabilities are unwanted for many applications in which constant pulse energy and high repetition rate are required. An analytical treatment of QML was done by Kärtner et al. [30] and experimental investigation of the transition between CWML and QML regimes was reported by Hönninger et al. [31]. The stability criterion against Q-switching, derived in [25], [30] and [31] for small modulation depths is:

$$E_P \frac{dR(E_P)}{dE_P}|_{\overline{E}_P} < \frac{T_R}{\tau_L} + \frac{E_P}{E_{sat,L}}, \tag{1.18}$$

where R is the nonlinear reflectivity of the saturable absorber mirror, E_P the intracavity pulse energy, τ_L and $E_{sat,L}$ are the upper-state lifetime and the saturation energy of the laser medium.

With the assumptions that the pulse energy is high enough to bleach the absorber (the pulse fluence should be approximately five times the absorber saturation fluence) and the laser operates far above threshold ($E_P \gg E_{sat,L}$), which is the case in most mode-locked lasers, the stability condition 1.18 becomes:

$$E_P^2 > E_{sat,L} E_{sat,A} \Delta R = F_{sat,L} A_{eff,L} F_{sat,A} A_{eff,A} \Delta R. \tag{1.19}$$

$F_{sat,A}$ and $F_{sat,L}$ are the saturation fluences of the saturable absorber and the laser medium respectively. $A_{eff,A}$ and $A_{eff,L}$ denote the effective mode arias. ΔR is the modulation depth of the saturable absorber.

There is a minimum intracavity pulse energy which is required for obtaining stable cw mode locking.

This theoretical predictions have been found to be in good agreement with the experimental results for many picosecond solid-state lasers. However, femtosecond soliton

mode-locked lasers show stable mode-locking in a regime in which they should actually be Q-switched mode locked according to this criterion. An extension for soliton lasers was derived by Hönninger et al. [31], in which the interplay of soliton effects and gain filtering was taken into account. The stability condition in this case can be written:

$$E_{sat,L} g K^2 E_P^3 + E_P^2 > E_{sat,L} E_{sat,A} \Delta R, \tag{1.20}$$

where $KE_P = f \equiv \Delta\nu(E_P)/\Delta\nu_g$ is the ratio of pulse bandwidth and gain bandwidth and depends on the pulse energy and on the pulse duration.

Another explanation for the decreased QML threshold was demonstrated to be the modified saturation characteristics of the absorber, namely the roll-over of the nonlinear reflectivity for higher pulse fluences [29, 32]. It has been shown that in semiconductor saturable absorber structures, nonlinear processes as TPA or FCA induce a so-called inverse saturable absorption (see figure 1.4) which reduces the tendency for QML [29]. This is not only due to the reduced effective modulation depth, but also to the reduced slope of the nonlinear reflectivity curve. A simple expression for the QML threshold including inverse saturable absorption and using only measurable parameters is [32]:

$$E_P^2 > \frac{E_{sat,A} \Delta R}{\frac{1}{E_{sat,L}} + \frac{1}{A_{eff,A} F_2}}, \tag{1.21}$$

where F_2 is the inverse slope of the induced absorption effect. For $F_2 \to \infty$ (i.e. without induced nonlinear losses) we retrieve the simpler equation 1.19.

1.4.3 Stability condition against the onset of multiple pulsing

It was shown in [16] that the stability of a soliton in the laser can be maintained as long as the loss l_s of the soliton are less than the loss l_c experienced by the continuum. The total energy loss of the soliton consists of filter loss l_f and absorption loss q_S:

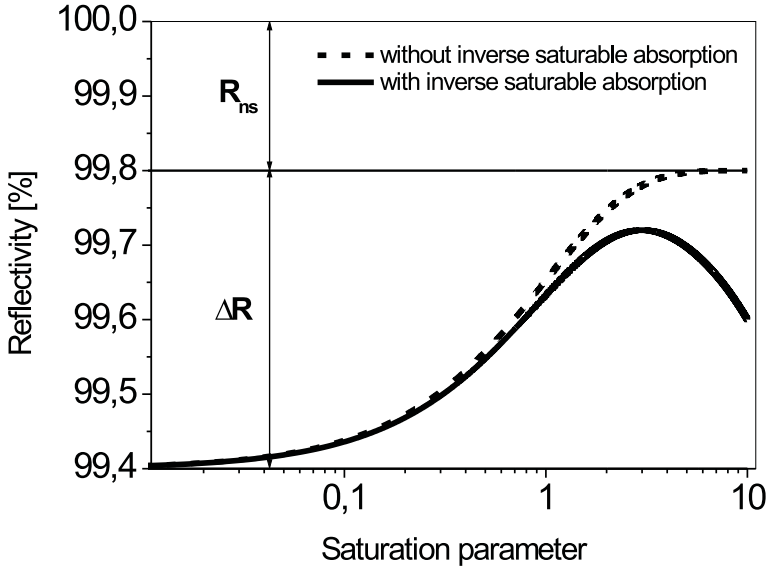

Figure 1.4: The saturation curve with (solid line) and without (dotted line) inverse saturable absorption induced by nonlinear processes such as TPA or FCA.

$$l_s = l_f + q_S(E_P) = \frac{D_{g,f}}{3\tau^2} + \frac{1}{2\tau}\int_{-\infty}^{+\infty} sech^2(\frac{t}{\tau})q(t)dt \tag{1.22}$$

where E_P is the soliton energy. In the case of an infinitely slow absorber, the response $q(t)$ for a sech-shaped pulse is explicitly given by [16]:

$$q(x) = q_0 \exp\{-\frac{y}{2}[1 + \tanh(x)]\} \tag{1.23}$$

where $x = t/\tau$ is the normalized time and $y = E_P/E_A$ is the ratio between the pulse energy and the saturation energy of the absorber.

However, stability against the continuum is not the only stability requirement. It was reported in many papers [33, 34] that the shortening of the pulses is limited by the onset of multiple pulsing. Decreasing the negative GVD in the cavity, the pulse becomes shorter until it breaks into two longer pulses. According to [24], this breakup

occurs due to the lower losses experienced in the case of double pulsing in comparison to single pulsing regime. As the two pulses are longer, they will experience a reduce loss due to the finite-gain bandwidth. On the other hand, they will suffer increased losses in the absorber, due to the reduced pulse energy. However, once the absorber is already too strongly saturated by the single-pulsing solution, it will also be saturated by the double-pulse solution. Consequently, the filter and absorber loss for the double pulsing regime l_2 can become lower than the loss l_1 for the single pulse regime.
The single-pulse solution is stable against breakup into double pulses as long as

$$l_1 < l_2 \tag{1.24}$$

i.e. the difference in the filter losses between the single and double-pulse solution is smaller than the difference in the saturable absorber losses

$$l_{f,1} - l_{f,2} < q_S(E_{P,2}) - q_S(E_{P,1}). \tag{1.25}$$

If the average power does not depend on the number of pulses in the cavity, one pulse of the double-pulse solution has about half of the energy of the single-pulse solution, i.e. $E_{P,2} = \frac{1}{2}E_{P,1}$. Therefore, the width of the double pulse is twice as large as that of the single pulse $\tau_2 = 2\tau_1$, according to [24]. This assumption is valid as long as the absorber and the filter losses are much smaller than the total cavity loss, that includes the transmission of the output coupler. In this case, l_1 and l_2 are given by

$$l_1 = \frac{D_{g,f}}{3\tau_1^2} + q_S(E_{P,1}) \tag{1.26}$$

$$l_2 = \frac{D_{g,f}}{12\tau_1^2} + q_S(\frac{E_{P,1}}{2}). \tag{1.27}$$

Then the equation 1.25 becomes

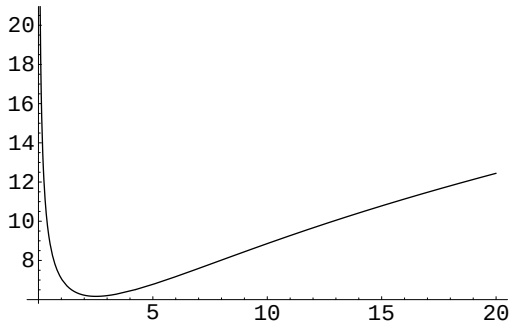

Figure 1.5: $\Delta q_S/q_0$ plotted as a function of the ratio E_P/E_A between the single pulse energy and the saturation energy of the absorber.

$$\frac{D_{g,f}}{4\tau_1^2} < \Delta q_S(E_{P,1}) = q_S(\frac{E_{P,1}}{2}) - q_S(E_{P,1}) \tag{1.28}$$

and the minimum pulse width scales with the square root of $\Delta q_S(E_{P,1})$ and $D_{g,f}$:

$$\tau_1 > \frac{1}{2}\sqrt{\frac{D_{g,f}}{q_0[\Delta q_S(E_{P,1})/q_0]}}. \tag{1.29}$$

Considering the equation 1.23 for a slow saturable absorber, $\Delta q_S/q_0$ depends only on the ratio between the single pulse energy and the saturation energy of the absorber. This dependence is shown in figure 1.5.
The optimum saturation ratio, where the shortest pulse can be expected before breakup into multiple pulsing occurs is about 3.

1.4.4 Multisoliton regime of the passively mode-locked lasers

Multiple pulse operation has been reported for many different mode-locked solid-state or fiber lasers [33]- [40]. Two or more than two pulses in the cavity have been observed either widely separated [40], or closely coupled [33–35]. In the first case, the spacing between pulses is much larger than the single-pulse width, is irregular and is the subject of spontaneous changes. In the other case, the pulses are closely coupled, with the pulse separation usually between 3 and 10 times the pulse width and the

regime can be very stable. However, a stable pulse separation of 37 times the pulse width was reported for an additive pulse mode-locking regime in a fiber laser [40]. Within the framework of NLSE, soliton-soliton interaction does not usually lead to fixing of soliton separation. An exception is the case of a train of solitons in quadrature, which is, nevertheless, not immune to perturbations [41]. However, the inclusion of other terms like distributed gain and losses or higher-order dispersion allows one to find stable bound states of pulses.

It was shown in 1.3.1 that the dynamics of passively mode-locked lasers can be well modelled by the CGLE, which is the NLSE plus the dissipative terms due to gain and loss. High-order soliton solutions of this equation have been extensively studied [42–44]. Using standard perturbation analysis for soliton interaction, it was shown that stationary solutions in the form of bound states of solitons, which are in-phase or out-of-phase, may exist. For analysing the stability properties and general dynamics of two-soliton solutions of the CGLE, Akhmediev et al [43] have proposed a two-dimensional plane (using distance and phase difference). For the lasers passively mode locked with a slow saturable absorber, stable soliton pairs with a phase difference of π or with rotating phase difference were predicted [44]. Figure 1.6 shows the interaction plane for this two types of solutions. The corresponding temporal shapes are shown in figure 1.7.

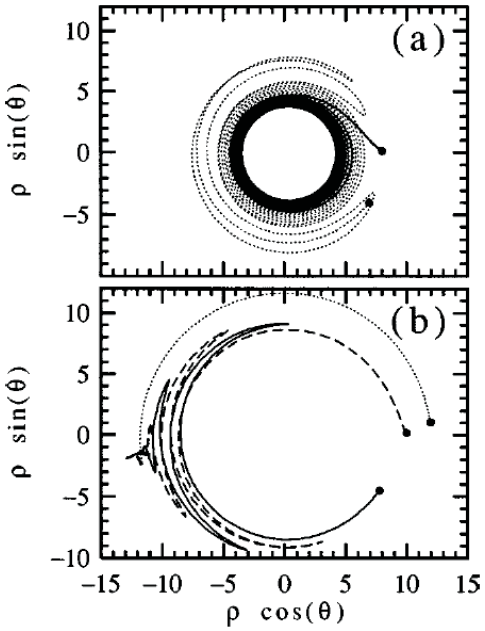

Figure 1.6: The interaction plane for soliton pairs with rotating phase difference (a) and with a phase difference of π (b) according to Akhmediev et al [41].

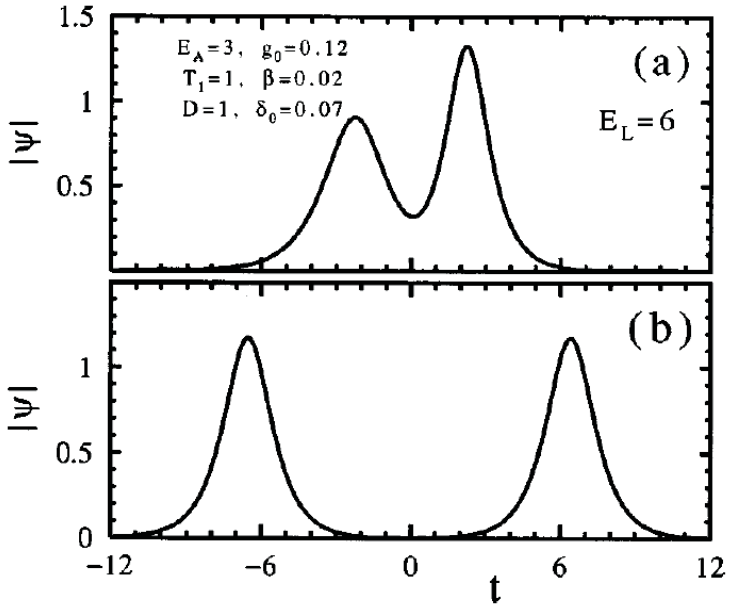

Figure 1.7: The temporal shapes corresponding to the solutions shown in figure 1.6 according to Akhmediev et al [41].

Chapter 2

Design of Passive Mode-Locked Lasers

2.1 Resonator design

A major part of the short pulse laser development is the resonator design. The cavity determines the beam diameters an intensities at different locations. Because for mode-locking an optical nonlinearity is required the intensities have to fulfill certain conditions.

The basic resonator geometry use for this work is displayed in figure 2.1. The resonator design is based on a delta-shaped cavity, which allows a small spot size and consequently a high intensity in the laser medium and on the saturable absorber, as required for the mode-locking regime. Basic properties regarding the resonator stability and the mode spot sizes in the cavity are derived using the matrix formalism. In this approach, the resonator modes are treated as Gaussian beams and the optical elements are described by using their ray-transfer matrices. The explicit forms of the matrices corresponding to the optical elements of the laser resonator, as well as the stability criterion and the formula of the mode radius can be found in [45]. It must be noticed that some elements like a curved mirror or a plane plate arranged at the Brewster angle are described by different matrices for the tangential and sagittal planes. Therefore the calculations must be done for the both planes. The stability

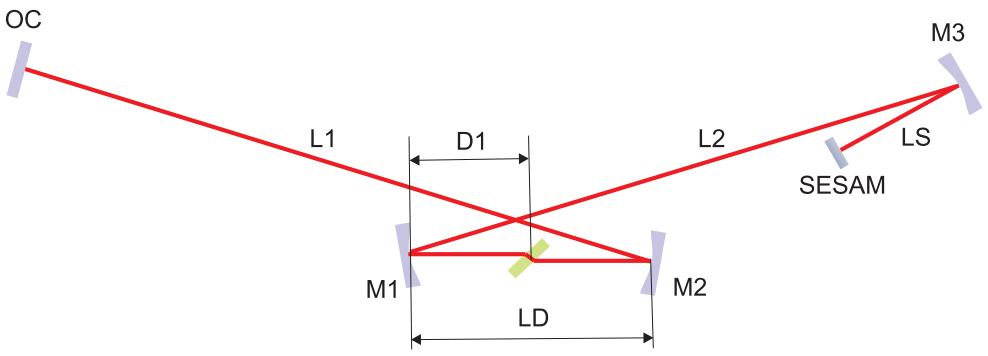

Figure 2.1: Layout of the laser resonator. M1-M3 - curved mirrors; R1-R3 - their radius of curvature; OC - plane output coupler; SESAM - plane saturable absorber mirror.

domain of the resonator will be the overlap between the two resulting stability regions. Another consequence is the elliptical shape of the modes, due to the different radii in the two planes. The calculations were made using a self written Mathematica programm.

A layout of the cavity is shown in figure 2.1. The active medium is arranged between the two folding mirrors M1 and M2, where the laser mode has its waist. The saturable absorber mirror is placed at the end of the cavity. The laser beam is focused on the saturable absorber by the curved mirror M3. The folding angles were kept lower than 5°. Around this values, the difference between the tangential and the sagittal planes introduced by the curved mirrors compensate the astigmatism due to the laser crystal (glass) arranged at the Brewster's angle. The calculations show only a small difference between the stability regions of the two planes and a slowly elliptical shape of the laser modes (see figure 2.2).

For certain radii of curvature of the mirrors, the stability region is determined by the folding distance L_D and the distance L_S (figure 2.1) between the focusing mirror and the saturable absorber mirror. Figure 2.2 shows the stability regions as functions of this distances. A variation of the arm lengths L_1 and L_2 has only a small influence on the laser modes. Also the insertion of a prism pair in one arm does not change the resonator stability.

There are three main requirements which we followed to fulfill by designing the laser

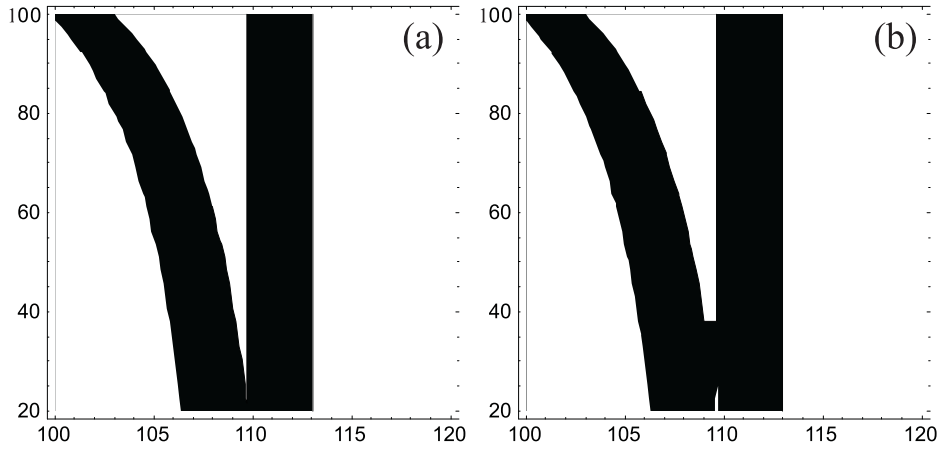

Figure 2.2: The stability diagram for the tangential (a) and sagittal (b) planes calculated with the parameters: R1 = R2 = 100 mm, R3 = 200 mm, L1= 400 mm, L2 = 800 mm. Horizontal axis: folding distance LD in mm. Vertical axis: distance LS between the focusing mirror and SESAM in mm.

resonator:

(1) *A good overlap between the pump beam and the laser mode in the active material.* The calculations show that the minimum mode size between the folding mirrors is proportional to their radius of curvature. To achieve a mode radius of 50 μm as the pumping scheme was designed, 100-mm curved mirrors are suitable (see figure 2.3).

(2) *A spot size on the saturable absorber mirror that results in a energy fluence larger than the saturable fluence of the device.*

For a stable mode locking regime, the energy fluence on the saturable absorber must be at least two times larger than the saturation fluence [16].

(3) *A very low divergence of the laser beam in the arm with the output coupler.*

This requirement must be fulfilled from the following considerations. To compensate the GVD introduced by the amplifying medium, a prism pair will be inserted in this arm. A divergent beam which propagates through a prism experiences higher losses at the prism surfaces in comparison to a parallel beam. Another reason is based on our experimentally observations that a divergent output beam shows strong instabilities on the edge. This is illustrated in figure 2.4. The pulse amplitude is almost constant in the center of the beam (a), but has a strong modulation at the edge (b).

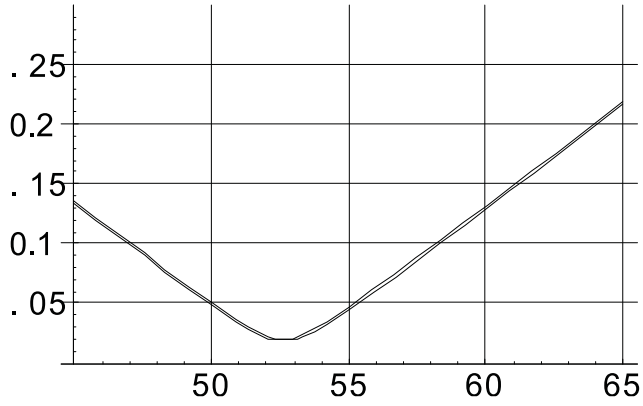

Figure 2.3: The mode radius at the crystal position for the tangential and the sagittal planes calculated with the parameters: R1 = R2 = 100 mm, R3 = 200 mm, L1= 400 mm, L2 = 800 mm. Horizontal axis: distance D1 in mm. Vertical axis: laser mode radius in μm.

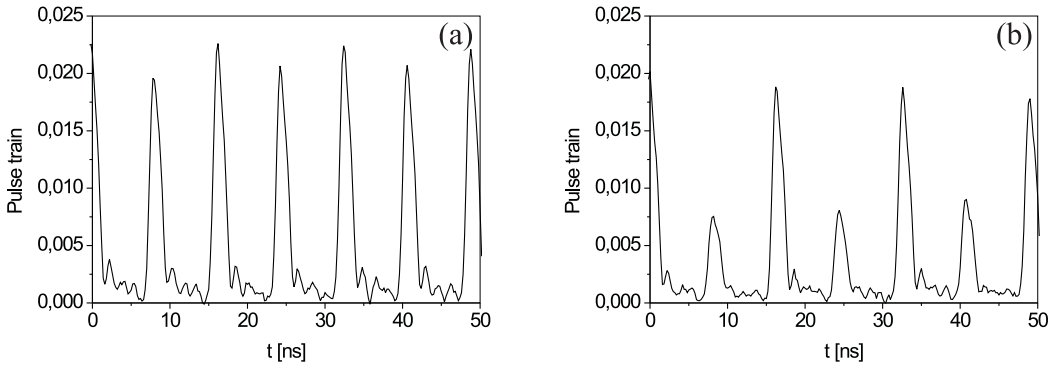

Figure 2.4: The pulse train in the center of the beam (a) and at the edge (b) for a divergent output beam.

2.2 Spectroscopic and laser properties of ytterbium-doped materials

The Yb^{3+}-ion [46] is a very suitable dopant for materials involved in ultrafast solid-state laser development. From a spectroscopic point of view, the Yb^{3+}-ion exhibits several advantages. Due to its simple electronic structure based on two electronic manifolds (see figure 2.5), undesired effects such as upconversion, excited-state absorption and concentration quenching do not occur. This allows the use of highly doped materials, leading to miniaturization of the devices. Ytterbium also presents a low quantum defect, which results in an improved efficiency of laser action and limits the heating of the laser rod.

The absorption band of Yb-doped materials is covered by high-power InGaAs laser diodes that permit direct diode pumping and the development of efficient and compact laser oscillators. In comparison to the corresponding Nd-doped laser materials, Yb-doped media show substantially broader emission spectra, which allow for shorter pulse generation and wider wavelength tuning.

However, an important drawback of Yb lasers is their quasi-three-level operating scheme, as the fundamental and terminal laser levels belong to the same $^2F_{7/2}$ manifold. Owing to this particular energy-level configuration, the spectroscopic and laser characteristics of ytterbium are particularly host dependent.

From the point of view of developing diode-pumped ultrashort-laser systems, it is crucial to look for Yb-doped media with the broadest emission spectrum. Among them, Yb-glasses exhibit very large emission bandwidths and thus have made possible the genertion of 58-fs pulses [47, 48], but their poor thermal properties and low emission cross sections constitute a big disadvantage because of subsequently induced low gain and very strong thermal effects. This is not the case for the Yb-doped crystals, which have a higher emission cross section and better thermal behavior [49]- [53]. The problem here is that the crystalline structure also tends to keep the emission and absorption bands narrow. In the last years, many investigations were done [54]-[63] in order to develop Yb-doped crystals with good thermal properties but with

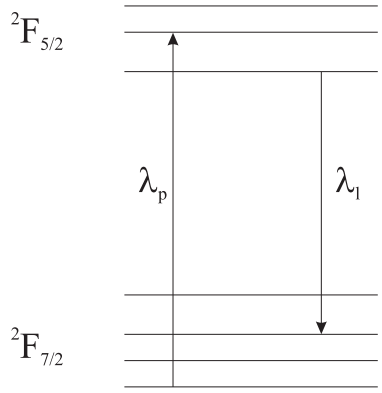

Figure 2.5: The energy levels of the Yb^{3+} ion. λ_p - pump wavelength, λ_l - laser wavelength.

spectral-emission broadness comparable to that of the glass.

In our experiments, we used Yb-doped fluoride-phosphate glass and two recently developed Yb-doped crystals, Yb:KGW and Yb:KYW which are very promising for ultrashort pulse generation [64]- [68]. Their spectroscopic and laser properties will be described in the following subsections.

2.2.1 Yb-doped fluoride-phosphate glass

The Yb-doped fluoride-phosphate glass (Yb:FP20) used in our experiments was developed at the University of Jena. The samples were doped with $8 \times 10^{20} cm^{-3} Yb^{3+}$ and had a 20-mol. % phosphate content. More details about the glass composition and preparation can be found in ref. [69]. The main parameters of the glass are listed in the table 2.1.

The figure 2.6 shows the measured absorption spectrum and the calculated emission spectrum using the reciprocity method [70]. The absorption spectrum allows for pumping in the range 935 - 975 nm. To get the highest pump efficiency, we pumped the laser around 972 nm, where the spectrum shows a peak. However, the pumping around 940 nm has the advantage of a highest stability against the temperature variations of the laser diode. The absorption cross section is almost constant in the range 935 - 955 nm, thus a small variation of the temperature and consequently of

Table 2.1: Parameters of Yb-doped fluoride-phosphate glass

Material	Yb:fluoride-phosphate glass
refractive index n_e at 1045 nm	1.50964
nonlinear refractive index n_2	$2.14 \times 10^{-16}\, cm^2/W$
lifetime ${}^2F_{5/2}$	1.39 ms
absorption coefficient at 975 nm	$11.6\, cm^{-1}$
absorption cross section at 975 nm	$14.5 \times 10^{-21}\, cm^2$
emission cross section at 1045 nm	$4.4 \times 10^{-21}\, cm^2$
saturation pump intensity at 975 nm	$9.4\ kW/cm^2$
gain saturation fluence	$75\ J/cm^2$
Thermal conductivity	$9 \times 10^{-3}\, W/cm/K$

the pump wavelength does not change the laser output power. This is a good choice for systems where a high output stability is required.

Using the emission and absorption spectra, the gain coefficient g can be calculated with the formula:

$$\begin{aligned} g &= 2L_g(N_2\sigma_{em}^{(L)} - N_1\sigma_{abs}^{(L)}) \\ &= 2L_g[N_2[\sigma_{em}^{(L)} + \sigma_{abs}^{L}) - N_{tot}\sigma_{abs}^{(L)}] \end{aligned} \tag{2.1}$$

where $\sigma_{em}^{(L)}$ and $\sigma_{abs}^{(L)}$ are the effective emission and absorption cross sections of the laser transition, N_1 and N_2 are the population densities in the lower and upper laser manifold. L_g is the length of the gain medium and the factor 2 results from the number of passes through the gain medium per cavity round trip. $N_{tot} = N_1 + N_2$ denotes the total number of active ions per unit volume.

At steady state, the laser gain just compensates for the cavity loss. This means that the excitation level, i.e. the fraction of active ions in the upper manifold is a fixed value, determined by the cavity loss, the length of the medium and the doping level. Figure 2.7 illustrates the gain spectra for various excitation levels N_2/N_{tot}, calculated

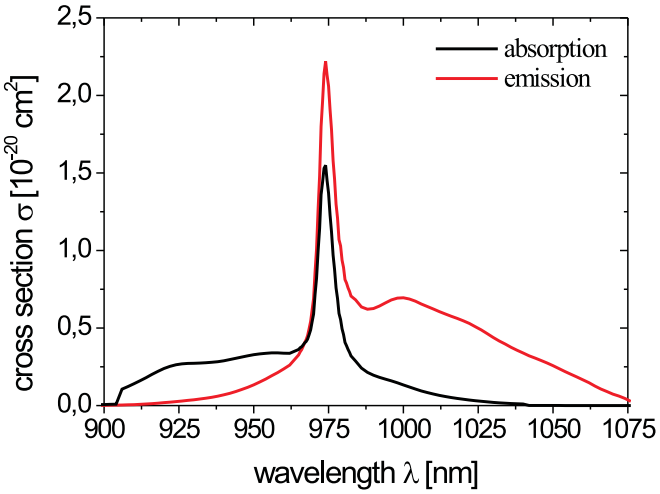

Figure 2.6: The absorption and emission spectra of Yb:fluoride-phosphate glass.

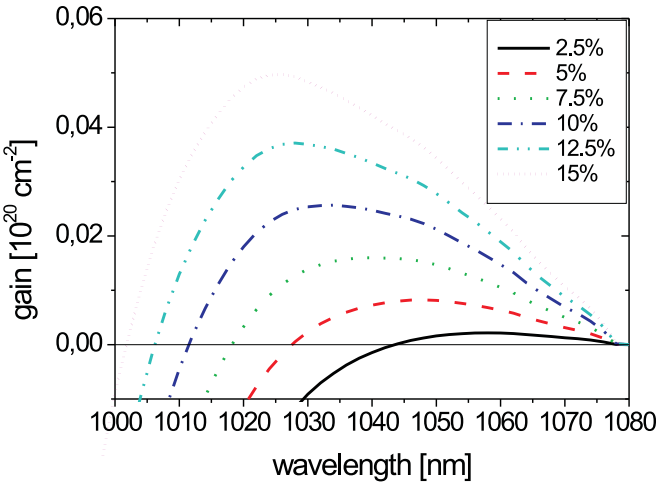

Figure 2.7: The calculated gain spectra of Yb:fluoride-phosphate glass for various excitation level N_2/N_{tot}.

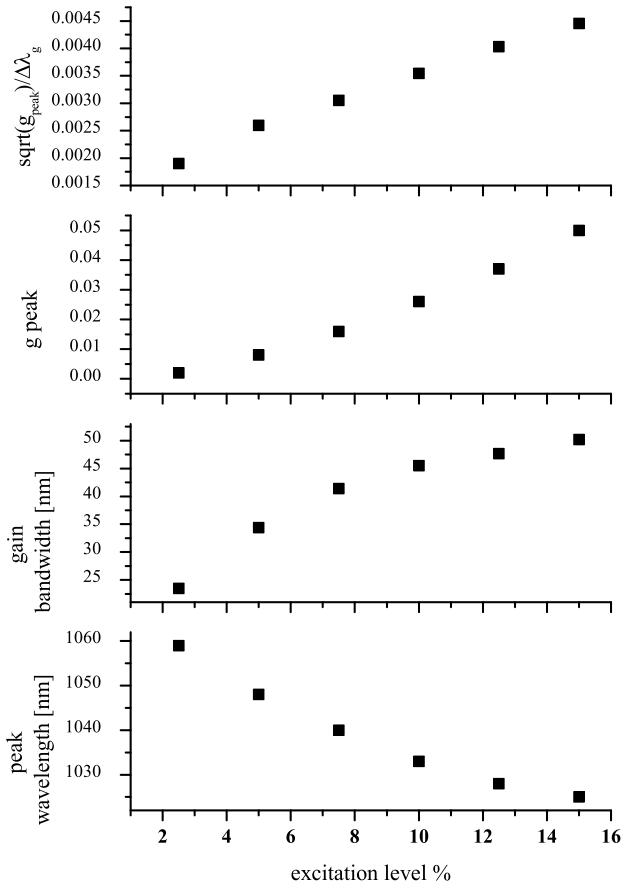

Figure 2.8: The calculated values of the ratio $(g_{peak})^{1/2}/\Delta\lambda_g$, the corresponding peak wavelength, gain bandwidth and maximum gain plotted as a function of excitation level.

from the data shown in figure 2.6. In contrast to four level systems, the peak wavelength and the gain bandwidth depend on the excitation level and thus on the cavity loss (figure 2.8). For higher gain, a shorter center wavelength and broader FWHM gain bandwidth is achieved. This explains the behavior we observed, that a cavity with a higher loss, which requires a higher excitation level works at a shorter wavelength. In mode locking regime, this considerations influence the achievable pulse duration. It was shown in the first chapter (equations 1.29 and 1.3) that the limiting effect of the gain filter depends not only on the FWHM gain bandwidth $\Delta\lambda_g$ but also on the peak gain coefficient g_{peak}. The minimum achievable pulse duration is

Table 2.2: Parameters of the unit cell for KGW and KYW

Crystal	KGW	KYW
crystal structure	monoclinic	monoclinic
point group	$C2/c$	$C2/c$
lattice parameters	$a = 8.05\mathring{A}$	$a = 8.05\mathring{A}$
	$b = 10.43\mathring{A}$	$b = 10.35\mathring{A}$
	$c = 7.588\mathring{A}$	$c = 7.54\mathring{A}$
	$\beta = 94.43°$	$\beta = 94°$

approximately proportional to $(g_{peak})^{1/2}/\Delta\lambda_g$. The calculated values of this ratio, as well as the corresponding peak wavelength, gain bandwidth and maximum gain are plotted in figure 2.8 as a function of excitation level. It can be noticed that the ratio increases with the excitation level. In effect, the minimum pulse duration of an Yb-based laser is obtained at a long wavelength (i.e. a low excitation level), despite the smaller value of $\Delta\lambda_g$ [47].

2.2.2 Yb-doped tungstates

Yb-doped potassium gadolinium tungstate $Yb : KGd(WO_4)_4$ (Yb:KGW) and Yb-doped potassium yttrium tungstate $Yb : KY(WO_4)_4$ (Yb:KYW) are two recently developed laser crystals [71–73] which are very attractive for ultrashort pulse generation. In comparison to other Yb-doped laser crystals such as Yb:YAG and Yb:YCOB, they have a much higher (13-17 times) absorption cross section, extremely low quantum defect ($\sim 4\%$), an emission cross section 9 times higher than Yb:YCOB, a broad emission band and therefore show the highest slope efficiency (87%) in a laser.
Rare-earth potassium tungstates have a monoclinic $C2/c$ (C_{2h}^6) structure [74]. The parameters of the unit cell for $KGd(WO_4)_4$ and $KY(WO_4)_4$ are given in the table 2.2. The Yb^{3+} ions substitutes the Gd^{3+} (or Y^{3+}) at a site with C_2 point symmetry. From the point of view of optical properties, KGW and KYW are biaxial crystals and the optical axes do not overlap with the crystallographic axes. The orientation

Table 2.3: Parameters of Yb:KGW and Yb:KYW

Material	Yb:KGW	Yb:KYW
Thermal expansion	$\alpha_a = 4 \times 10^{-6}/°C$	-
	$\alpha_b = 3.6 \times 10^{-6}/°C$	-
	$\alpha_c = 8.5 \times 10^{-6}/°C$	-
Thermal conductivity	$K_a = 2.6\,W/mK$	-
	$K_b = 3.8\,W/mK$	-
	$K_c = 3.4\,W/mK$	-
Density	$7.27\,g/cm^3$	$7.27\,g/cm^3$
Mohs hardness	4-5	4-5
Melting temperature	$1075\ °C$	-
Transmission range	0.35-5.5 μm	0.35-5.5 μm
refractive index at 1.06 μm	$n_g = 2.033$	-
	$n_p = 2.0337$	-
	$n_m = 1.986$	-
temperature dispersion	$0.4 \times 10^{-6}\,K^{-1}$	$0.4 \times 10^{-6}\,K^{-1}$
nonlinear refractive index n_2	$24 \times 10^{-16}\,cm^2/W$	$8.7 \times 10^{-16}\,cm^2/W$
lifetime ${}^2F_{5/2}$	0.6 ms	0.6 ms
absorption peak and bandwidth	$\alpha_a = 26\,cm^{-1}$	$\alpha_a = 40\,cm^{-1}$
	$\lambda = 981\,nm$	$\lambda = 981nm$
	$\Delta\lambda = 3.7\,nm$	$\Delta\lambda = 3.5\,nm$
absorption cross section at 981 nm	$1.2 \times 10^{-19}\,cm^2$	$1.33 \times 10^{-19}\,cm^2$
emission cross section $(E\|\|a)$	$2.6 \times 10^{-20}\,cm^2$	$3 \times 10^{-20}\,cm^2$
saturation pump intensity at 975 nm	$9.4\ kW/cm^2$	
gain saturation fluence	$7.42\ J/cm^2$	$6.43\ J/cm^2$
Stark levels energy (in cm^{-1})		
of the ${}^2F_{5/2}$ manifolds of Yb^{3+} at 77K	10682, 10471, 10188	10695, 10476, 10187
Stark levels energy (in cm^{-1})		
of the ${}^2F_{7/2}$ manifolds of Yb^{3+} at 77K	535, 385, 163, 0	568, 407, 169, 0

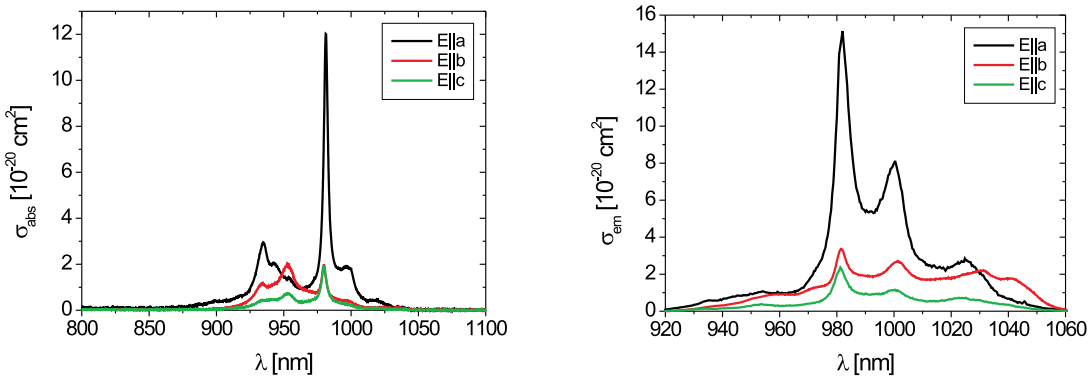

Figure 2.9: Polarised absorption and emission spectra of Yb:KGW.

of the indicatrix in the KGW crystal, as well as the dispersion of the refractive index can be found in [75]. Other main parameters of these laser materials are listed in the table 2.3. The nonlinear refractive indexes were taken from [76] and [77].

Yb:KGW gain spectra. The polarized absorption and emission spectra at room temperature are shown in figure 2.9. A strong absorption line is observed at $\sim$ 981 nm for all polarizations, with a peak absorption coefficient of 26 cm^{-1} ($E \parallel a$) and a linewidth (FWHM) of 3.7 nm.
Using this data and the equation. 2.1, the gain spectra were calculated for different excitation levels. They are plotted in figure 2.10 for polarizations parallel to a axis and parallel to c axis. It can be noticed that the Yb-doped crystals show structured gain spectra unlike the smooth spectra of Yb:glass. This could cause an increased tendency of the laser to work in double pulsing regime, in which phase-locked solitons with structured spectra would experience lower losses.

Yb:KYW gain spectra. The gain spectra of Yb:KYW have been calculated in a similar manner. Polarized absorption and emission spectra of Yb:KYW are shown in figure 2.11 and the calculated gain spectra for polarizations parallel to a and c axis are shown in figure 2.12.

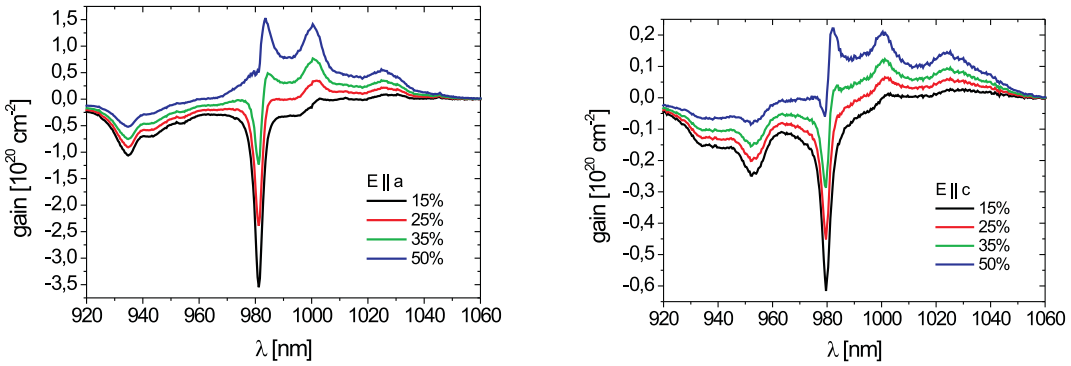

Figure 2.10: Polarised gain spectra of Yb:KGW for various excitation level N_2/N_{tot}.

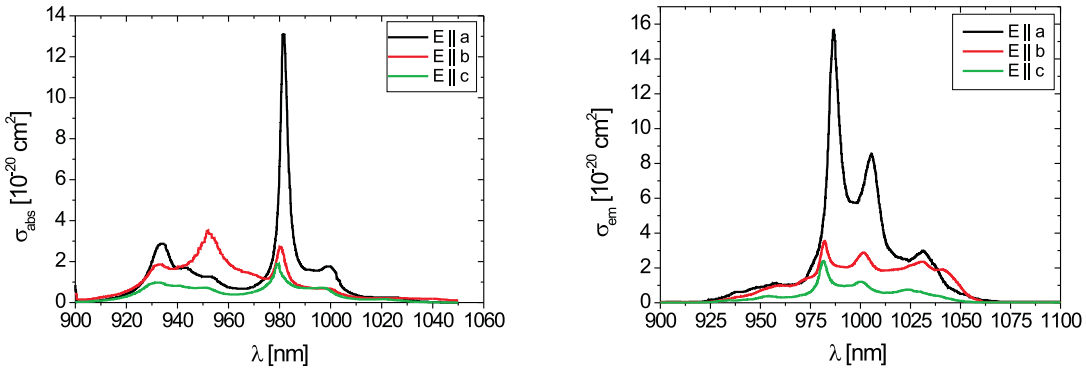

Figure 2.11: Polarised absorption and emission spectra of Yb:KYW.

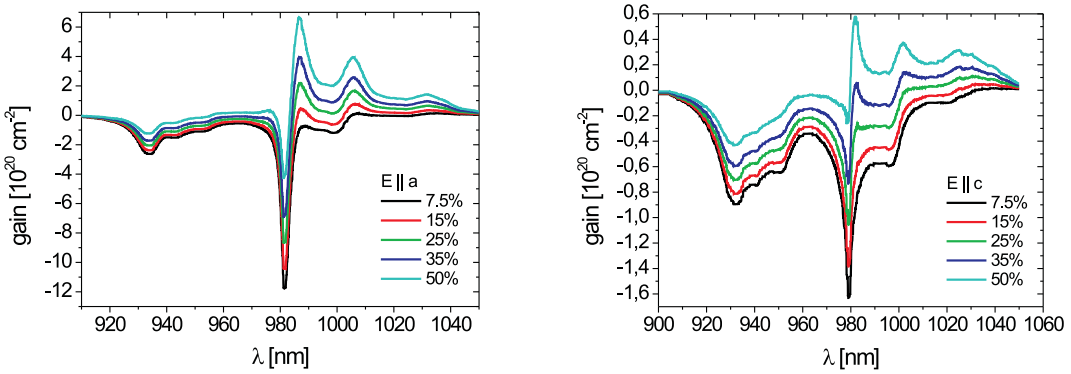

Figure 2.12: Polarised gain spectra of Yb:KYW for various excitation level N_2/N_{tot}.

2.3 Pumping systems

The absorption spectra of the ytterbium doped materials are well covered by the InGaAs/AlGaAs laser diodes emitting in the spectral range 940 - 980 nm. In order to achieve a high pump intensity in the gain medium as the quasi-3-level systems require, a high power and also a good beam quality are necessary. Another requirement is the mode matching between laser and pump beams. To get the highest possible pumping efficiency, the pump beam has to be focused to a pump spot area that is as small as possible, while maintaining a good overlap of the pump beam with the laser mode over at least an absorption length. In standard laser cavities, without the use of cylindrical optics, the laser modes are more or less circular. Therefore, the pump beam has to be focused to a circular spot inside the gain medium. A typical semiconductor laser emitter has an active surface of $\approx 100 \times 1\mu m^2$. For this reason, the spatial profile of typical diode lasers is very asymmetric in terms of beam size and mode quality. The axis parallel to the diode junction, the so called fast axis, is approximately diffraction limited, so only one mode can propagate through the waveguide structure. This mode is strongly diffracted at the emitter edge, which leads to a high divergence in this direction. The slow axis, perpendicular to the diode junction, allows the oscillation of many modes and the diffraction on the emitter edge induces only a low divergence. The generation of a focused circular spot requires the use of some beam shaper which symmetrizes the beam quality in both directions.
In our experiments, we tested two types of high power laser diodes, which are commercially available. They will be described in the following subsections. The advantages and the limitations for both systems will be shown.

2.3.1 Both sides pumping using single emitter laser diodes

The first pumping system we tested consists of two Polaroid laser diodes, model 2000-977-TO3-MCL-BW [78]. They have a single emitter with an active area of $100 \times 2\mu m^2$ and deliver a maximum output power of 2 W. The emitted radiation is linear polarized and has a divergence of $10° \times 2°$. A cylindrical microlens is placed in the front of

the emitter in order to collimate the fast axis [79]. This allows us to use spherical optics to focus the beam. The diode is placed in a 6 pin package (TO-3) on a heatsink (SDL-800) and supplied from a control device (SDL-822) which allows the adjustment of the temperature. Precise wavelength control is possible at high optical power.
The light was focused with two achromatic lenses with a focal length of 100 mm. The diode exhibits the typical difference in the beam quality. The measurements showed a beam quality M^2 of 1.3 for the fast axis and a M^2 of 10 for the slow axis [45].
Using this pumping scheme, the laser has a strong tendency to work in higher spatial modes. A single mode could be obtained only with a considerably decreasing of the output power.

2.3.2 One side pumping with a high brightness fiber coupled laser diode

Another tested pumping system was a high brightness fiber coupled laser diode from Unique-Mode, model UM5200/50/15 [80]. It provides an output power up to 5 W. The fiber has a core diameter of 50 μm and an effective numerical aperture (N.A.) of 0.15, which leads to a beam quality of $M^2 = 12$. The unique brightness is achieved by transforming the asymmetric radiation from two single emitters into a symmetrical beam using a patented micro optics. This beam can be coupled into a fiber with a very small core and N.A. with a high efficiency.
The output beam from the fiber has a circular shape, thus we used spherical optics to focus it on the laser medium. A beam radius of 50 μm was achieved with two achromatic lenses with 75 mm and 150 mm focal length [81].
This pumping system allowed an output power almost double than with the first pumping scheme. The laser could be easily arranged to work in single mode at maximum output power. This is due to a better overlap with the laser mode and smoother spatial profile of the pump beam. However, there are also some limitations. With the glass, the maximum pump power could not be applied because of its low thermal conductivity. This is not a problem if a crystal is used as gain material, but

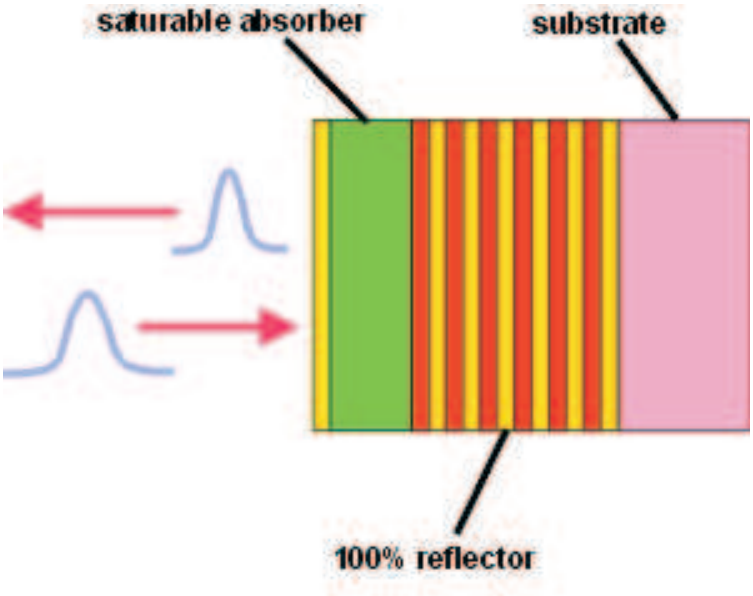

Figure 2.13: Basic layer structure of a semiconductor saturable absorber mirror.

in this case the absorption is strongly dependent on the pump beam polarization. As the radiation from the diode is not polarized, we did not work at minimum absorption length.

2.4 Semiconductor saturable absorber mirrors

To mode lock the laser, we used semiconductor saturable absorber mirrors with different modulation depths, provided by BATOP Optoelectronics [82].

The basic SESAM layer structure is shown in figure 2.13. It consists of a Bragg-mirror on a semiconductor wafer like GaAs, covered by a structure which embeds an saturable absorber layer and a more or less sophisticated top film system. The saturable absorption region can consist of one or more quantum wells or quantum dots layers. The top layer determines the field amplitude distribution across the mirror structure, and thus the saturable losses.

SESAMs structure

The detailed structure of the samples used in our experiments is explained in the tables 2.4 and 2.5.

Table 2.4: SESAMs structure (1)

Layer		Function
Si or Ta oxide		dielectric cover
71.2 nm GaAs		barrier
InGaAs		low temperature grown quantum well
71.2 nm GaAs		barrier
74.7 nm GaAs 88.4 nm AlAs	27×	Bragg mirror
GaAs		substrate

Table 2.5: SESAMs structure (2)

Sample	Quantum Well	Coating	Relative field amplitude
1	10,2 nm $In_{0,28}Ga_{0,72}As$	90 nm SiO_2	0.69
2	11,8 nm $In_{0,25}Ga_{0,75}As$	182 nm SiO_2	0.87
3	10,3 nm $In_{0,28}Ga_{0,72}As$	126 nm Ta_2O_5	1.24

The Bragg mirror has a reflectivity higher than 99.9% in the spectral range 900 - 1100 nm, as can be seen in figure 2.14.

The values of the relative field amplitude given in table 2.5 were calculated using a Filmwizard programm [83]. The electric field distribution (modulus of the electric field) for the three samples are presented in the figures 2.15, 2.16 and 2.17. The intensity of the input wave in the free space, averaged over a period, was considered to be equal to 1. The position of the saturable absorber (one quantum well) overlaps in all cases with a maximum of the electric field. Different choices of the cover layer change only the value of this maximum.

SESAMs macroscopic parameters

The macroscopic properties of the SESAMs relevant for the mode-locking process are listed in the table 2.6. Their experimental determination will be described in details in the chapter 4.

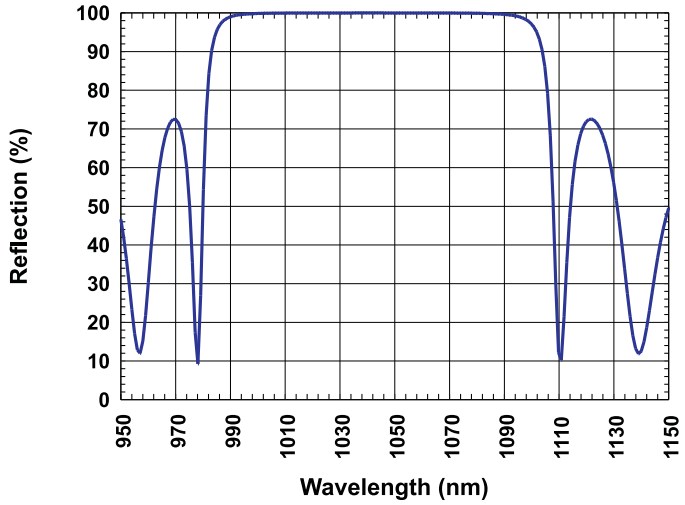

Figure 2.14: Reflectivity of the Bragg mirror containing 27 layers.

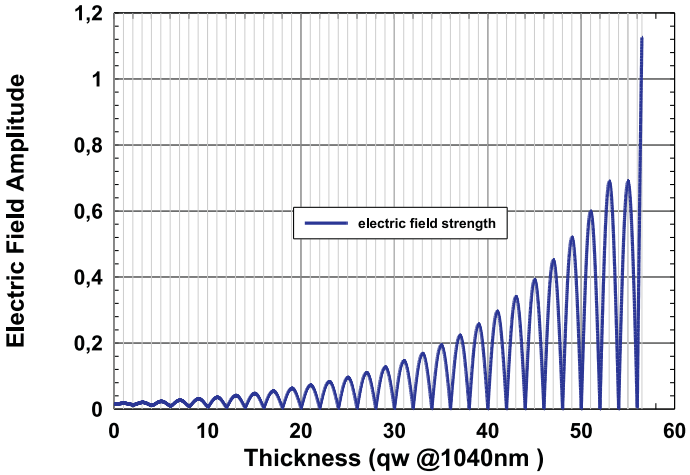

Figure 2.15: The electric field distribution (modulus of the electric field) for the sample 1.

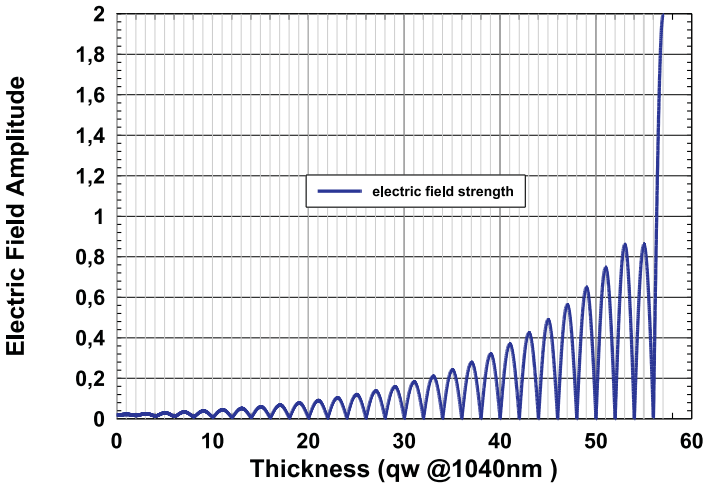

Figure 2.16: The electric field distribution (modulus of the electric field) for the sample 2.

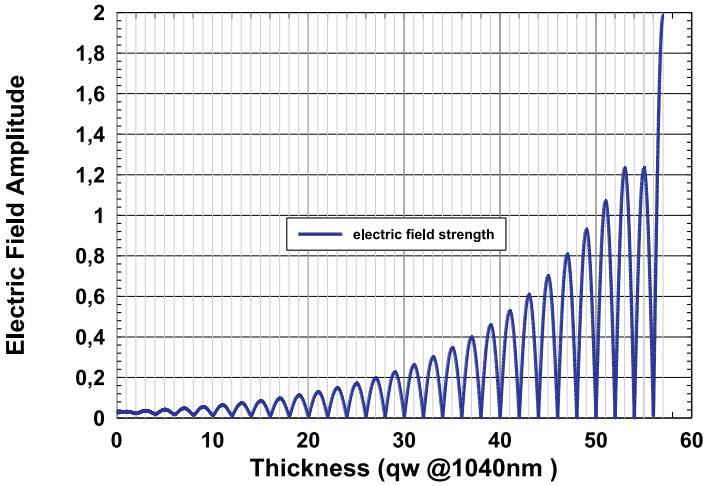

Figure 2.17: The electric field distribution (modulus of the electric field) for the sample 3.

Table 2.6: SESAMs macroscopic parameters

Sample	Modulation depth	Linear losses	Saturation fluence
1	0.9 %	1.55 %	14 $\mu J/cm^2$
2	1.3 %	2.31 %	59 $\mu J/cm^2$
3	2.0 %	4.39 %	6 $\mu J/cm^2$

2.5 Dispersion management

It was shown in the chapter 1 that the soliton mode-locking regime is generated by the balance between the negative group velocity dispersion (GVD) and the positive self-phase modulation (SPM). A source of negative GVD is then required to compensate for the usually positive material dispersion. The most common way to generate negative GVD is to use a prism pair. A broadband laser beam experiences negative angular dispersion between the prisms and positive material dispersion proportional to the path length in the prism. The magnitude of the negative GVD is determined by the prisms separation and the dispersion of the material.

Beside the GVD, the higher order dispersion terms influence also the passive mode locking [84]- [88].

The expressions of the second order (GVD) and third order (TOD) dispersion introduced by a pair of identical prisms are given further according to [8]. The approach is to analyze the sequence of optical elements by ray-optical techniques and calculate the optical beam path P as function of frequency ω. The phase delay between the rays corresponding to the arbitrary frequency ω and the central frequency ω_l is

$$\Psi(\omega) = \frac{\omega}{c} l \cos(\alpha) \tag{2.2}$$

where l is the distance between the prisms and α the angle between the two rays (see figure 2.18).

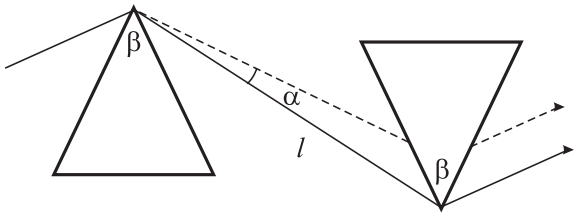

Figure 2.18: Two prism sequence for the GVD compensation.

At minimum deviation arrangement for the component ω_l (symmetrical beam path through the prisms) and with the apex angle chosen to fulfill Brewster's condition, the second order dispersion term is given by:

$$\Psi''(\omega_l) = \frac{d^2\Psi}{d\omega^2}|_{\omega_l} \approx -4l\frac{\lambda_l^3}{2\pi c^2}(\frac{dn}{d\lambda}|_{\lambda_l})^2, \tag{2.3}$$

where n is the refractive index of the prism material and $\frac{dn}{d\lambda}|_{\lambda_l}$ describes the material dispersion at center wavelength λ_l. The equation was derived by neglecting the terms which are usually much smaller than those considered above.
In the same way, the third order dispersion term can be written for this particular geometry

$$\begin{aligned}\Psi'''(\omega_l) &= \frac{d^3\Psi}{d\omega^3}|_{\omega_l} \\ &\approx \frac{12l\lambda_l^4}{(2\pi)^2c^3}(\frac{dn}{d\lambda})^2[1-\lambda_l\frac{dn}{d\lambda}(n^{-3}-2n)] + \lambda_l(\frac{dn}{d\lambda}\frac{d^2n}{d\lambda^2})|_{\lambda_l}.\end{aligned} \tag{2.4}$$

The previous two equations describe the effect of the angular dispersion only. In practice, the beam also passes through a certain amount of glass in each prism which contributes to the dispersion. If the cumulative mean glass path is L, the additional second-order and third-order dispersion terms are

$$\Psi''_L(\omega_l) = \frac{\lambda_l^3}{2\pi c^2}L\frac{d^2n}{d\lambda^2}|_{\lambda_l}. \tag{2.5}$$

and respectively

$$\Psi_L^{'''}(\omega_l) = -\frac{\lambda_l^2}{(2\pi)^2 c^3} L[3\lambda_l^2 \frac{d^2 n}{d\lambda^2} + \lambda_l^3]|_{\lambda_l}. \tag{2.6}$$

The total dispersion of the prism sequence is:

$$\Psi_{tot}^{''}(\omega_l) \approx \frac{\lambda_l^3}{2\pi c^2}[Ln^{''} - 4ln^{'2}] \tag{2.7}$$

and

$$\Psi_{tot}^{'''}(\omega_l) \approx \frac{\lambda_l^4}{(2\pi)^2 c^3}[12l(n^{'2}[1 - \lambda_l n^{'}(n^{-3} - 2n)] + \lambda_l n^{'} n^{''}) - L(3n^{''} + \lambda_l n^{'''})]. \tag{2.8}$$

The terms $n^{'}$, $n^{''}$ and $n^{'''}$ denote the derivatives of n with respect to λ taken at λ_l. While the angular dispersion (second term in equation 2.7) always results in negative group delay dispersion, the finite glass path (first term) gives rise to positive GVD in the visible and near infrared spectral range where $d^2n/d\lambda^2 > 0$. This offers the possibility of tuning the GVD by changing L. The common method is to simply translate one of the prisms perpendicularly to its base, which alters the glass path while keeping the beam deflection constant.

To design a mode-locked laser cavity, we need to chose the suitable prism material and prism separation, so that the introduced negative GVD to compensate the positive GVD of the other elements. To estimate the dispersion introduced by a pair of prisms we need to know the dependence of the refractive index on the wavelength and also the derivatives $n^{'}$, $n^{''}$ and $n^{'''}$. This can be calculated using the Sellmayer equation:

$$n^2(\lambda) - 1 = B_1 \frac{\lambda^2}{\lambda^2 - C_1} + B_2 \frac{\lambda^2}{\lambda^2 - C_2} + B_3 \frac{\lambda^2}{\lambda^2 - C_3} \tag{2.9}$$

The equation is especially suitable for the progression of refractive index in the wavelength range from the UV through the visible to the IR area (to 2.3 m). It is derived

from the classical dispersion theory and allows the description of the progression of refractive index over the total transmission region with one set of data and to calculate accurate intermediate values. The Sellmeyer coefficients B_{1-3} and C_{1-3} for different glasses are given in [89]. The determination of the coefficients was performed for all glass types on the basis of precision measurements by fitting the dispersion equation to the measurement values.

According to the dispersion requirements, we used three types of prisms in our lasers: fused silica, BK7 and SF10. The Sellmeier coefficients for this materials are given in the table 2.7.

Table 2.7: Sellmeier coefficients of the prism glasses

	fused silica	BK7	SF10
B1	$6.69422575 \times 10^{-1}$	1.15150	1.61625977
B2	$4.34583937 \times 10^{-1}$	1.18584×10^{-1}	$2.59229334 \times 10^{-1}$
B3	$8.71694723 \times 10^{-1}$	1.26301	1.07762317
C1	$4.48011239 \times 10^{-3}$	1.05984×10^{-2}	$1.27534559 \times 10^{-2}$
C2	$1.32847049 \times 10^{-2}$	-1.18225×10^{-2}	$5.81983954 \times 10^{-2}$
C3	9.53414824×10^{1}	1.29618×10^{2}	1.1660768×10^{2}

The next figures show the calculated values for the refractive index and the first three derivatives in the wavelength range from 1020 to 1070 nm.

To make the right choice between this materials, we have to estimate the positive GVD introduced by the amplifying media and the other elements in the cavity (mirrors, saturable absorber mirror).

For the Yb:KGW crystal we used the parameters given in ref. [75] for the undoped KGW crystal. They measured the refractive indices corresponding to the three optical axis in the visible and near-infrared regions. The refractive index variations have been described by an infrared-corrected Sellmeyer law:

$$n(\lambda) = A + \frac{B}{1 - (\frac{C}{\lambda})^2} - D\lambda^2 \tag{2.10}$$

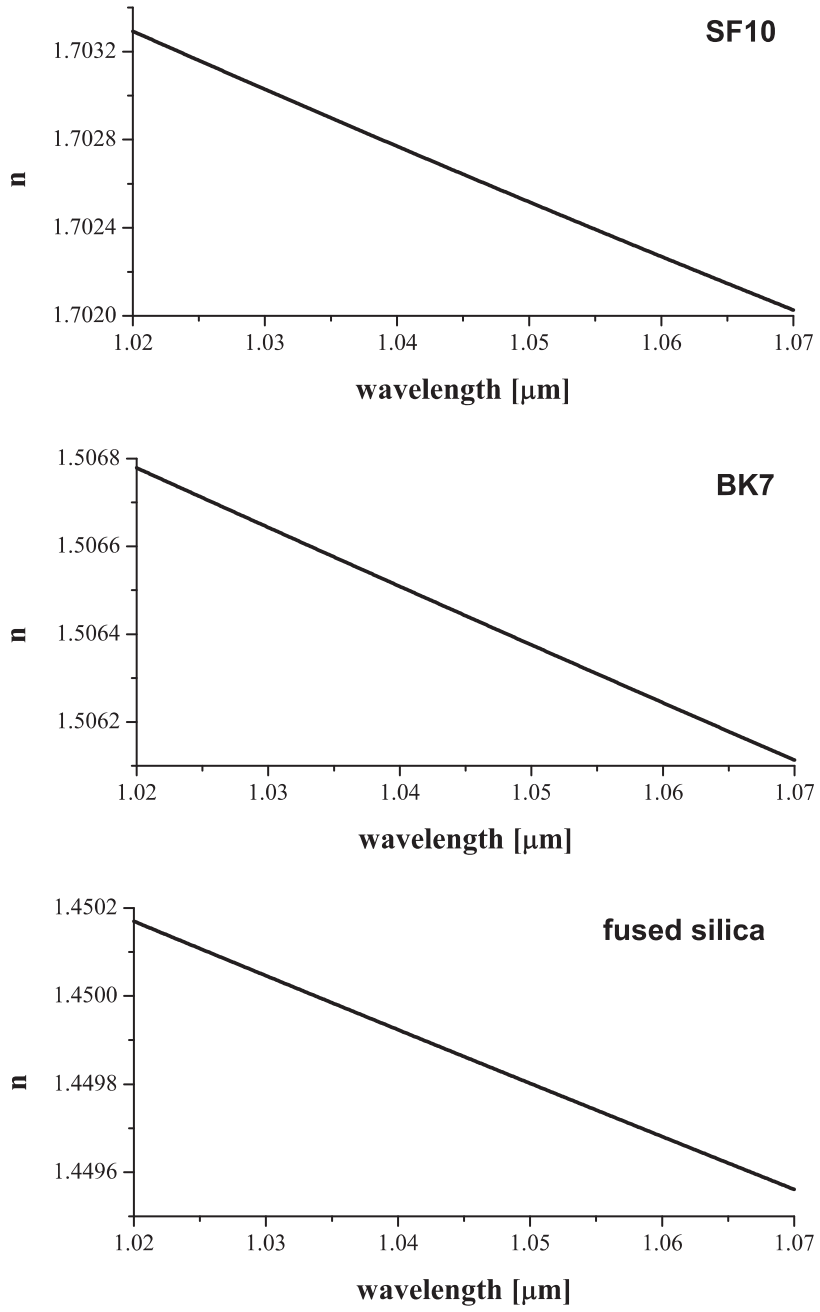

Figure 2.19: The refractive index of the prism materials in the wavelength range 1020–1070 nm.

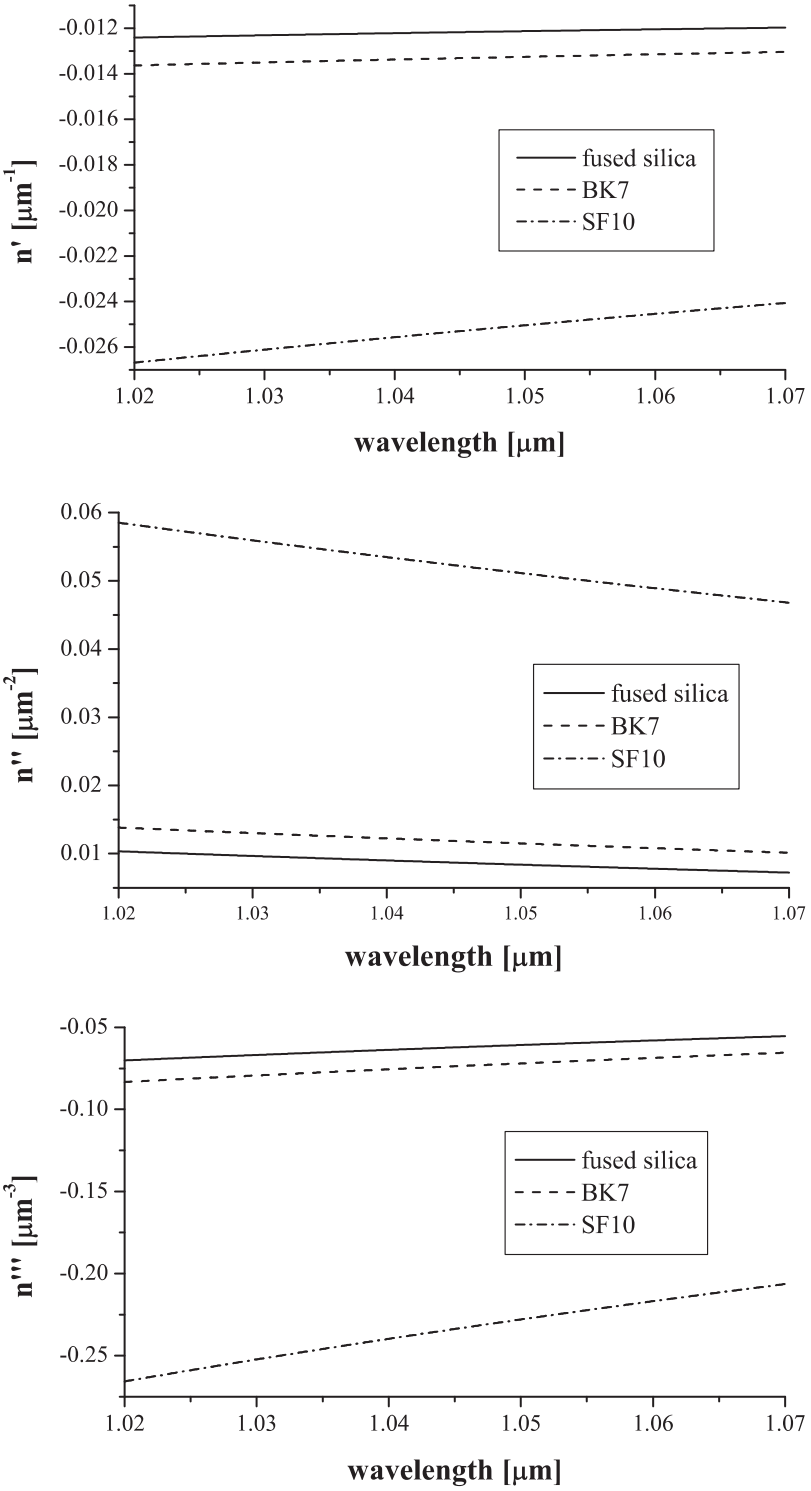

Figure 2.20: The first three derivatives of the refractive index of the prism materials.

The parameters A, B, C and D obtained from the fits of the experimental results are given in the table 2.8.

Table 2.8: Sellmeier coefficients of the room-temperature refractive indices of undoped KGW crystal according to Pujol et al [75]

	A	B	C/nm	D/nm^{-2}
n_g	1.3867	0.6573	170.02	0.2913×10^{-9}
n_m	1.5437	0.4541	188.91	2.1567×10^{-9}
n_p	1.5344	0.4360	186.18	2.0999×10^{-9}

Chapter 3

Laser Experiments

3.1 Laser setup

As it was shown in section 2.3, we used two pumping schema for our lasers. The setups corresponding to each pumping system will be described in the next subsections.

3.1.1 Both sides pumped laser setup

The first experiments were performed using the two Polaroid laser diodes described in subsection 2.3.1, in the setup shown in figure 3.1. As laser medium we used an 1.8 mm thick Yb:fluoride phosphate glass provided by the Otto-Schott-Institut, University of Jena [69]. The doping level was $8 \times 10^{20} ion/cm^3$.

Each diode has a 100 μm emission aperture and emits 1.4 W at 975 nm. The two pump beams are imaged with four achromatic lenses onto the both sides of the laser glass resulting in a pump spot diameter of approximately 60 μm. The cavity was designed for a mode waist of 50 μm inside the glass. An 100 mm curved mirror focuses the laser beam onto the SESAM in order to achieve a beam radius of 50 μm. A pair of SF13 prisms separated by 14 cm were used to compensate the group-velocity dispersion introduced by the amplifying medium. The glass was arranged at Brewster angle. Using two lambda-half plates, the polarization of the pump beams was rotated to achieve the maximum absorption in the glass.

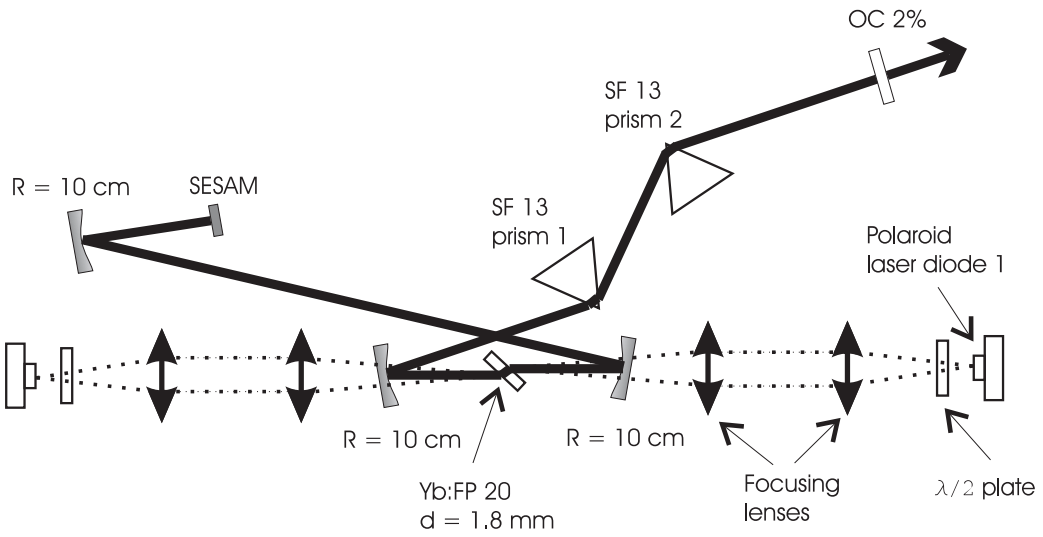

Figure 3.1: Both sides pumped laser setup. R, radius of curvature; SESAM, semiconductor saturable absorber mirror; OC, output coupler.

3.1.2 One side pumping using a fiber coupled laser diode

An other pumping system we tested was a high-brightness fiber-coupled laser diode, which provides an output power up to 5W (see subsection 2.3.2). The fiber has a core diameter of 50 μm and an effective numerical aperture of 0.15, which leads to a beam quality of $M^2 = 12$.

The laser setup (figure 3.2) consists of a delta-shaped cavity with one arm folded by the plane mirror M4, in order to achieve a compact design. The laser medium (Yb-doped glass or crystal) was placed in the cavity at the Brewster angle.

The pump beam is focused with two antireflective coated achromatic lenses, resulting in a measured pump spot diameter of 100 μm, which fits well to the designed laser mode in the material. The folding mirrors M1 and M2 have a radius of curvature of 100 mm and a reflectivity $> 99.9\%$ in the range 1020-1070 nm. The laser beam was focused onto the SESAM using the spherical mirror M3 with 100 or 200-mm radius of curvature. A pair of SF10 prisms separated by 34 cm were inserted in the arm with the output coupler OC. They compensate for the group-velocity dispersion introduced by the amplifying medium.

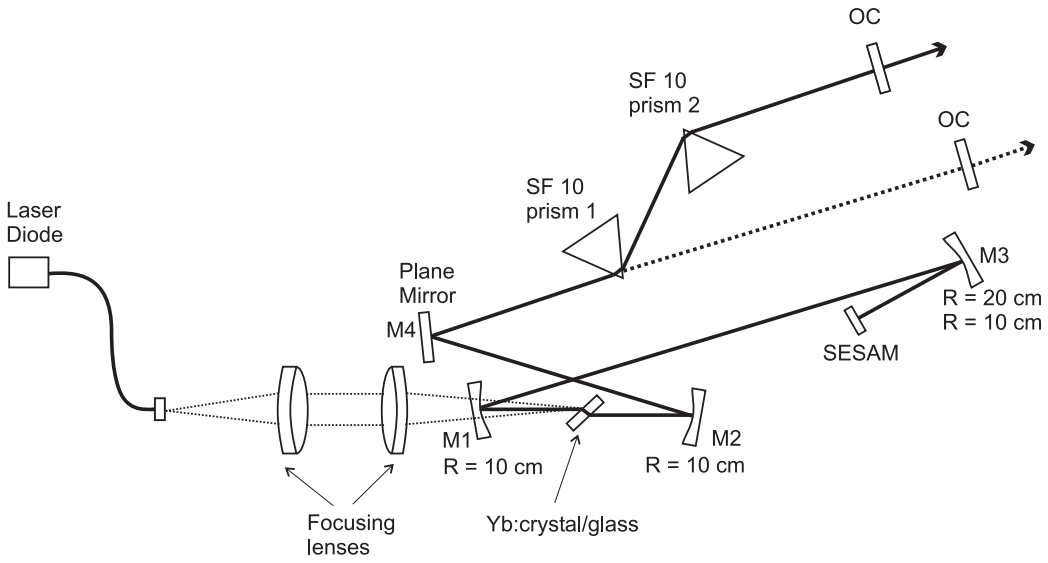

Figure 3.2: Experimental setup for mode-locked Yb-based lasers. M1 - M3, curved mirrors; R, radius of curvature; M4, high-reflective plane mirror; OC1 - OC2, output couplers with different transmissions; SESAM, semiconductor saturable absorber mirror.

3.2 Beam diagnostics

To monitor the pulse train we used a silicon photodiode with a rise time of about 2 ns. The amplified photodiode signal was visualized with a Tektronix sampling oscilloscope with 500 MHz bandwidth and 5 GS/s sample rate. The signal was also sent to a frequency spectrum analyzer in order to observe the eventually modulations of the pulse amplitude.

The spectral properties of the laser were monitored by a grating spectrometer from OceanOptics, with a resolution of 0.3 nm.

For the temporal characterization of the laser pulses we built a second order autocorrelator, which is schematically shown in figure 3.3.

It has a 50% transmission beam-splitter BS and one corner mirror in each arm. One of them (CM1) is placed on a motorized translation stage which is used to vary automatically the path length. We used a 200 μm thick BBO crystal to generate the second harmonic (SH) radiation. The two arms are focused onto the nonlinear crystal

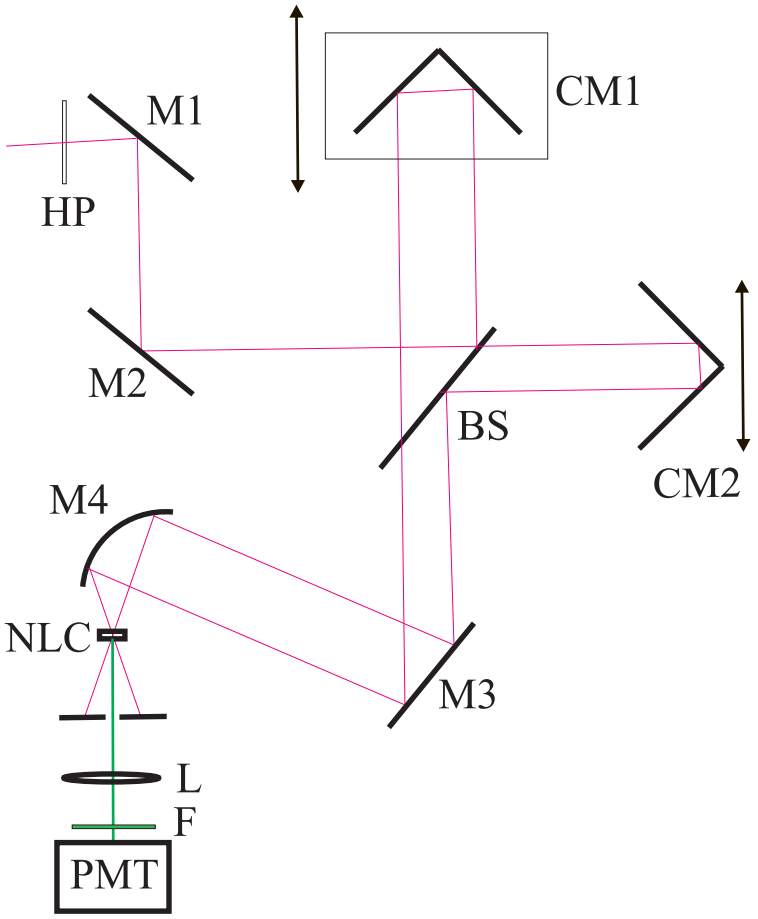

Figure 3.3: Second order autocorrelator for pulse length measurement. BS - beam-splitter with 50% transmission, M1-3 - plane mirrors, M4 - spherical mirror, CM1-2 - corner mirrors, HP - lambda half plate, NLC - nonlinear crystal, L - lens, F - interferential filter, PMT - photomultiplier tube.

using the spherical mirror M4 with a 50-mm radius of curvature. The non-collinear SH beam was collimated to the entry of the photomultiplier tube PMT and the signal sent to a PC. The lambda-half plate HP was used to rotate the polarization in order to achieve the highest SH intensity. By translating the corner mirror CM2 along the axis perpendicular to the incident beam, the setup can be also arranged to record the interferometric autocorrelation trace.

We also used a commercial scanning real-time autocorrelator in order to notice immediately the changes in the pulse length.

3.3 Experimental results

3.3.1 Mode-locking performance

Yb:fluoride phosphate glass

The first mode-locking experiments were performed using the setup described in subsection 3.1.1 and an 1.8 mm thick Yb:fluoride phosphate glass as laser medium. At 1.9 W absorbed power, and with a 2% transmission output coupler, we achieved an output power of up to 100 mW in mode locked operation. Using a high reflective mirror instead of the SESAM, the output power was 225 mW and 420 mW with and without dispersion prisms, respectively. Pulses as short as 110 fs, assuming a $sech^2$ pulse shape, are generated at a repetition rate of 122 MHz. Figure 3.4a shows the interferometric autocorrelation trace of 110-fs-pulses. The corresponding optical spectrum (figure 3.4b) is centered at 1057 nm and has a bandwidth of 11 nm.

The laser performance of Yb:glass was definitely improved using the setup described in subsection 3.1.2.

With a high reflective mirror instead of the SESAM and without dispersion prisms, an output power of 950 mW in the TEM_{00} operation was achieved at 4 W pumped power. For comparison with the previous setup: 2.8 W pumping power, 420 mW output power and a strong tendency to higher transverse modes. In CW mode-locked regime, using the SESAM with 2% saturable absorption, the output power was 180 mW (45 mW with the previous setup).

The shortest autocorrelation width obtained with this setup is 162 fs (see figure 3.5a), which corresponds to a pulse width of 95 fs assuming a hyperbolic secant shape, respectively 105 fs for a gaussian pulse shape. The optical spectrum, shown in figure 3.5b is centered at 1062 nm and has a broadness of 14.2 nm. The time-bandwidth product is 0.36.

The shortest pulse reported so far in the literature for an Yb:fluoride phosphate glass laser is 60 fs [48] at 1057 nm, with a broadness of 22.4 nm and a time-bandwidth product of 0.358.

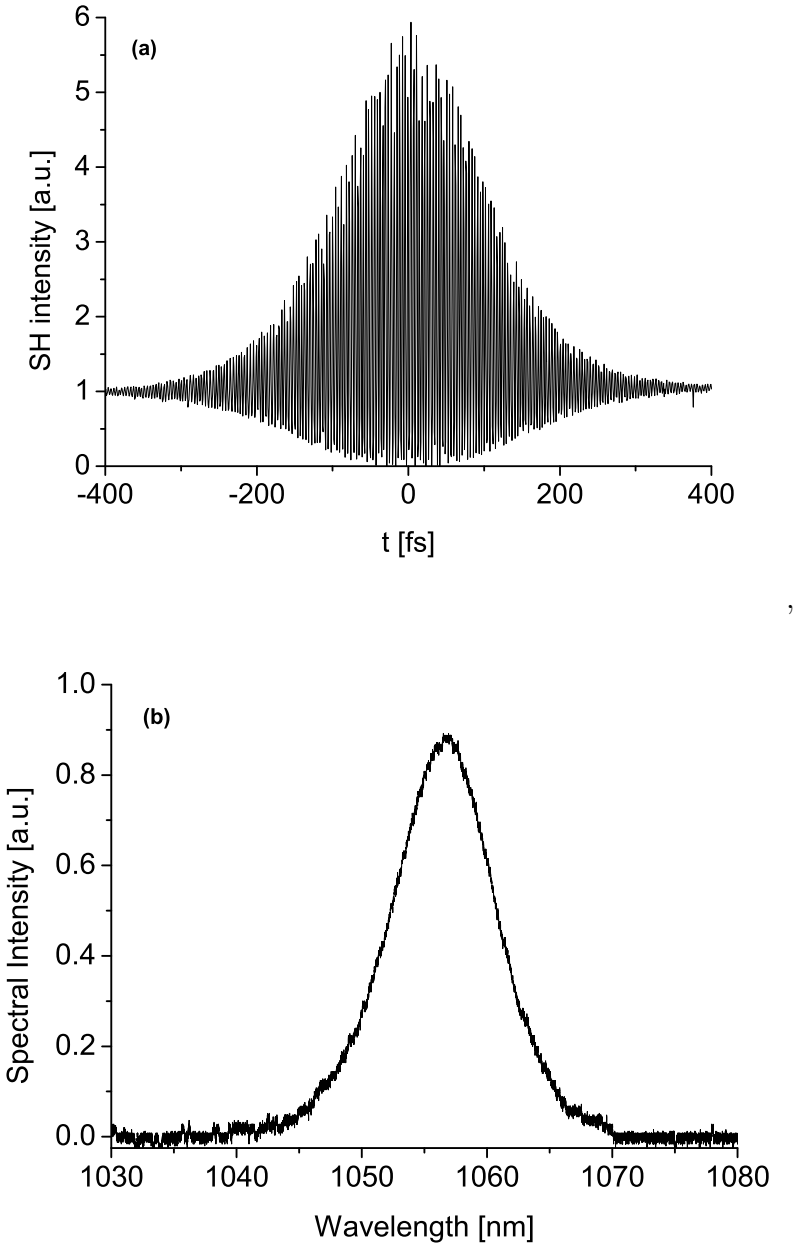

Figure 3.4: (a) Interferometric autocorrelation trace and (b) the corresponding optical spectrum of 110 fs pulses obtained with the laser oscillator described in 3.1.1.

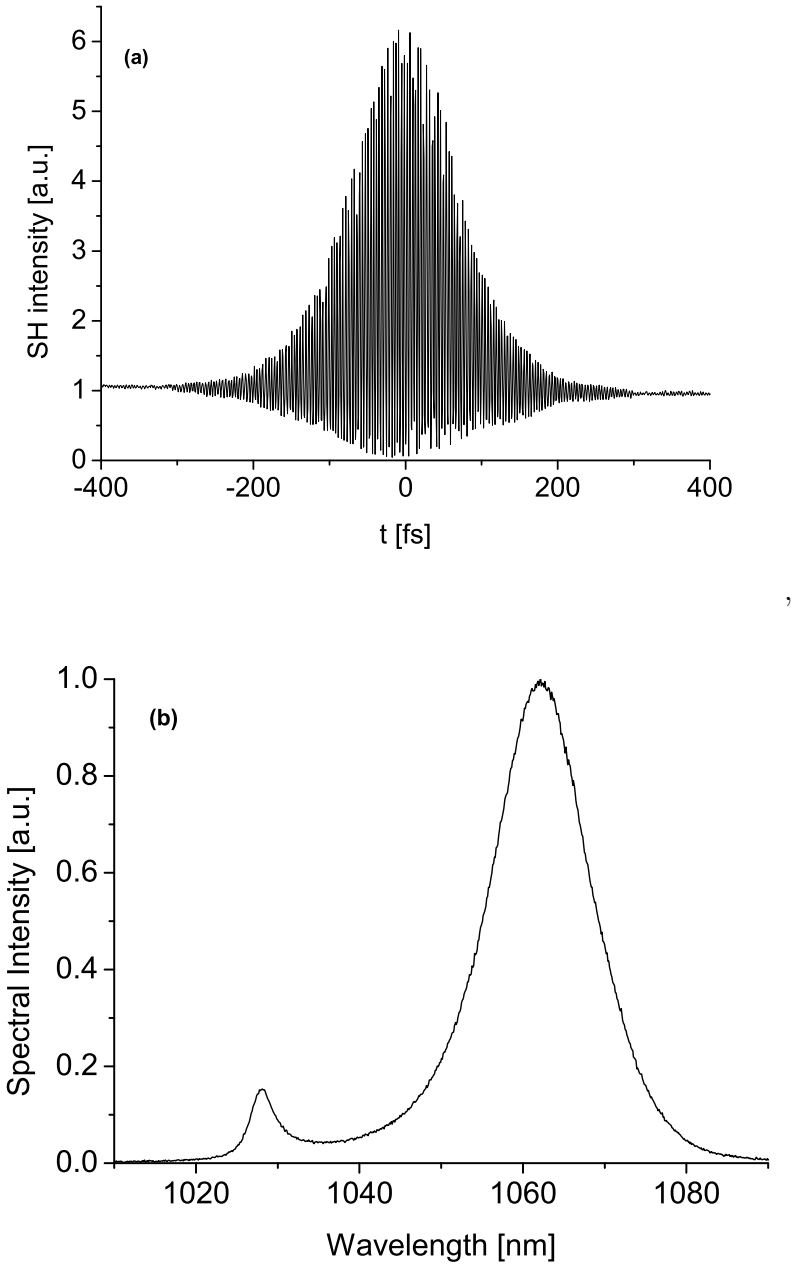

Figure 3.5: (a) Interferometric autocorrelation trace and (b) the corresponding optical spectrum of 95 fs pulses obtained with the laser oscillator described in 3.1.2.

Yb:KGW

The experiments were performed with a 1-mm-thick Yb:KGW crystal arranged in the setup described in subsection 3.1.2. The crystal was doped with 5 at.% of Yb^{3+} ions and cut for pumping along the b axis.

Using a 2% transmission output coupler and the SESAM with 2% modulation depth, pulses as short as 100 fs were achieved. Figure 3.6a shows the intensity autocorrelation trace and the fit assuming a $sech^2$ pulse shape. The corresponding optical spectrum (figure 3.6b) is centered at 1037.4 nm and has a bandwidth of 13.4 nm. This results in a time-bandwidth product of 0.373, which is with 18% more than the theoretical value of 0.315 for a $sech^2$-pulse shape. This is the shortest pulse length reported so far for this material [90]. As the time-bandwidth product is 18% larger than the theoretical value, the pulses may be shortened further. The output power was 126 mW and the repetition rate 108 MHz. This corresponds to an energy per pulse of 1.17 nJ and to a peak power of 11.7 kW. The CW mode-locking regime was selfstarting and stable.

Using a saturable absorber with 0.9% modulation depth and a 3% transmission output coupler, an output power between 360 and 430 mW was achieved. In this case the shortest pulse had a duration of 174 fs and a spectral bandwidth of 7.2 nm.

In the cw configuration, with a high reflective mirror instead of the saturable absorber and with a 3% output coupler, the output power was 630 mW without the prisms and 520 mW after the prisms insertion.

Yb:KYW

Similar results were obtained using a Yb:KYW crystal. It had the same thickness and Yb concentration as the Yb:KGW crystal and was tested using the same set-up. A comparison between the laser performances of the two crystals is given in table 3.1. For both amplifying media, the shortest pulse length was achieved with a 2% saturable-absorption mirror and a 2% transmission output coupler, as the highest output power was delivered for an 0.6% saturable-absorption mirror and 3%, respectively 4% transmission output couplers.

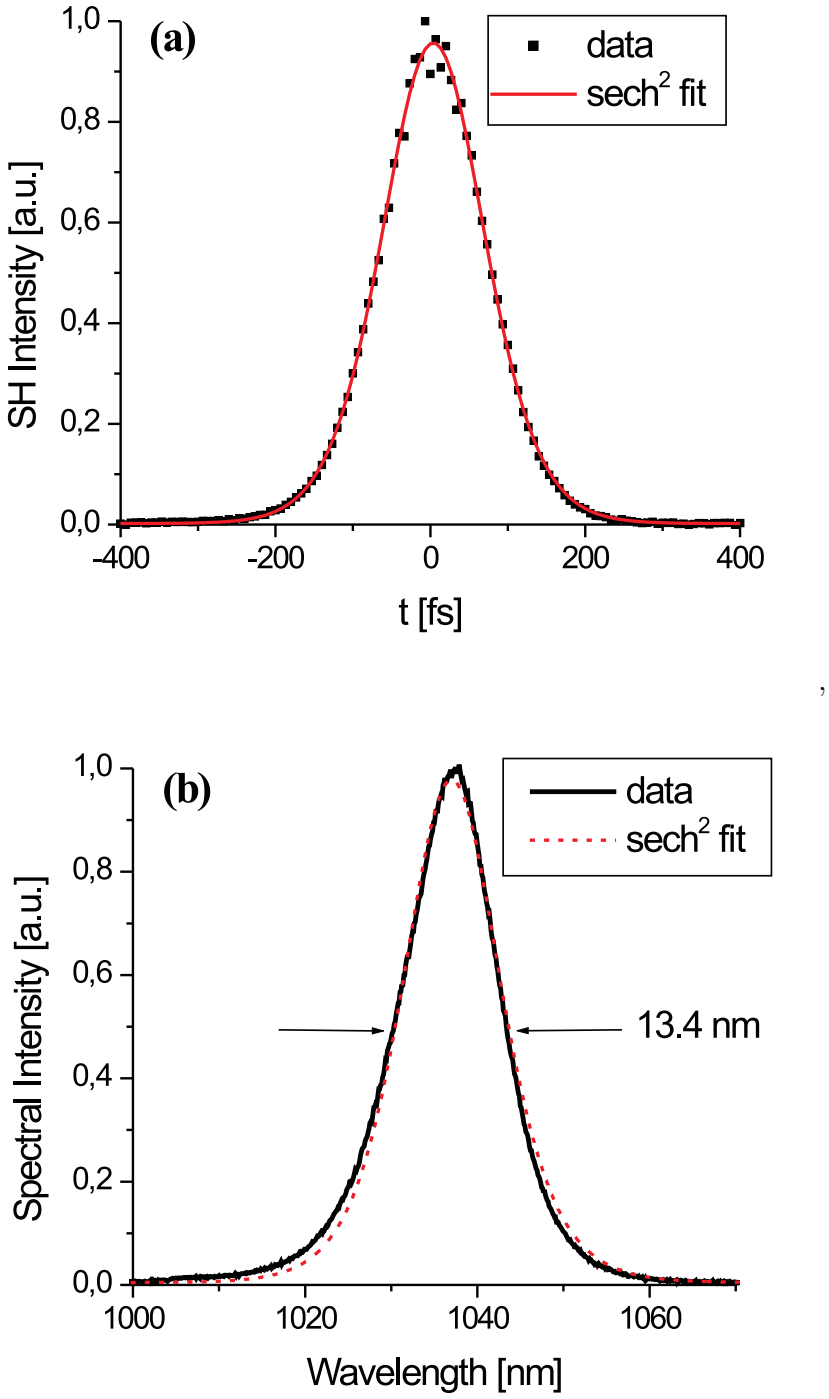

Figure 3.6: Yb:KGW mode-locked laser. (a) Measured intensity autocorrelation of 100-fs pulses and its fit for a $sech^2$ pulse shape. (b) Optical spectrum of the pulses and the $sech^2$ fit.

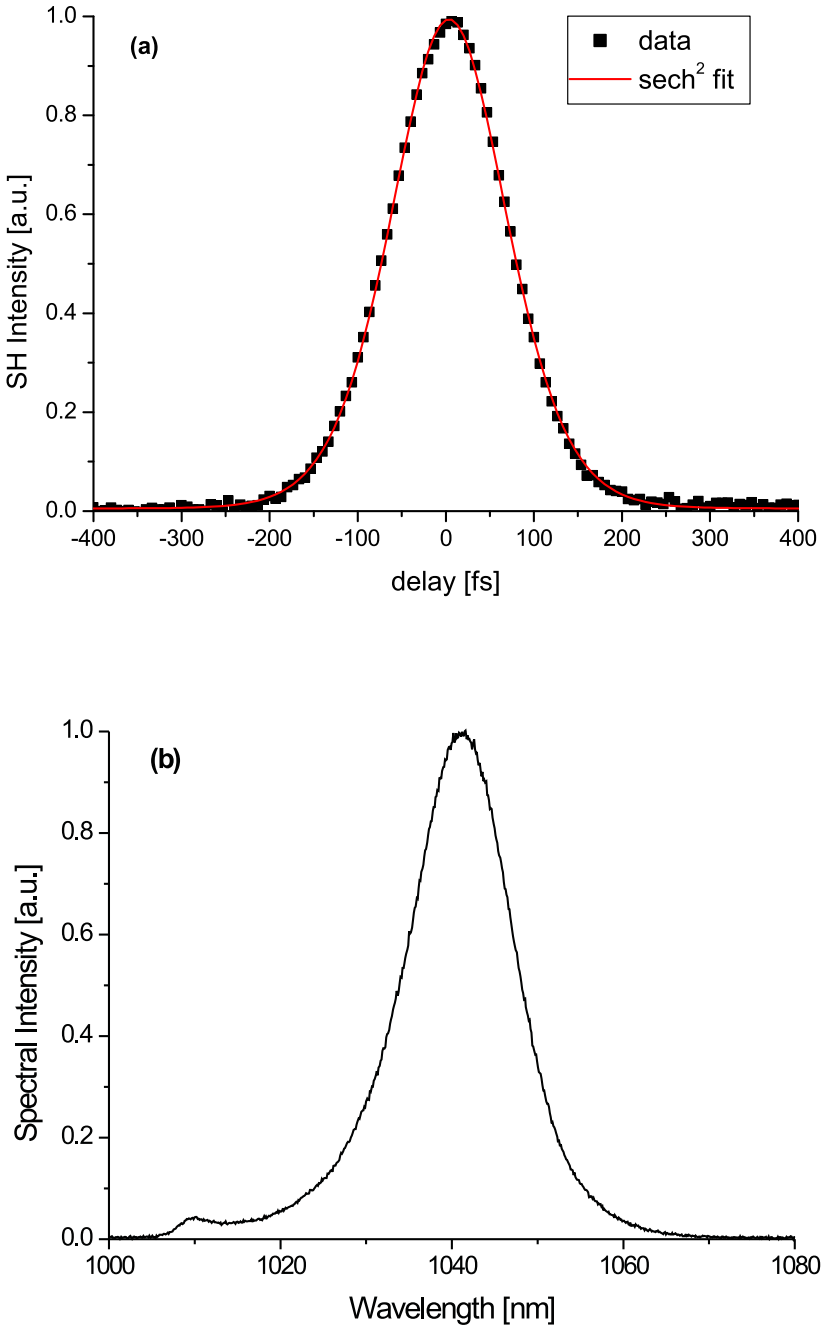

Figure 3.7: Yb:KYW mode-locked laser. (a) Measured intensity autocorrelation of 100-fs pulses and its fit for a $sech^2$ pulse shape. (b) Optical spectrum of the pulses.

Table 3.1: Comparison between Yb:KGW and Yb:KYW mode-locked lasers. The laser parameters are given for the shortest pulses and the highest output power respectively.

	τ_p [fs]	P_{output} [mW]	λ [nm]	$\tau_p \times \Delta\nu$	T_{OC}	Saturable absorption
Yb:KGW	**100**	126	1037.4	0.373	2%	2%
	218	**430**	1035	0.342	3%	0.9%
Yb:KYW	**106.5**	92	1039	0.380	2%	2%
	247	**289**	1032.2	0.343	4%	0.9%

3.3.2 Influence of GVD on the laser parameters

As reported previously [10, 33, 34, 91], the pulse shortening in soliton mode-locking is limited by the onset of multiple pulsing. The pulse becomes shorter decreasing the negative GVD, i.e. increasing the prism insertion, until it breaks in two longer pulses. In the single pulsing regime, the simplest relation between the pulse duration and the intracavity GVD is obtained from the solution of the non-linear Schrödinger equation [16]:

$$\tau_p = 1.763 \times \frac{2|D|}{|\gamma_{SPM}|E_p} \tag{3.1}$$

where D is the GVD per cavity round-trip, γ_{SPM} is the self phase modulation (SPM) coefficient and E_p is the intracavity pulse energy. The equation 3.1 does not express the influence of the modulation depth and the non-saturable losses on the pulse parameters. In our laser cavity, the pulse experiences positive SPM in the amplifying medium and negative SPM in the saturable absorber mirror, due to the negative nonlinear refractive index of the semiconductor. Using the field distribution A(z) of the standing wave along the semiconductor structure, we estimated the product $\gamma_{SPM}Ep$ for the SESAM to be less than 0.5% from those of the crystal, so we can

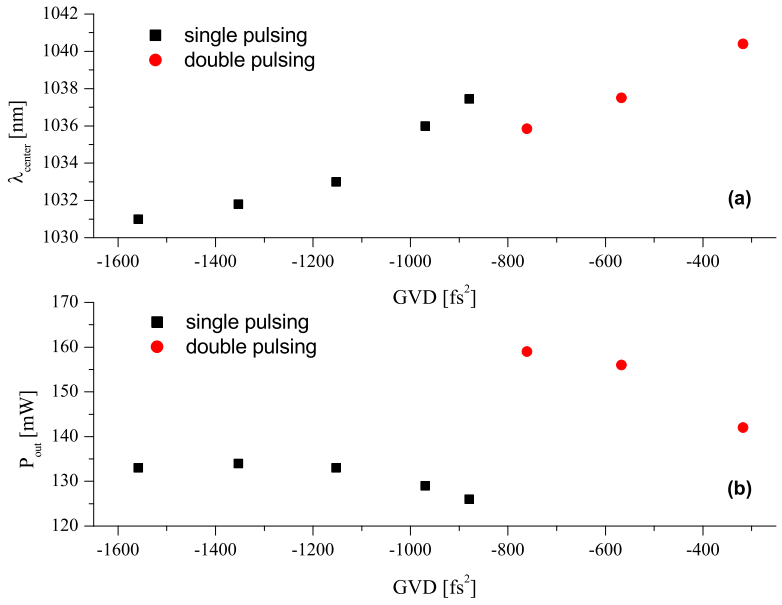

Figure 3.8: Variation with the negative GVD of the center wavelength (a) and output power (b).

neglect it further. The SPM coefficient for the crystal is given by:

$$\gamma_{SPM} = \frac{2\pi}{\lambda} n_2 \frac{d}{\pi w^2/2} = \frac{4 n_2 d}{\lambda w^2} \tag{3.2}$$

where d is the thickness of the medium for a round trip, n_2 the nonlinear refractive index, λ and w are the wavelength and the radius of the Gaussian beam which propagates through the medium. The variation of the GVD induces a wavelength shift and a change of the output power as it is shown in figure 3.8.

Because not any efforts were undertaken in order to maintain constant wavelength and output power, we can not consider a linear relation between the pulse duration and the GVD. Figure 3.9a shows the measured pulse duration as a function of the group velocity dispersion in single pulsing and double pulsing regime. The hollow squares show the theoretical values calculated using the equations 3.1 and 3.2 and the experimental values shown in figure 3.8. For the calculation of the intracavity

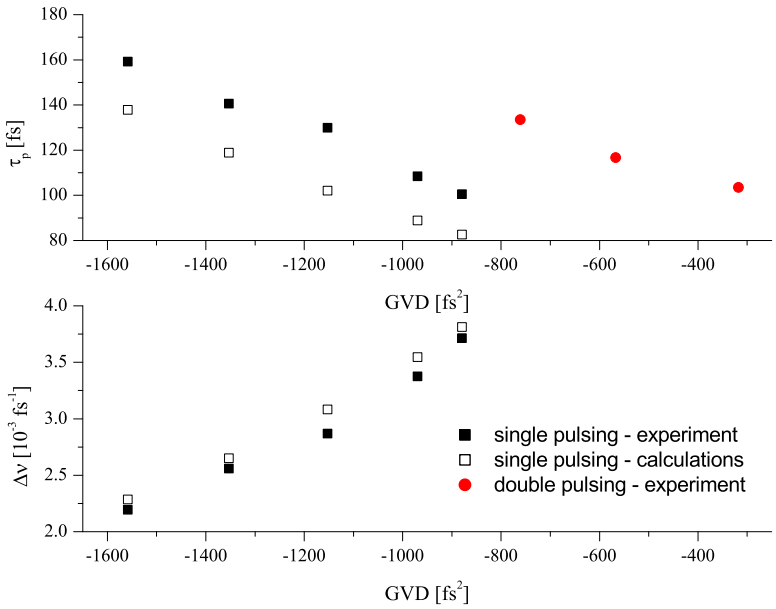

Figure 3.9: Variation with the negative GVD of the pulse duration assuming a $sech^2$ pulse shape (a) and spectral bandwidth (b).

GVD, we considered the negative contribution of the prism refraction and the positive GVD of the prism glass, mirrors and laser crystal. To calculate the contribution of the crystal, we used the Sellmeier coefficients given in [75]. The parameters for the mirrors were supplied by the mirror vendor (Layertec GmbH). The nonlinear refractive index of the Yb:KGW was taken from [76] as $21 \times 10^{-16} cm^2/W$. Figure 3.9b shows the measured values of the spectral bandwidth (full squares) and the theoretical ones (hollow squares), calculated with formula 3.1 and assuming $sech^2$-shaped pulses.

3.3.3 Multiple pulsing regime

In the double pulsing regime, the separation between pulses was less than 1 ps, which requires autocorrelation measurements on a longer time scale. Figure 3.10 shows the interferometric autocorrelation trace (a) and the corresponding optical spectrum (b). We measured a pulse spacing of 917.5 fs, which remains constant once the multiple pulsing regim is started. The ratio between the pulse separation and the pulse width

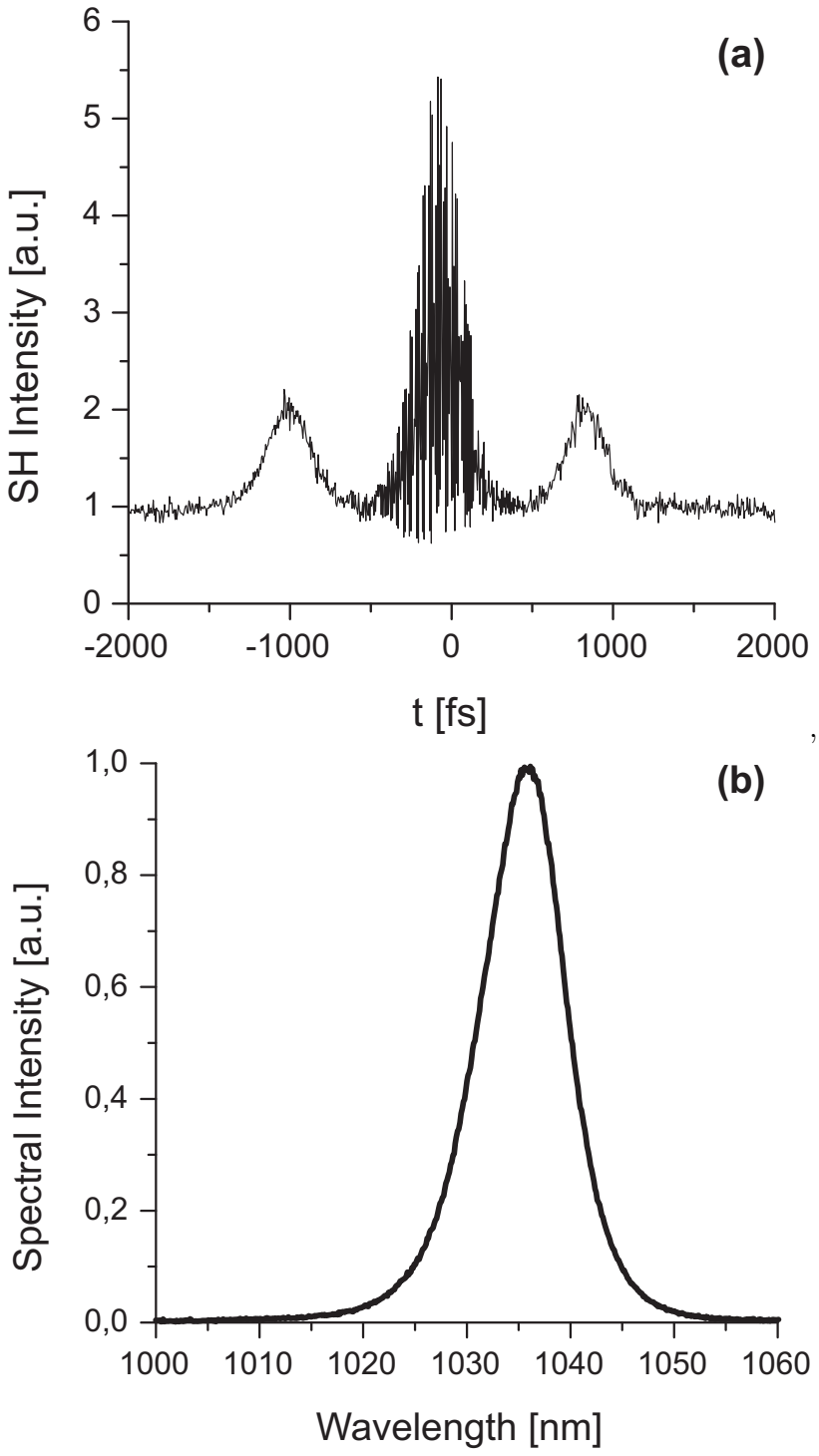

Figure 3.10: Interferometric autocorrelation on a 4 ps time range (a) and the corresponding optical spectrum (b).

was in the range 6.7 - 9. As the two lateral peaks in figure 3.10a corresponding to the overlap in time of consecutive pulses do not show interferometric structure, we can conclude that the phases of the two solitons are independent. The generation of soliton pairs with rotating phase difference in lasers passively mode locked with slow saturable absorbers was predicted in a stability analysis of the complex Ginzburg-Landau equation [35,44] and experimentally observed in a Ti:sapphire laser. [35] The rotating phase difference is confirmed also by the absence of fringes which appear in phase-locked soliton pairs spectra. Increasing further the prism insertion, more than two pulses could be observed delayed up to half cavity round-trip time. In this regime, the oscillator was stable only for a few seconds.

3.3.4 Influence of saturable absorber parameters on the mode-locking performance

We compared the mode-locking performances of three SESAMs with different parameters (table 2.6). The experiments were performed using the setup described in 3.1.2 and the Yb:KYW crystal as laser medium. For each SESAM, we tried to achieve the shortest pulse duration by using output couplers with different transmissions and by changing the pump power. "The shortest pulse duration" denotes the minimum pulse length obtained by decreasing the negative GVD, at which the pulse is still stable against the splitting in two pulses (figure 3.9a).

According to equation 1.29, the SESAM parameter that strongly influences the pulse duration is the modulation depth. Therefore our attempt was to test SESAMs with different values of this parameter, as listed in table 2.6. The shortest pulse durations obtained with different output coupler transmissions are plotted in figure 3.11 as a function of the modulation depth.

The technique used to increase the modulation depth (saturable losses) was to change the relative field distribution across the mirror structure. This induces also an increase in the nonsaturable losses, and therefore the laser output power will decrease for SESAMs with higher modulation depth. This can be noticed in figure 3.12 which

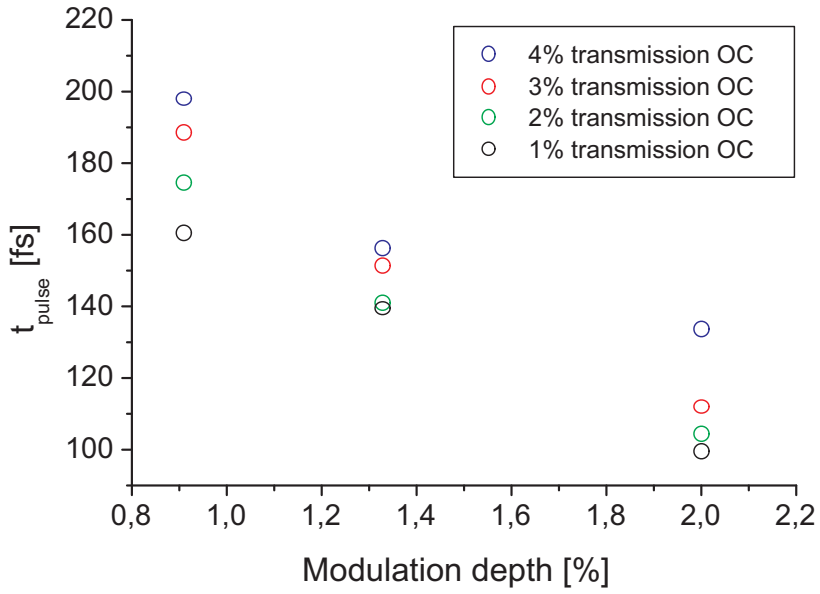

Figure 3.11: The shortest pulse duration plotted as a function of the SESAM modulation depth.

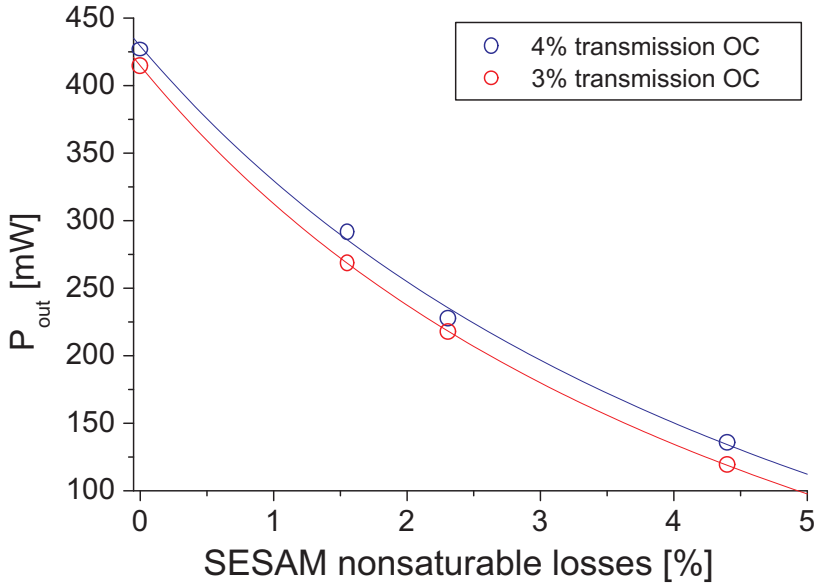

Figure 3.12: Laser output power plotted as a function of the SESAMs nonsaturable losses. The solid lines show the theoretical curves described by the equation 3.3. For both output coupler transmissions, the fit delivers almost the same parameters: $L_{res} \approx 2.5\%$, $g_0 \times l \approx 0.073$ and $A \times I_S \approx 17000\,mW$.

shows the dependence of the output power on the measured nonsaturable losses introduced by the SESAMs. The values corresponding to zero losses were measured by replacing the SESAM with a high reflective mirror. The solid lines show the theoretical curves for laser output according to equation 3.56 from [92]:

$$P_{out} = A(\frac{1-R}{1+R})I_s(\frac{2g_0 l}{L - lnR} - 1). \tag{3.3}$$

In this equation, A and l are the cross-section and the length of the amplifying medium, respectively, I_S is a materials parameter, and R is the reflectivity of the output coupler. g_0 denotes the unsaturated gain coefficient and L the resonator losses. For our laser, L is given by $L = A_{lin,SESAM} + L_{res}$, where $A_{lin,SESAM}$ are the SESAM nonsaturable losses (linear absorption) and L_{res} are the losses introduced by other intracavity elements such as mirrors, prisms etc.

It can be noticed that the data are very well fitted with the equation 3.3. For both output coupler transmissions, the fit delivers almost the same parameters: $L_{res} \approx 2.5\%$, $g_0 \times l \approx 0.073$ and $A \times I_S \approx 17000\,mW$. Thus we can conclude that the laser output power in mode-locking regime is mainly determined by the nonsaturable losses of the SESAM.

An other dependence which can be observed is illustrated in figure 3.13. For all three SESAMs, the pulse length decreases at longer center wavelength. This is due to the fact that the Yb-based lasers show a broader gain spectrum at longer center wavelength (see subsection 2.2.1).

3.3.5 Experimental observations of the output coupler influence onto the pulse duration

It was shown in [47] that for Yb based mode-locked lasers, the achievable pulse duration increases with the excitation level (see subsection 2.2.1). This is determined by the total cavity losses, including the output coupler transmission. Therefore we would expect to achieve shorter pulses by using output couplers with lower transmissions.

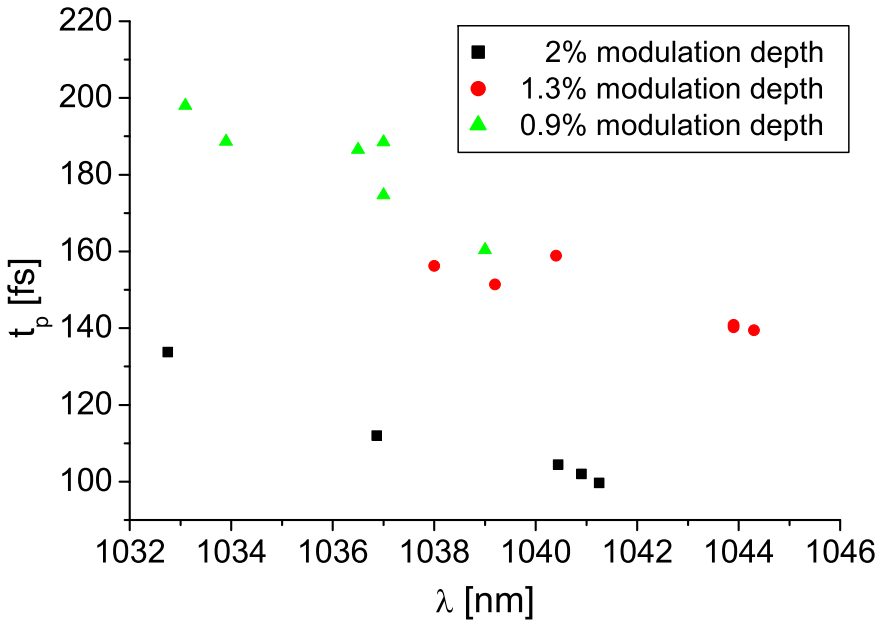

Figure 3.13: Pulse duration plotted as a function of the center wavelength.

Our experimental observations are illustrated in figures 3.14, 3.15, 3.16 for SESAMs 1, 2 and 3 respectively. The shortest pulse length achieved and the corresponding output power are plotted as a function of the output coupler transmission T_{OC}. For T_{OC} higher than 2%, the shortest achievable pulse length decreases with T_{OC}. Decreasing T_{OC} below 2% and maintaining the same pump power, the pulse length remains the same (samples 1 and 3) or even begins to increase (sample 2). However, it can be shortened if the pump power is reduced. The hollow symbols show the pulse length after decreasing the pump power. This behavior could be explained by the increased intracavity power at low output coupler transmissions and consequently the higher fluence incident on the saturable absorber. Under stronger saturation, the pulse breakup occurs at longer pulse durations [24].

Nevertheless, this experimental measurements can not be compared with the theoretical predictions from [24]. The shortest pulse duration before the onset of multiple pulsing was estimated to be a function of the modulation depth, the fluence incident on the saturable absorber and the linear intracavity losses including the output cou-

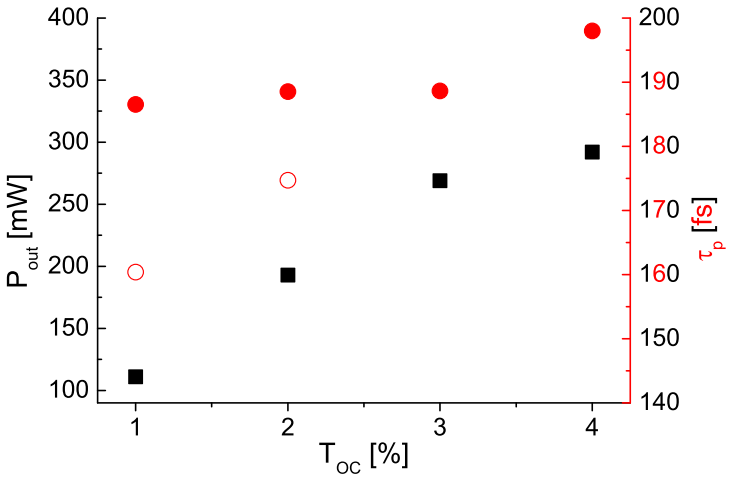

Figure 3.14: Pulse duration (red points) and output power (black points) plotted as a function of the output coupler transmission. The hollow symbols show the pulse duration after decreasing the pump power. The laser was mode locked using the SESAM 1.

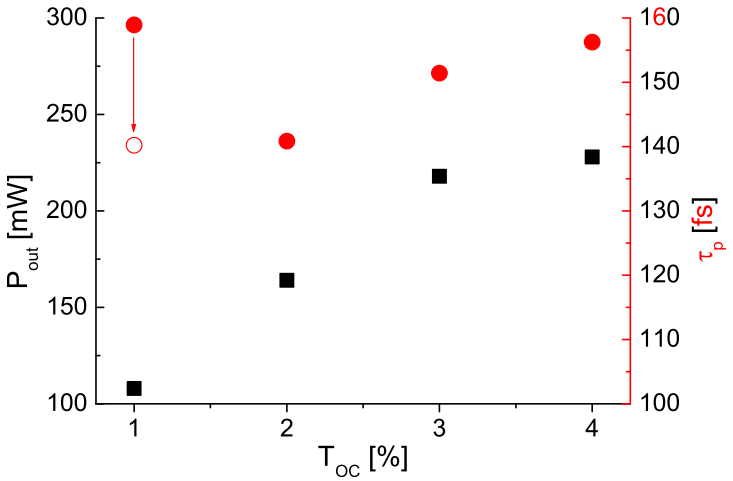

Figure 3.15: Pulse duration (red points) and output power (black points) plotted as a function of the output coupler transmission. The hollow symbols show the pulse duration after decreasing the pump power. The laser was mode locked using the SESAM 2.

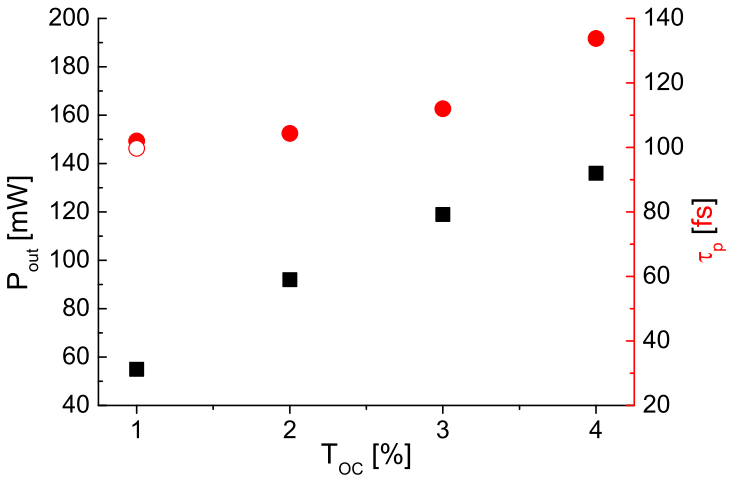

Figure 3.16: Pulse duration (red points) and output power (black points) plotted as a function of the output coupler transmission. The holow symbols show the pulse duration after decreasing the pump power. The laser was mode locked using the SESAM 3.

pler transmission (see equation 1.29). An experimental verification would suppose the variation of one parameter, while the other two are keeping constant. This is not the case for this experiments because the change of the output coupler transmission induces the change of the incident fluence. To keep it constant, supplementary measures should be taken.

However, the described experimental observations could be very useful to adjust the laser to work at the parameters needed for a specific application.

Chapter 4

Optical Characterization of the Saturable Absorber Mirrors

It was shown in chapter 1 that the laser dynamic and the mode-locking performance are determined by a number of parameters of the saturable absorber, such as modulation depth, saturation fluence, recovery time and nonsaturable losses. The semiconductor structure design and the growth technology allow a wide range of these parameters, therefore they need to be measured with high accuracy and under the operation conditions.

The modulation depth, saturation fluence and nonsaturable losses can be obtained from nonlinear reflectivity measurements [93]. To determine the dynamic response of the saturable absorber, one should perform pump-probe experiments, in which the mirror reflectivity is measured as a function of the delay time between the pump and probe pulses.

This kind of measurement becomes challenging for saturable absorber mirrors with a low modulation depth or a high saturation fluence, due to the requirements on high power and detection sensitivity.

For laser media with small signal gain, as is the case for Yb-doped materials, the laser shows the highest efficiency for low output coupler transmissions, of the order of a few percent. The intracavity pulse energy is 20 - 100 times higher than the delivered pulse energy. For this reason, it is difficult to arrange a pump-probe experiment that

fits the intracavity conditions in terms of pulse length, center wavelength and energy fluence onto the saturable absorber.

We performed two types of experiments to characterize the saturable absorbers. The first attempt was to arrange a collinear cross-polarizations pump-probe setup in which the fluence on the saturable absorber can be adjusted in the same range like the intracavity fluence, but the pulse length is about 8 ps, while the pulses generated from our lasers are in the range 100 - 400 fs.

Another experimental method we developed was to characterize the saturable absorber *in situ*, in an operating mode-locked laser. This is a new technique we demonstrated and reported in [94]. The experiments were performed using a Yb:KGW laser, which allows the generation of a stable pulse train without Q-switching modulations. *In situ* characterization of semiconductor saturable absorbers yields the absorber parameters, in particular the modulation depth and the dynamic response, under the exact laser operation conditions, which is not necessarily achieved by other methods. The technique may also be an alternative to the classical pump-probe measurements in situations where the intracavity parameters such as incident energy fluence, pulse length and center wavelength are difficult to reproduce simultaneously with available lasers.

This experiments will be described in the following subsections.

4.1 Pump probe experiments using a pulsed laser in picosecond regime

The measurements were performed with a $Nd:YVO_4$ laser from HighQ [95], delivering an output power of 4 W at 1064 nm. It is a passive mode-locked laser, without GVD compensation, generating 8-ps pulses with a repetition rate of 84 MHz.

We used a collinear cross-polarizations pump-probe technique. The experimental setup is shown in figure 4.1. The beam-splitter BS divides the laser radiation in two beams, which are further s and p polarized using two polarizing cubes. The

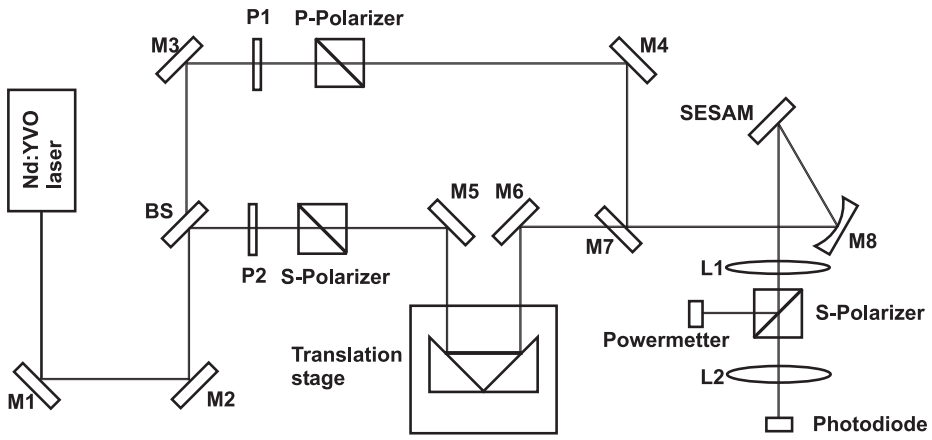

Figure 4.1: Experimental setup for pump-probe measurements. M1 - M7, plane mirrors; M8, curved mirror with 50 mm radius of curvature; SESAM, saturable absorber mirror; BS, beam-splitter; L1 - L2, lenses; P1 - P2 , half wavelength plates used to adjust beams intensity.

lambda-half plates P1 and P2 were used to set the intensities of the two beams. A corner mirror placed on a motorized translation stage formes an optical delay line. The mirrors M1-4 are high reflective for both polarizations at 45° incidence angle. The pump and probe beams are overlapped on the mirror M7 and focused onto the SESAM with the 50-mm-curvature mirror M8.

The spot radius on the SESAM was measured using the knife-edge method and estimated to about 15 μm in the focal plane. Nevertheless, due to the strong focalization, a very small displacement from the focal plane determines a strong variation of the spot size and consequently of the fluence onto the SESAM. The incidence angle was 5° and taking into account the high reflective index of the GaAs, we can consider the same direction through the semiconductor like in the normal incidence case. The reflected pump and probe beams are separated with a polarizer. The probe beam is focused onto a photodiode with the lens L2, while the pump beam is used to check the stability of the laser power. The lens L1 was used to collimate the reflected beams. The signal from the photodiode is directed to a lock-in amplifier. As only the pump beam was modulated, the signal from the amplifier will be proportional to the pump-induced change of the reflected probe beam intensity.

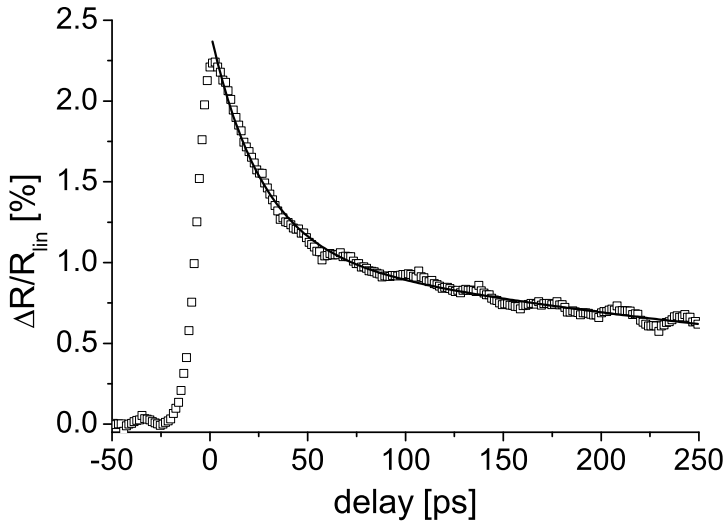

Figure 4.2: Differential reflectivity measurement at a pump fluence of 193 $\mu J/cm^2$. $\Delta R/R_{lin} = (R - R_{lin})/R_{lin}$ is plotted as a function of the delay between pump and probe pulses. R, R_{lin} - reflectivity with and without pump pulse, respectively. The solid line shows the double exponential fit, with a fast time constant of 25 ps and a slow time constant of 450 ps.

Using the experimental setup described so far, we tried to measure different saturable absorber mirrors. We measured modulation depths in the range 2 - 5 % and recovery times higher than 10 ps. An example can be seen in the figures 4.2 (pump-probe trace) and 4.3 (saturation curve) for a saturable absorber with a modulation depth of 2.5% and a saturation fluence of 94 $\mu J/cm^2$. The pump-probe trace in figure 4.2 was recorded at a pump fluence of 572 $\mu J/cm^2$. It can be observed a bitemporal impulse response of the saturable absorber, with a fast time constant of 25 ps and a slow time constant of about 450 ps. The SESAM has a linear absorption of 4.4 % and a low fluence reflectivity R_{lin} of 93.06 % (figure 4.3).

Such devices with high modulation depth can not be used to mode-locked Yb-based lasers. The setup was not suitable to characterize SESAMs used successfully for mode-locking experiments. Any pump-probe trace could not be recorded for this samples. One reason is that some of this SESAMs have a subpicosecond fast time

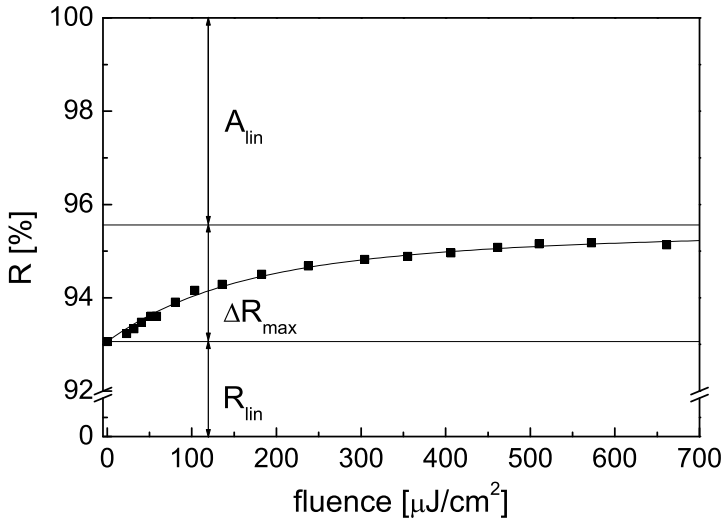

Figure 4.3: Nonlinear reflectivity plotted as a function of the energy fluence on the saturable absorber. The solid line shows the theoretical curve assuming a modulation depth ΔR_{max} of 2.5% and a saturation fluence of 94 $\mu J/cm^2$. The linear absorption $A_{lin} = 4.4$ % and the low fluence reflectivity $R_{lin} = 93.06$ %

constant, as it will be shown in the next subsection. Using much longer pulses, the modulation depth can decrease below the detection sensitivity threshold or the noise level.

4.2 *In situ* characterization of saturable absorber mirrors in an operating mode-locked laser

The problems referred so far can be overcome by measuring the SESAMs parameters *in situ* in the operating mode-locked laser. It was developed a new technique for SESAMs characterization that yields their parameters under the exact operation conditions.

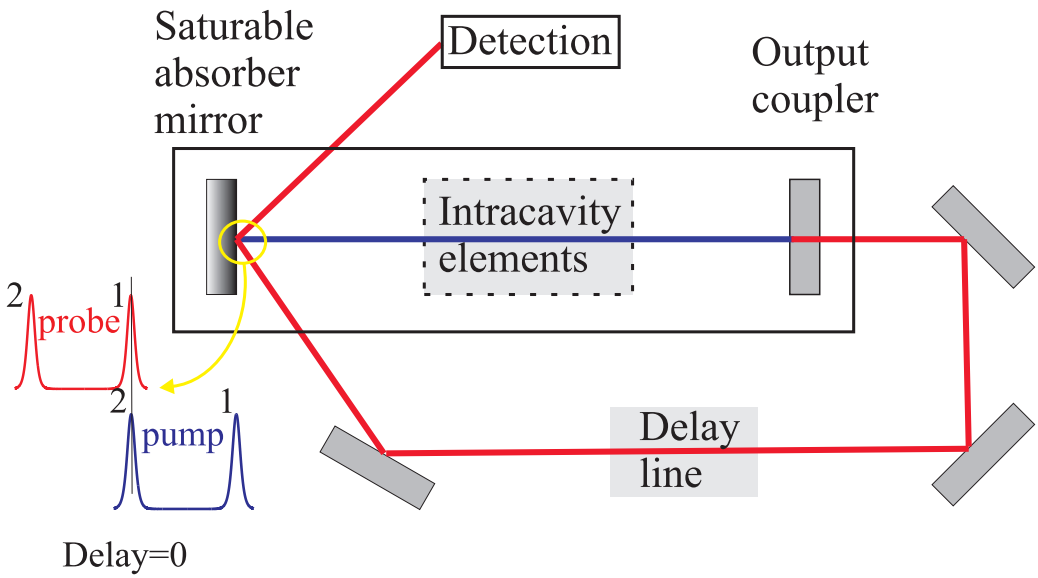

Figure 4.4: The schematic of the *in situ* SESAMs characterization technique.

4.2.1 Principle of the method

The principle of this new method is illustrated in figure 4.4. The saturable absorber mirror and the output coupler are arranged as end mirrors in the resonator. The technique can be described as a pump-probe experiment in which the intracavity beam acts as a pump beam, while the output beam of the laser is used to monitor the change in SESAM reflectivity. The optical path at zero delay is arranged such that the probe pulse overlaps in time with the subsequent intracavity pulse. Using the significant intracavity power of a CW-mode-locked laser oscillator opens the way for time resolved saturation measurements in cases where amplified pulses would be needed. With this *in situ* technique high average power comes for free.

4.2.2 Experimental setup

The layout of the laser resonator is shown in figure 4.5a and the following experimental arrangement for SESAM characterization is displayed in figure 4.5b.

The laser setup is the same like described in section 3.1.2.

The laser generates a very stable pulse train, without Q-switching modulations. This was verified by observing the temporal development of the pulse amplitude (figure

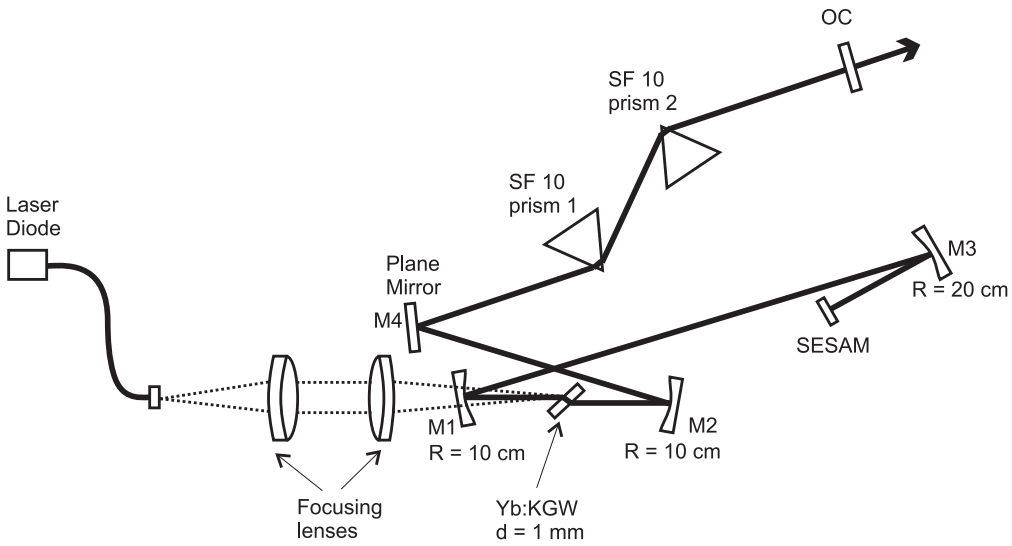

(a)

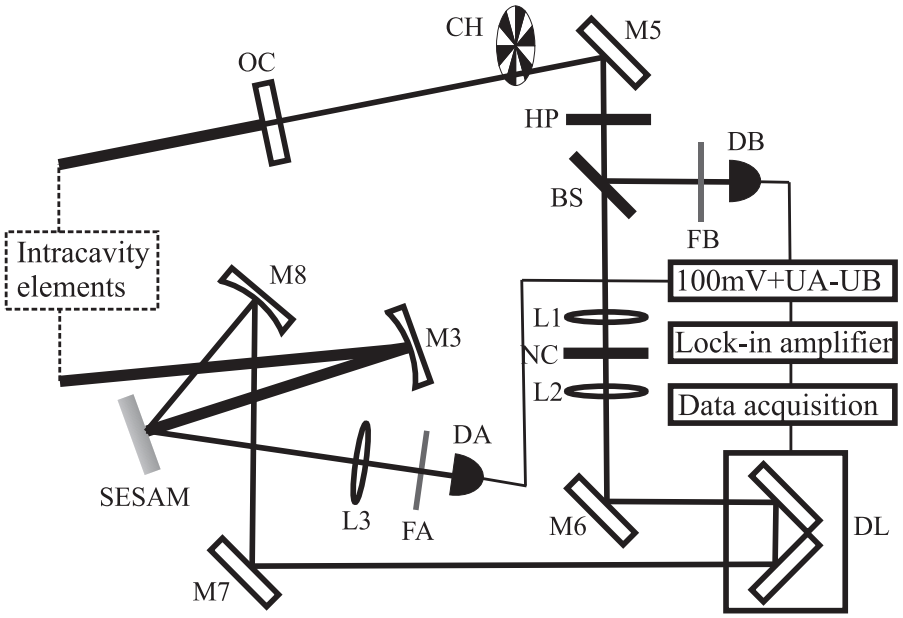

(b)

Figure 4.5: (a) Yb:KGW laser cavity and (b) experimental setup for *in situ* characterization of the saturable absorber. M1 - M3, curved mirrors; R, radius of curvature; M4, high-reflective plane mirror; OC, output coupler; SESAM, saturable absorber mirror; M5 - M7, plane mirrors; M8 - curved mirror; CH, chopper; BS, beam-splitter; L1 - L3, lenses; NC, nonlinear crystal for SH generation; HP, half wavelength plate used to adjust the SH intensity; DL, delay line; DA, DB - photodiodes; FA, FB - neutral density filters.

4.6) as well as the frequency spectrum which shows only the cavity frequency, without any sidebands (figure 4.7). A pulse amplitude constant in time is extremely important for high accuracy measurements.

The output laser beam is used further to monitor the intracavity beam-induced change in SESAM reflectivity, as it is shown in figure 4.5b. Pump and probe pulses are delayed with respect to each other using the optical delay line DL. The probe beam is focused onto the active area of the saturable absorber by the curved mirror M8, which has a 50-mm radius of curvature. The angle between the pump and probe beams is 30°.

Because the sample to be investigated is a component of the laser, there are some experimental particularities concerning the spatial overlap and the detection system. The laser output coupler has a transmission of 2% or 3%. This results in a contrast between the probe and pump beam that is smaller than 3:100, which can not be increased due to the geometrical limitations of the resonator. In this condition, the spatial overlap of the two beams is difficult to arrange. In our experiments, the intracavity peak power was high enough to generate a weak - but visible - second harmonic (SH) signal in the semiconductor structure. We used the 200-μm-thick nonlinear crystal NC to generate an SH beam that propagates on the same path as the probe beam. The intensities of this SH signals are similar, and their spatial overlap can be achieved much more easily.

In most pump-probe experiments, where small probe signal variations are measured, a chopper is positioned in the pump beam path so that the pump-induced changes in the reflected probe beam can be measured differentially with a lock-in amplifier. This is not possible in our experimental configuration, because the modulation of the intracavity beam would provoke the breakdown of the mode-locking regime. We modulated the probe beam with chopper CH and we used two photodiodes, DA and DB, and an analog device that amplifies the difference between the two signals. The reflected probe beam is directed to the detector DA and a reference beam taken from beam-splitter BS is sent on to detector DB. With a proper choice of transmission of the filter, the signal sent to the lock-in amplifier may be adjusted to a level similar to that of the measured signal.

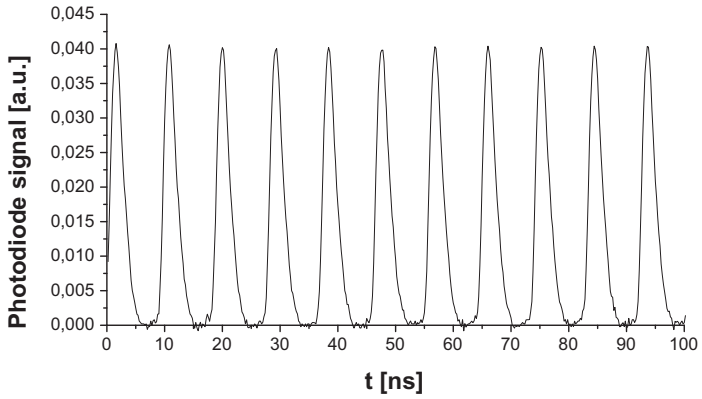

Figure 4.6: The pulse train recorded with a sampling oscilloscope and a photodiode.

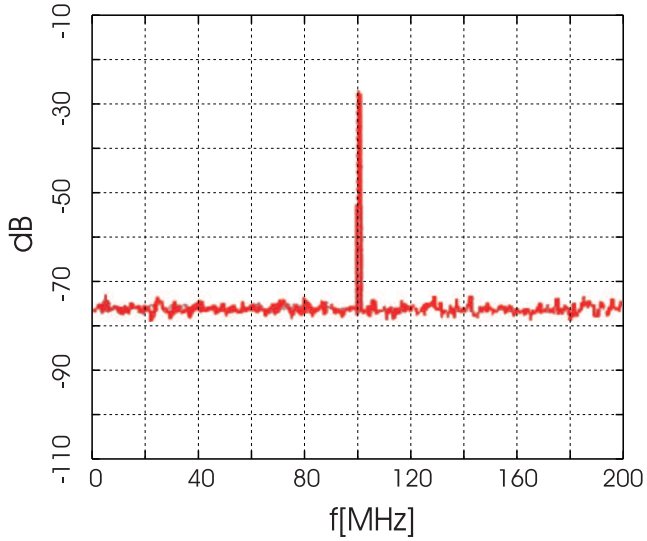

Figure 4.7: The frequency spectrum recorded with a frequency spectrum analyzer and a photodiode. The central frequency is 108 MHz.

Using the experimental setup described above, we measured the dynamic response of the saturable absorber at different values of the pump fluence. The delay-dependent differential reflectivity $\Delta R(t)/R_{lin} = (R(t) - R_{lin})/R_{lin}$ is given by the signal $[(S_{DA} - S_{DB})(t) - (S_{DA} - S_{DB})(-\infty)]/S_{DA}(-\infty)$, where S_{DA} and S_{DB} are the signals of photodiodes DA and DB respectively. R(t) denotes the SESAM reflectivity at a time delay t between the pump and probe pulses and R_{lin} is the reflectivity at low fluence.

4.2.3 Measurement of the laser spot size onto the SESAM

For a good estimation of the incident fluence, one needs to know precisely the laser spot radius onto the SESAM. This was measured using the following experimental method: The SESAM was replaced with a plane dielectric mirror which has a transmission of 1%. The laser will operate in a CW regime. The transmitted beam is a divergent gaussian beam with the waist at the reflecting surface. This is a required condition for the resonator stability. Using the knife-edge method, the beam radius was measured at different distances z from the mirror surface (see figure 4.8). The data are plotted in figure 4.9 as a function of the optical path which is given by $z_{opt} = z + d_{glass}(n_{glass} - 1)$. d_{glass} and n_{glass} are the thickness and the refractive index of the mirror glass substrate. The solid line shows the fit using the formula:

$$\omega(z) = \omega_0 \sqrt{1 + (\frac{\lambda M^2 z}{n\pi\omega_0})^2} \tag{4.1}$$

where ω_0 is the beam waist, $\omega(z)$ the beam radius at distance z from the focal plane, λ the pump wavelength, n the refractive index of the medium and M^2 the quality factor of the beam.

Using this method, the radius of the laser beam onto the SESAM was estimated to 82 μm.

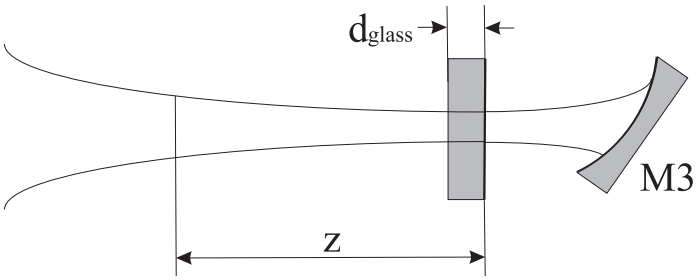

Figure 4.8: Schematic of the spot size measurement.

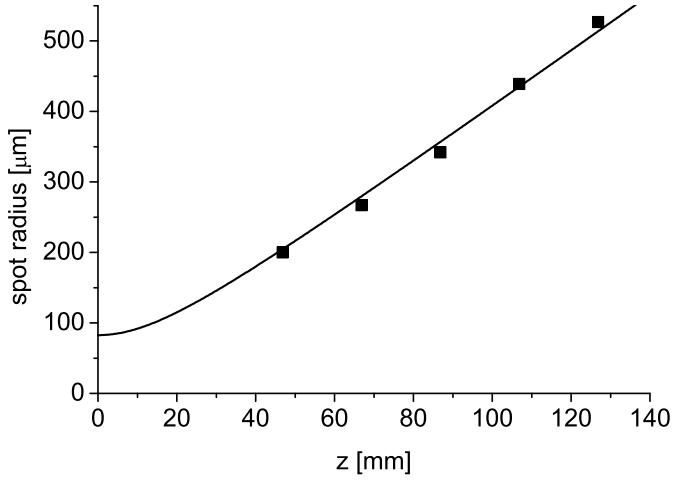

Figure 4.9: The measured beam radius plotted as a function of the distance to the SESAM. The solid line shows the fit with the equation 4.1 assuming a spot radius of 82 μm at the SESAM position.

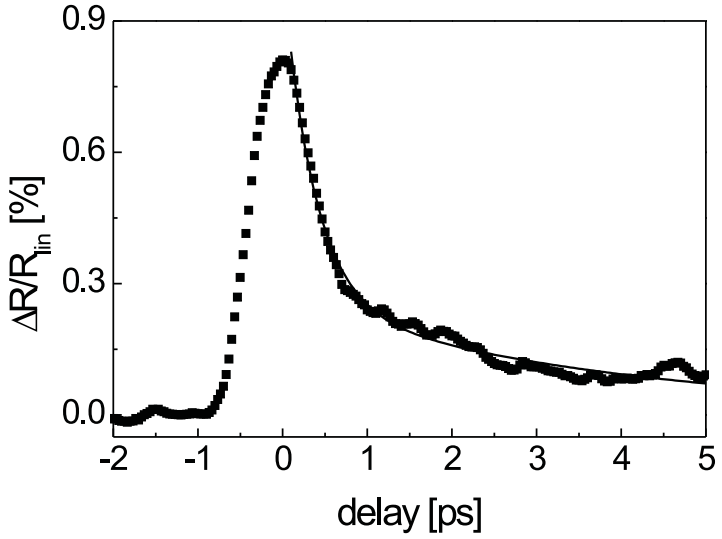

Figure 4.10: Differential reflectivity measurement at a pump fluence of $126\ \mu J/cm^2$. $\Delta R/R_{lin} = (R - R_{lin})/R_{lin}$ is plotted as a function of the delay between pump and probe pulses. R, R_{lin} - reflectivity with and without pump pulse, respectively. The solid line shows the double exponential fit, with a fast time constant of 370 fs and a slow time constant of 3.9 ps.

4.2.4 Experimental results

Sample 1.

The experiments were performed with 296 fs pulses at a center wavelength of 1031 nm. The intracavity pulse energy was modified by changing the pump power. To keep the pulse length and center wavelength fixed we adjusted the intracavity GVD by modifying the prism insertion. Figure 4.10 shows the pump-probe differential reflectivity trace at a pump fluence of $126\ \mu J/cm^2$. The nonlinear response exhibits a bitemporal behavior, as reported many times for semiconductor saturable absorbers [26, 96, 97]. The fast component is usually attributed to spectral hole burning [26], while the slow one is attributed to carrier recombination and trapping [1]. The solid line depicts a double exponential fit with a fast time constant of about 370 fs and a slow time constant of about 3.9 ps.

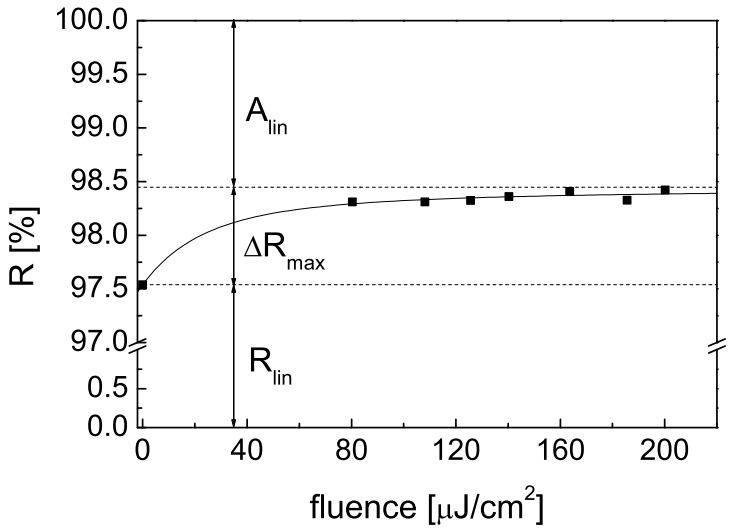

Figure 4.11: Nonlinear reflectivity plotted as a function of the energy fluence on the saturable absorber. The solid line shows the theoretical curve assuming a modulation depth of 0.91% and a saturation fluence of 14 $\mu J/cm^2$.

Figure 4.11 shows the SESAM reflectivity as a function of the incident energy fluence. The differential reflectivity at zero delay was extracted from the pump-probe measurements. R_{lin} was measured using the laser in CW operation and referenced to a high reflective dielectric mirror. At 1031 nm, $R_{lin} = 97.54 \pm 0.1\%$.
The data describe only part of the saturation curve because a stable mode-locking regime does not occur at small fluences on the saturable absorber. However, it can be noticed that the reflectivity remains almost constant with increasing pump fluence. This leads to an accurate determination of the effective modulation depth $\Delta R_{max} = 0.91 \pm 0.05\%$ and of the linear loss $A_{lin} = 1 - \Delta R_{max} - R_{lin} = 1.55 \pm 0.15\%$. The saturation fluence is estimated to 14 $\mu J/cm^2$.

Sample 2.

The measurements were performed with 220 fs pulses at a center wavelength of 1037 nm. The output coupler has a transmission of 2%. Unlike the other two samples, the pump-probe traces do not show a fast time constant. This can be observed in figure

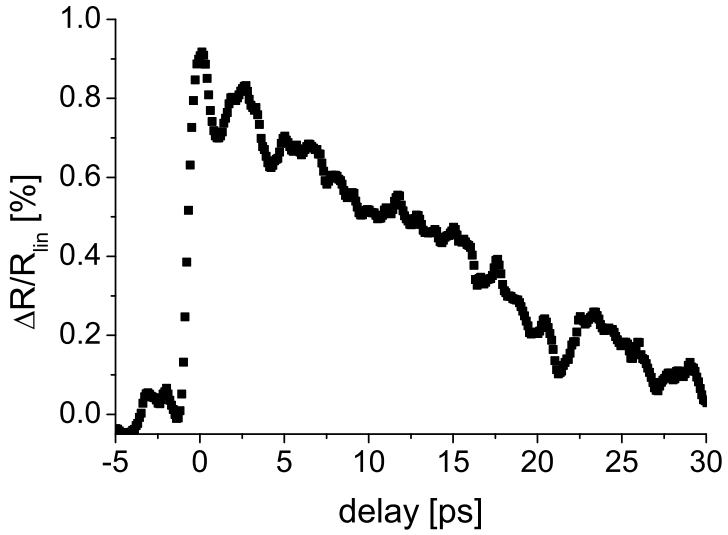

Figure 4.12: Differential reflectivity measurement at a pump fluence of 193 $\mu J/cm^2$. $\Delta R/R_{lin} = (R - R_{lin})/R_{lin}$ is plotted as a function of the delay between pump and probe pulses. R, R_{lin} - reflectivity with and without pump pulse, respectively.

4.12, where the differential reflectivity of the sample is plotted as a function of the delay time. The data can not be fitted with an exponential function. The recovery time is about 30 ps. A possible explanation is that the SESAM exhibits a fast time constant much shorter than the minimum pulse duration which can be achieved with this laser medium. Therefore, in this case, only the slow time constant is relevant for mode-locking. the generation of femtosecond pulses using a saturable absorber with a recovery time of 30 ps is due to soliton formation.

The SESAM reflectivity is plotted in figure 4.13 as a function of the incident energy fluence. The values were calculated in the same manner as described for sample 1. At 1037 nm, we measured the low fluence reflectivity $R_{lin} = 96.36 \pm 0.1\%$.

The solid line shows the theoretical curve assuming a modulation depth $\Delta R_{max} = 1.33 \pm 0.05\%$ and a saturation fluence of 59 $\mu J/cm^2$. The linear losses are $A_{lin} = 1 - \Delta R_{max} - R_{lin} = 2.31 \pm 0.15\%$.

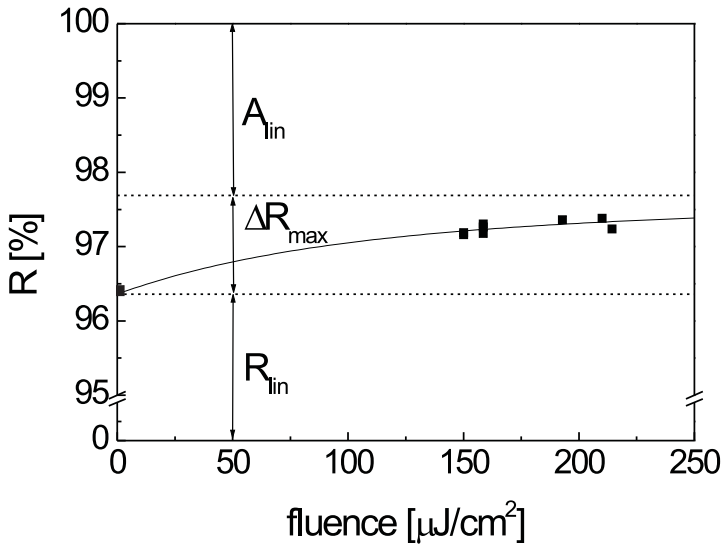

Figure 4.13: Nonlinear reflectivity plotted as a function of the energy fluence on the saturable absorber. The solid line shows the theoretical curve assuming a modulation depth of 1.33% and a saturation fluence of 59 $\mu J/cm^2$.

Sample 3.

With the same experimental method, we measured the dynamic response of the saturable absorber. The pulse length was about 175 fs and the center wavelength about 1033 nm. The intracavity pulse energy could be modified by changing the pump power. Figure 4.14 shows the pump-probe differential reflectivity traces for different values of the pump fluence. The nonlinear response exhibits an ultrafast time constant on the order of the pulse autocorrelation, that is usually attributed to spectral hole burning [26].

Figure 4.15 shows the maximum change of reflectivity $\Delta R/R_{lin}$ extracted from the pump-probe measurements as a function of the energy fluence onto the SESAM. The data describe only a segment of the saturation curve because a stable mode-locking regime could be achieved only for a restricted range of the energy fluence. However, it can be noticed that the reflectivity decreases almost linearly with increased pump fluence. This means the SESAM works at energy fluences situated on the so-called

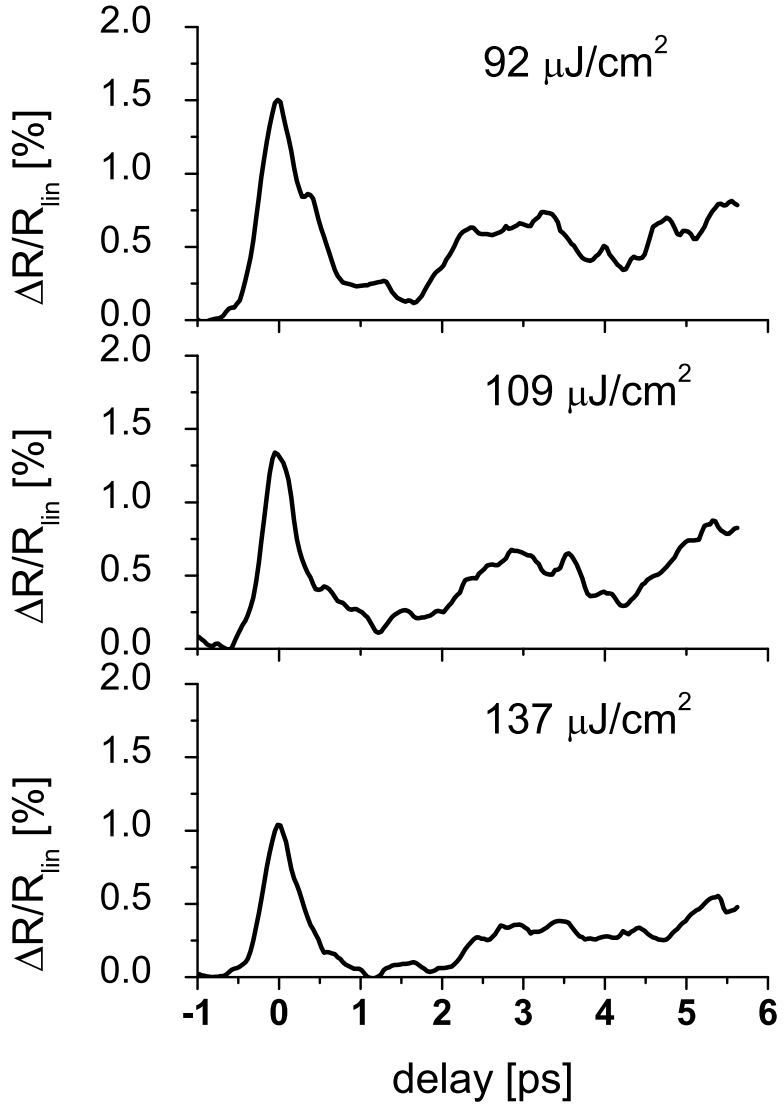

Figure 4.14: Differential reflectivity measurements for different values of the pump fluence. $\Delta R/R_{lin} = (R - R_{lin})/R_{lin}$ is plotted as a function of the delay between pump and probe pulses. R, R_{lin} - reflectivity with and without pump pulse, respectively.

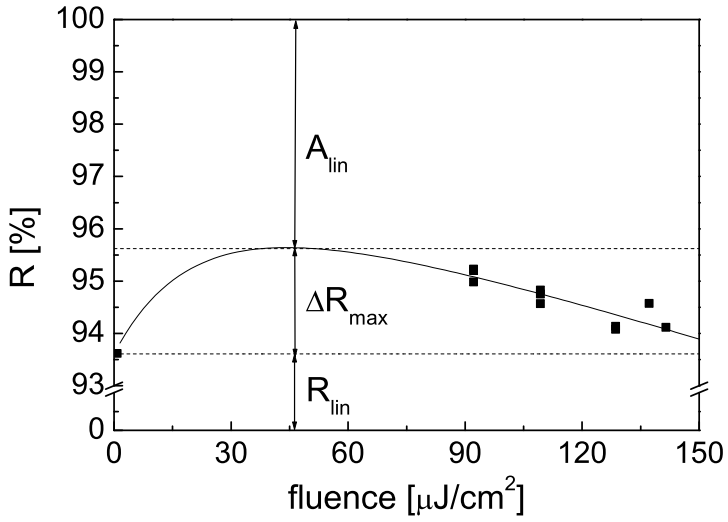

Figure 4.15: Nonlinear reflectivity plotted as a function of the energy fluence on the saturable absorber. The solid line shows the theoretical curve for SESAM reflectivity considering the two photon absorption process.

roll-over of the saturation curve [29,32], which is attributed to nonlinear non-saturable processes, such as two photon absorption [28]. The solid line shows the theoretical curve for SESAM reflectivity considering the two photon absorption process. The maximal change in reflectivity is $\Delta R_{max} = 2.01 \pm 0.4\%$. The incident fluence necessary to increase the reflectivity with 1/e from this value is 6 $\mu J/cm^2$.

The low fluence reflectivity at 1033 nm was measured $R_{lin} = 93.61 \pm 0.1\%$. The linear losses are $A_{lin} = 1 - \Delta R_{max} - R_{lin} = 4.39 \pm 0.5\%$.

Conclusions

This thesis treated the development of diode-pumped femtosecond lasers based on ytterbium-doped solid-state materials and the investigation of their dynamics. Specifically, a mode-locked laser suitable to seed the amplifier chain of the POLARIS system with ultrashort pulses was developed.

The first part of the work concentrates on the development of compact and stable laser oscillators with a pulse duration of about 100-fs and an energy higher than 1-nJ. Different Yb-doped materials were tested as gain medium. The first experiments were performed using Yb-doped fluoride-phosphate glass. Pulses as short as 95-fs have been achieved at a center wavelength of 1062 nm, which is about 25 nm longer than the targeted value. Therefore further experiments were done using two recently developed Yb-doped crystals, Yb:KGW and Yb:KYW, which are very promising for ultrashort pulse generation.

In the frame of this thesis, the generation of 100-fs pulses from a Yb:KGW mode-locked laser was demonstrated. This is the shortest pulse length reported so far for this material. The output power was 126 mW and the repetition rate 108 MHz, that corresponds to an energy per pulse of 1.17 nJ and to a peak power of 11.7 kW. The mode-locked laser was tuned in the spectral range 1031 - 1037.4 nm. Using the Yb:KYW crystal, similar results have been obtained. The achieved parameters show that the laser is suitable to seed the amplifiers of the POLARIS system.

Laser performances concerning the pulse duration and the output power strongly depend on the saturable absorber characteristics. In order to get the suitable values, SESAMs with different parameters have been tested. As expected from theoretical predictions, the pulse duration decreases by increasing the modulation depth. An-

other experimental observation is that the output power in mode-locking regime is mainly determined by the nonsaturable losses of the SESAM. The reason is that the SESAMs under test have nonsaturable losses of the same order like the modulation depth and output coupler transmission.

As reported previously for soliton mode-locking, the pulse shortening is limited by the onset of multiple pulsing. In the multiple pulsing regime, bound states of solitons with rotating phase difference were observed.

The second part of this work was dedicated to the optical characterization of the semiconductor saturable absorber mirrors. Their macroscopic parameters such as modulation depth, saturation fluence, recovery time and nonsaturable losses are decisive for the laser dynamic and the mode-locking performance. Therefore they need to be measured with high accuracy and under exactly operation conditions.

Classical methods i.e. nonlinear reflectivity measurements and pump-probe experiments, are not easy to perform for SESAMs used to mode-lock Yb-based lasers due to the requirements on high power densities and detection sensitivity.

A major result from the research performed for this thesis is the development of a new technique to characterize the SESAMs used for passive mode-locking. This novel technique can be described as a pump-probe experiment in which the intracavity beam acts as a pump beam, while the output beam of the laser is used to monitor the change in SESAM reflectivity. The optical path at zero delay is arranged such that the probe pulse overlaps in time with the subsequent intracavity pulse. The experiments were performed with a Yb:KGW laser, which allows the generation of a stable pulse train without Q-switching modulations.

It was demonstrated that *in situ* SESAM characterization is a reliable method in situations where the intracavity parameters such as incident energy fluence, pulse length and center wavelength are difficult to reproduce simultaneously without amplified femtosecond pulses.

In situ characterization of semiconductor saturable absorbers yields the absorber parameters, in particular the modulation depth and the dynamic response, under the exact laser operation conditions, which is not necessarily achieved by other methods.

Most of the SESAMs investigated using this method showed a bitemporal impulse response, with a fast time constant of few hundred femtoseconds and a slow time constant in the picosecond range. However, one of the samples under test exhibits only a relaxation time constant of about 30 ps, while the achieved pulse duration with the laser was about 200 fs due to the soliton formation.

It was also observed that the nonsaturable losses are considerably higher for SESAMs with increased modulation depths. Therefore the shortening of the pulses by increasing the modulation depth induces a significant drop in the output power.

The performance of the lasers could be improved further by using SESAMs that exhibit simultaneously a high modulation depth and low nonsaturable losses. If this can be achieved, shorter pulses will be generated with much higher output power.

Zusammenfassung

Diese Dissertation behandelt die Entwicklung von diodengepumpten Lasern auf der Basis von Ytterbium-dotierenden Materialen und die Untersuchung der Dynamik derartiger Laser. Es war das Ziel, einen modengekoppelten Laser zu entwickeln, der als Front-End für das POLARIS System verwendbar ist.

Der erste Teil dieser Arbeit wurde der Realisierung von kompakten und stabilen Laseroszillatoren mit einer Pulsdauer von etwa 100-fs und einer Pulsenergie größer als 1 nJ gewidmet.

Verschiedene Yb-dotierende Materialen wurden als Verstärkungsmedium getestet. Erste Experimente wurden mit Yb-dotiertem Fluorid-Phosphat-Glas durchgeführt. Bei einer Zentralwellenlänge von 1062 nm, die ungefähr 25 nm größer als der Zielwert ist, wurden Impulse von 95 fs Dauer erreicht. Um die Zentralwellenlänge entsprechend zu verringern, wurden weitere Experimente mit zwei neuerlich entwickelten Yb-dotierten Laserkristallen Yb:KGW und Yb:KYW, die sehr aussichtsreich für Kurzenpulserzeugung sind, durchgeführt.

So konnte im Rahmen dieser Dissertation die Erzeugung von 100-fs Pulsen in einem modengekoppelten Yb:KGW Laser gezeigt werden. Dies ist die kürzeste bis dahin berichtete Impulsdauer für dieses Material. Die Ausgangleistung des Lasers betrug 126 mW bei einer Repetitionsrate von 108 MHz. Dies entspricht einer Pulsenergie von 1.17 nJ und einer Spitzenleistung von 11.7 kW. Die Zentralwellenlänge des modengekoppelten Lasers konnte im Bereich von 1031 nm bis 1037.4 nm durchgestimmt werden. Ähnliche Ergebnisse wurden mit dem Yb:KYW Kristall erreicht. Die erhaltenen Parameter zeigen, dass der Laser als Impulsgenerator für das POLARIS-System geeignet ist.

Die Lasereigenschaften bezüglich der Impulsdauer und der Ausgangleistung sind stark von den Eigenschaften des sättigbaren Absorbers abhängig. Um optimale Werte zu erreichen, wurden SESAMs mit verschiedenen Parametern getestet. Übereinstimmend mit der Theorie ergaben die Experimente, dass die Pulsdauer mit der Erhöhung der Modulationstiefe kleiner wird. Eine andere experimentelle Beobachtung ist, dass die Ausgangleistung im Regime der Modenkopplung hauptsächlich von den nicht sättigbaren Verlusten des SESAMs bestimmt werden. Der Grund ist, dass die getesteten SESAMs nicht sättigbare Verluste in der gleichen Größenordnung wie die Modulationstiefe und die Transmission des Ausgangsspiegels haben.

Wie bereits früher für Soliton-Modenkopplung berichtet, ist die Pulsverkürzung durch die Entstehung von Mehrfachpulsen beschränkt. Im Mehrfachpulsensregime können gebundene Zustände von Solitonen mit variierender Phase beobachtet werden.

Der zweite Teil dieser Arbeit wurde der optischen Charakterisierung von sättigbaren Halbleiterabsorberspiegeln gewidmet. Ihre makroskopischen Parameter wie Modulationstiefe, Sättigungsenergiedichte, Relaxaktionszeit und der Betrag der nicht sättigbaren Verluste sind entscheidend für die Laserdynamik und die Modenkopplungseigenschaften. Deshalb müssen sie mit einer hohen Genauigkeit und unter genau den Betriebsbedingungen gemessen werden, wie sie im Laserresonator anzutreffen sind.

Die klassische Methoden wie die Bestimmung der nichtlinearen Reflektivität durch Pump-Probe Experimente sind in diesem Falle nicht adäquat durchzuführen, da beim Modenkoppeln von Lasern basierend auf Yb-dotierten Verstärkermaterialien hohe Leistungsdichten auftreten und eine hohe Nachweismpfindlichkeit benötigt wird.

Ein Hauptergebnis dieser Arbeit stellt die Entwicklung eines neuen Verfahrens zur Charakterisierung der SESAMs dar. Die SESAMs werden dabei im Laserresonator vermessen. Dieses neuartige Verfahren kann als Pump-Probe Experiment beschrieben werden, bei dem der Laserstrahl im Resonator als der Pumpenstrahl verwendet wird, während die Ausgangsimpulse des Lasers als Testimpulse fr die Messung der Reflektivität der SESAM benutzt werden.

Es wurde gezeigt, dass diese *in situ*-SESAM-Charakterisierung eine verlässliche Methode in Situationen ist, in denen die Parameter Pulsdauer, Energiedichte und Zen-

tralwellenlänge ohne verstärkte Femtosekundenpulse nicht gleichzeitig reproduziert werden können. Die *in situ*-Charakterisierung der sättigbaren Halbleiterabsorber gibt die Parameter Modulationstiefe und Relaxaktionszeitkonstante unter genau den Laserbetriebenbedingungen wieder, die mit anderen Methoden nicht erreicht werden können.

Die meisten SESAMs, die mit dieser Methode untersucht wurden, zeigten eine zeitliche Impulsantwort mit einer schnellen Zeitkonstante von einigen hundert Femtosekunden und einer langsamen Zeitkonstante im Pikosekundenbereich. Bei einer der getesteten Proben wurde nur eine langsame Zeitkonstante von 30 ps gemessen, wobei die im Laser erreichte Pulsdauer ungefähr 200 fs betrug. Dieses Verhalten ist der Solitonsausbildung zuzuschreiben.

Für SESAMs mit größerer Modulationstiefe wurden zudem deutlich größere nicht sättigbare Verluste beobachtet. Daraus folgt, dass bei der Erzeugung kürzerer Laserimpulse durch Erhöhung der Modulationstiefe eine geringere maximale Ausgangsleistung erreicht wird.

Die Ausgangsparameter des Lasers könnten durch SESAMs mit größerer Modulationstiefe und gleichzeitig geringerer nicht sättigbarer Verluste optimiert werden, das bedeutet kürzere Impulse können bei gleichzeitig höherer Ausgangsleistung erzeugt werden.

Bibliography

[1] U. Keller, "Recent developments in compact ultrafast lasers", Invited Paper, Nature, vol. 424, 831-838, 2003.

[2] W. Sibbett, W. h. Knox, "Applications of ultrashort pulse lasers," in *Advances in lasers and applications*, edited by D. M. Finlayson and B. D. Sinclair, printed by J. W. Arrowsmith Bristol, 1998.

[3] A. H. Zwail, "Femtochemistry: atomic-scale dynamics of chemical bond," J. Phys. Chem. A 104, 5660-5694, 2000.

[4] A. H. Zwail, "Femtochemistry: Recent progress in studies of dynamics and control of reactions and their transition states," J. Phys. Chem. A 100, 12701, 2000.

[5] Jagdeep Shah, *Ultrafast Spectroscopy of Semiconductors and Semiconductor Nanostructures*, Springer Verlag, 1996.

[6] C. Rose-Petruck, R. Jimenez, T. Guo, A. Cavalleri, C. W. Siders, F. Raksi, J. A. Squier, B. C. Walker, K. R. Wilson, C. P. J. Barty: Nature 398, 310 (1999).

[7] H. Schwoerer, P. Gibbon, S. Düsterer, R. Behrens, C. Ziener, C. Reich, R. Sauerbrey, Phys. Rev. Lett. 86, 2317-2320, 2001.

[8] J.-C. Diels, W. Rudolph, *Ultrashort Laser Pulse Phenomena*, Academic Press, 1996.

[9] C. Rullière, *Femtosecond laser Pulses*, Springer-Verlag Berlin Heidelberg, 1998.

[10] U. Keller, "Semiconductor nonlinearities for solid-state laser modelocking and Q-switching," in *Nonlinear Optics in Semiconductors*, A. Kost and E. Garmire, Eds. Boston, MA: Academic, 1998.

[11] G. H. C. New, "Mode-locking of quasi-continuous lasers", Opt. Commun. 6, 188-192, 1972.

[12] H. A. Haus, "Theory of Mode Locking with a Slow Saturable Absorber", IEEE J. Quantum Electron. QE-11, 736-746, 1975.

[13] H. A. Haus, "Theory of Mode Locking with a Fast Saturable Absorber", J. Appl. Phys. 46, 3049-3058, 1975.

[14] H. A. Haus, E. P. Ippen, "Self-Starting of Passively Mode-Locked Lasers", Opt. Lett. 16, 1331-1333, 1991.

[15] F.X. Kärtner, and U. Keller, "Stabilization of Soliton-Like Pulses with a Slow Saturable Absorber", Opt. Lett. 20, 16-18, 1995.

[16] F.X. Kärtner, I.D. Jung and U. Keller, "Soliton Mode-Locking with Saturable Absorbers", *Special Issue on Ultrafast Electronics*, Photonics and Optoelectronics, IEEE J. Select. Topics Quantum Electron. 2, 540-556, 1996.

[17] I.D. Jung, F.X. Kärtner, L. R. Brovelli, M. Kamp, and U. Keller, "Experimental Verification of Soliton Modelocking Using Only a Slow Saturable Absorber", Opt. Lett. 20, 1892-1894, 1995.

[18] D. E. Spence, P. N. Kean, and W. Sibbett, "60-fsec Pulse-Generation from a Self-Mode-Locked Ti:Sapphire Laser", Opt. Lett. 16, 42-44, 1991.

[19] U. Morgner, F. Kärtner, S. Cho, Y. Chen, H. Haus, J. Fujimoto, E. Ippen, V. Scheuer, G. Angelow, and T. Tschudi, "Sub-two-cycle pulses from a Kerr-lens mode-locked Ti:sapphire laser," Opt. Lett. 24, 411-413, 1999.

[20] R. Ell, U. Morgner, F. Kärtner, J. Fujimoto, E. Ippen, V. Scheuer, G. Angelow, T. Tschudi, M. Lederer, A. Boiko, and B. Luther-Davies, "Generation of 5-fs pulses and octave-spanning spectra directly from a Ti:sapphire laser," Opt. Lett. 26, 373-375, 2001.

[21] G. Cerullo, S. De Silvestri, V. Magni, "Self-Starting Kerr Lens Mode-Locking of a Ti-Saphhire Laser", Opt. Lett. 19, 1040-1042, 1994.

[22] G. Cerullo, S. De Silvestri, V. Magni, L. Pallaro, "Resonators for Kerr Lens Mode-Locked Femtosecond Ti-Saphhire Lasers", Opt. Lett. 19, 807-809, 1994.

[23] D. J. Kaup, "Perturbation Theory for Solitons in Optical Fibers", Phys. Rev. A 42, 5689-5694, 1990.

[24] F.X. Kärtner, I. Aus der Au and U. Keller, "Mode-Locking with Slow and Fast Saturable Absorbers - What's the Difference?", *Special Issue on Ultrafast Electronics*, Photonics and Optoelectronics, IEEE J. Select. Topics Quantum Electron. 4, 159-168, 1998.

[25] H. A. Haus, "Parameter Ranges for CW Passive Mode Locking", IEEE J. Quantum Electron. QE-12, 169-176, 1976.

[26] P. Langlois, M. Joschko, E. R. Thoen, E. M. Koontz, F. X. Kärtner, E. P. Ippen and L. A. Kolodziejski, "High fluence ultrafast dynamics of semiconductor saturable absorber mirrors", Appl. Phys. Lett. 75, 3841-3843, 1999.

[27] M. Joschko, P. Langlois, E. R. Thoen, E.M. Koontz, E. P. Ippen and L. A. Kolodziejski, "Ultrafast hot-carrier dynamics in semiconductor saturable absorber mirrors", Appl. Phys. Lett. 76, 1383-1385, 2000.

[28] E. R. Thoen, E.M. Koontz, M. Joschko, P. Langlois, T.R. Schibli, F. X. Kärtner, E. P. Ippen and L. A. Kolodziejski, "Two-photon absorption in semiconductor saturable absorber mirrors", Appl. Phys. Lett. 74, 3927-3929, 1999.

[29] T.R. Schibli, E.R. Thoen, F.X. Kärtner, E.P. Ippen, "Suppresion of Q-switched mode locking and break-up into multiple pulses by invers saturable absorption", Appl. Phys. B 70 [Suppl.], S41-S49, 2000.

[30] F.X. Kärtner, L.R. Brovelli, D. Kopf, M. Kamp, I. Calasso, and U. Keller, "Control of solid-state laser dynamics by semiconductor devices", Opt. Eng. 34, 2024-2036, 1995.

[31] C. Hönninger, R. paschotta, F. Morier-Genoud, M. Moser and U. Keller, "Q-switching stability limits of continuous-wave passive mode-locking", J. Opt. Soc. Am. B 16, 46-56, 1999.

[32] R. Grange, H. Haiml, R. Paschotta, G.J Spühler, L. Krainer, M. Golling, O. Ostinelli, U. Keller, "New regime of inverse saturable absorption for self-stabilizing passively mode-locked lasers", Appl. Phys. B, 2004.

[33] J. Aus der Au, D. Kopf, F. Morier-Genoud, M. Moser, and U. Keller, "60-fs pulses from a diode-pumped Nd:glass laser", Opt. Lett. 22, 307-309, 1997.

[34] B. C. Collings, K. Bergman and W. H. Knox, "True fundamental solitons in a passively mode-locked short-cavity $Cr^{4+} : YAG$ laser", Opt. Lett. 22, 1098-1100, 1997.

[35] M. J. Lederer, B. Luther-Davies, H. H. Tan, C. Jagadish, N. N. Akhmediev, J. M. Soto-Crespo, "Multiple operation of a Ti:sapphire laser mode locked by an ion-implanted semiconductor saturable-absorber mirror," J. Opt. SOC. Am. B 16, 895-904, 1999.

[36] D. Y. Tang, W. S. Man, H. Y. Tam, P. D. Drummond, "Observation of bound states of solitons in a passively mode-locked fiber laser", Phys. Rev. A 64, 1-3, 2001.

[37] S. Zhao, G. Chen, Y. Wang, L. Yu, "Mechanism of pulse shaping in femtosecond lasers based on the high-order soliton," Optics & Laser Technology 32, 251-253, 2000.

[38] Ph. Grelu, F. Belhache, F. Gutty, J.-M. Soto-Crespo, "Phase-locked soliton pairs in a streched-pulse fiber laser," Opt. Lett. 27, 966-968, 2002.

[39] B. Chassagne, G. Jonusauskas, J. Oberlé, C. Rullière, "Multipulse operation regime in a self-mode-locked Cr^{4+}:forsterite femtosecond laser," Opt. Comm. 150, 355-362, 1998.

[40] B. Ortac, A. Hideur, M. Brunel, "Binding widely-separated pulses with a passively mode-locked Yb-doped double-clad fiber laser", Appl. Phys. B 79, 185-192, 2004.

[41] N. N. Akhmediev, A. Ankiewicz, "Generation of a train of solitons with arbitrary phase difference between neighboring solitons", Opt. Lett. 19, 545-547, 1994.

[42] B. A. Malomed, "Bound solitons in the nonlinear Schrödinger-Ginzburg-Landau equation", Phys. Rev. A 44, 6954-6957, 1991.

[43] N. N. Akhmediev, A. Ankiewicz, J. M. Soto-Crespo, "Multisoliton Solutions of the Complex Ginzburg-Landau Equation", Phys. Rev. Lett. 79, 4047-4051, 1997.

[44] J. M. Soto-Crespo, N. N. Akhmediev, "Multisoliton regime of pulse generation by lasers passively mode locked with a slow saturable absorber," J. Opt. Am. B 16, 674-677, 1999.

[45] J. Philipps, *Kompakte diodengepumpte Erbium-Ytterbium-Glaslaser*, Dissertation, Jena, 2001.

[46] E. Biémont, H. P. Garnir, Z. S. Li, V. Lokhnygin, P. Palmeri, P. Quinet, S. Svanberg, J. F. Wyart and Z. G. Zhang, "Experimenzal and theoretical energy levels, transition probabilities and radiative lifetimes in Yb_{III}", J. Phys. B: At. Mol. Opt. Phys. 34, 1869-1876, 2001.

[47] C. Hönninger, R. Paschotta, M. Graf, F. Morier-Genoud, G. Zhang, M. Moser, S. Biswal, J. Nees, A. Braun, G. Mourou, I. Johannsen, A. Giesen, W. Seeber, U. Keller, "Ultrafast ytterbium-doped bulk lasers and laser amplifiers", Appl. Phys. B 69, 3-17, 1999.

[48] C. Hönninger, F. Morier-Genoud, M. Moser, U. Keller, L. R. Brovelli and C. Harder, "Efficient and tunable diode-pumped femtosecond Yb:glass lasers", Opt. Lett. 23, 126-128, 1998.

[49] C. Hönninger, F. X. Kärtner, G. Zhang, U. Keller and A. Giesen, "Femtosecond Yb:YAG laser using semiconductor saturable absorbers", Opt. Lett. 20, 2402-2404, 1995.

[50] J. Aus der Au, S. F. Schaer, R. Paschotta, C. Hönninger and U. Keller, "High-power diode-pumped passively mode-locked Yb:YAG lasers", Opt. Lett. 24, 1281-1283, 1999.

[51] J. Aus der Au, G. J. Spühler, T. Südmeyer, R. Paschotta, R. Hövel, M. Moser, S. Erhard, M. Karszewski, A. Giesen and U. Keller, "16.2-W average power from a diode-pumped femtosecond Yb:YAG thin disk laser", Opt. Lett. 25, 859-861, 2000.

[52] F. Brunner, R. Paschotta, J. Aus der Au, G. J. Spühler, F. Morier-Genoud, R. Hövel, M. Moser, S. Erhard, M. Karszewski, A. Giesen and U. Keller, "Widely tunable pulse durations from a passively mode-locked thin-disk Yb:YAG laser", Opt. Lett. 26, 379-381, 2001.

[53] E. Innerhofer, T. Südmeyer, F. Brunner, R. Häring, A. Aschwanden, R. Paschotta, C. Hönninger, M. Kumkar and U. Keller, "60-W average power in 810-fs pulses from a thin-disk Yb:YAG laser", Opt. Lett. 28, 367-369, 2003.

[54] B. Viana, J. Petit, R. Gaumé, D. Vivien, F. Druon, F. Balembois, P. M. George, "Yb^{3+}-doped laser materials for high-power or ultrafast applications", in Solid

State Lasers and Amplifiers, Proc. of SPIE Vol. 5460 (SPIE, Bellingham, Wa, 2004), 145-156.

[55] P. H. Haumesser, R. Gaumé, B. Viana and D. Vivien, "Determination of laser parameters of ytterbium-doped oxide crystalline materials", J. Opt. Soc. Am. B 19, 2365-2375, 2002.

[56] A. Aznar, R. Sole, M. Aguilo, F. Diaz, U. Griebner, R. Grunwald, V. Petrov, "Growth, optical characterization, and laser operation of epitaxial Yb^{3+} : $KY(WO_4)_2/KY(WO_4)_2$ composites with monoclinic structure", Appl. Phys. Lett. 85, 4313-4315, 2004.

[57] S. Chénais, F. Druon, F. Balembois, P. Georges, R. Gaumé, P. H. Haumesser, B. Viana, G. P. Aka and D. Vivien, "Spectroscopy and efficient laser action from diode pumping of a new broadly tunable crystal : $Yb^{3+} : Sr_3Y(BO_3)_3$", J. Opt. Soc. Am. B 19, 1083-1091, 2002.

[58] D. A. Hammons, J. M. Eichenholz, Q. Ye, B. H. T. Chai, L. Shah, R. E. Peale, M. Richardson, H. Qiu, "Laser action in $Yb^{3+} : YCOB$ (Yb^{3+} : $YCa_4O(BO_3)_3$)", Opt. Comm. 156, 327-330, 1998.

[59] H. Zhang, X. Mang, P. Wang, L. Zhu, X. Liu, R. Cheng, J. Dawes, P. Dekker, S. Zhang, L. Sun, "Slope efficiency of up to 73% for $Yb : Ca_4YO(BO_3)_3$ crystal laser pumped by a laser diode", Appl. Phys. B 68, 1147-1149, 1999.

[60] V. A. Lebedev, I. V. Voroshilov, A. N. Gavrilenko, B. V. Ignatiev, "Kinetic and spectroscopic investigations of $Yb : YCa_4O(BO_3)_3$ (Yb:YCOB) single crystals", Optical Materials 14, 171-173, 2000.

[61] F. Druon, F. Balembois, P. Georges, A. Brun, A. Courjaud, C. Hönninger, F. Salin, A. Aron, F. Mougel, G. Aka and D. Vivien, "Generation of 90-fs pulses from a mode-locked diode-pumped Yb3+:Ca4GdO(BO3)3 laser", Opt. Lett. 25, 423-425, 2000.

[62] F. Druon, S. Chénais, P. Raybaut, F. Balembois, P. Georges, R. Gaumé, G. Aka, B. Viana, S. Mohr and D. Kopf, "Diode-pumped $Yb : Sr_3Y(BO_3)_3$ femtosecond laser", Opt. Lett. 27, 197-199, 2002.

[63] F. Druon, S. Chénais, P. Raybaut, F. Balembois, P. Georges, R. Gaumé, G. Aka, B. Viana, D. Vivien, J. P. Chambaret, S. Mohr and D. Kopf, "Largely tunable diode-pumped sub-100-fs Yb:BOYS laser", Appl. Phys. B 74, 201-203, 2002.

[64] F. Brunner, G. J. Spühler, J. Aus der Au, L. Kreiner, F. Morier-Genoud, R. Paschotta, N. Lichtenstein, S. Weiss, C. Harder, A. A. Lagatsky, A. Abdolvand, N. V. Kuleshov, and U. Keller, "Diode-pumped femtosecond $Yb : KGd(WO_4)_2$ laser with 1.1-W average power", Opt. Lett. 25, 1119-1121, 2000.

[65] A. Major, L. Giniunas, N. Langford, A. I. Ferguson, D. Burns, E. Bente, and R. Danelius, "Saturable Bragg reflector-based continuous-wave mode locking of $Yb : KGd(WO_4)_2$ laser", J. Mod. Opt. 49, 787-793, 2002.

[66] H. Liu, J. Nees, G. Mourou, "Diode-pumped Kerr-lens mode-locked $Yb : KY(WO_4)_2$ laser", Opt. Lett. 26, 1723-1725, 2001.

[67] P. Klopp, V. Petrov, U. Griebner, G. Erbert, "Passively mode-locked Yb:KYW laser pumped by a tapered diode laser", Opt. Express 10, 108-113, 2002.

[68] F. Brunner, T. Südmeyer, E. Innerhofer, F. Morier-Genoud, R. Paschotta, V. E. Kissel, V. G. Shcherbitsky, N. V. Kuleshov, J. Gao, K. Contag, A. Giesen, and U. Keller, "240-fs pulses with 22-W average power from a mode-locked thin-disk $Yb : KY(WO_4)_2$ laser", Opt. Lett. 27, 1162-1164, 2002.

[69] D. Ehrt and T. Töpfer, Preparation, structure and properties of Yb^{3+} FP laser glass, Proceeding of SPIE, Vol. 4102 (2000).

[70] T. Töpfer, *Diodengepumpte Hochleistungsglaslaser - Lasermaterialien, Pumplaserdioden und Verstärker für den POLARIS-Laser*, Dissertation, Jena, 2001.

[71] N. V. Kuleshov, A. A. Lagatsky, A. V. Podlipensky, V. P. Mikhailov, and G. Huber, "Pulsed laser operation of Yb-doped $KY(WO_4)_2$ and $KGd(WO_4)_2$", Opt. Lett. 22, 1317-1319, 1997.

[72] P. Klopp, U. Griebner, V. Petrov, X. Mateos, M. A. Bursukova, M. C. Pujol, R. Sole, J. Gavalda, M. Aguilo, F. Güell, J. Massons, T. Kirilov, F. Diaz, "Laser operation of the new stoichiometric crystal $KYb(WO_4)_2$", Appl. Phys. B 74, 185-189, 2002.

[73] website of EKSMA Lasers, Optics, Electronics Company:
$http://www.eksma.lt$.

[74] N. V. Kuleshov, A. A. Lagatsky, V. G. Shcherbitsky, V. P. Mikhailov, E. Heumann, T. Jensen, A. Diening, G. Huber, "CW laser performance of Yb and Er, Yb doped tungstates", Appl. Phys. B 64, 409-413, 1997.

[75] M. C. Pujol, M. Rico, C. Zaldo, R. Sole, V. Nikolov, X. Solans, M. Aguilo, F. Diaz, "Crystalline structure and optical spectroscopy of Er^{3+}-doped $KGd(WO_4)_2$ single crystals", Appl. Phys. B 68, 187-197, 1999.

[76] A. Major, I. Nikolakakos, J. S. Aitchison, A. I. Ferguson, N. Langford, P. W. E. Smith, "Characterization of the nonlinear refractive index of the laser crystal $Yb : KGd(WO_4)_2$", Appl. Phys. B 77, 433-436, 2003.

[77] K. V. Yumashev, N. N. Posnov, P. V. Prokoshin, V. L. Kalashnikov, F. Mejid, I. G. Poloyko, V. P. Mikhailov, V. P. Kozich, "Z-scan measurements of nonlinear refraction and Kerr-lens mode-locking with $Yb^{3+} : KY(WO_4)_2$", Optical and quantum Electronics 32, 43-48, 2000.

[78] Polaroid Inc., "Laser diode manufacturing and developement", Product Literature, 1998.

[79] K. Baxter, D. Goodmann, "Laser assembly with integral beam-shaping lens", U.S. Patent 5.793.792, 1998.

[80] website of unique-m.o.d.e. AG:
$http://www.unique-mode.com.$

[81] R. Flaig, *Entwicklung eines diodengepumpten Femtosekunden-Lasers*, Masterthesis, Universität Jena, Januar 2003.

[82] website of BATOP GmbH optoelectronics: $http://www.batop.de.$

[83] website of Scientific Computing International: $http://www.sci-soft.com.$

[84] I. Walmsley, L. Waxer and C. Dorrer, "The role of dispersion in ultrafast optics", Rev. of Scientific Instruments 72, 1-29, 2001.

[85] H. A. Haus, J. D. Moores and L. E. Nelson, "Effect of third-order dispersion on passive mode locking", Opt. Lett. 18, 51-53, 1993.

[86] J. Herrmann, V. P. Kalosha and M. Müller, "Higher-order phase dispersion in femtosecond Kerr-lens mode-locked solid-state lasers: sideband generation and pulse splitting", Opt. Lett. 22, 236-238, 1997.

[87] J. N. Elgin, "Soliton propagation in an optical fiber with third-order dispersion", Opt. Lett. 20, 1409-1410, 1992.

[88] T. Kellner, F. Heine, G. Huber, C. Hönninger, B. Braun, F. Morier-Genoud, M. Moser and U. Keller, "Soliton mode-locked Nd:YalO3 laser at 930 nm", J. Opt. Soc. Am. B 15, 1663-1666, 1998.

[89] website of SCHOTT AG:
$http://www.schott.com.$

[90] G. Paunescu, J. Hein, R. Sauerbrey, "100-fs diode-pumped Yb:KGW mode-locked laser", Appl. Phys. B 79, 555-558, 2004.

[91] S. Spälter, M. Böhm, M. Burk, B. Mikulla, R. Fluck, I.D. Jung, G. Zhang, U. Keller, A. Sizmann, G. Leuchs, "Self-starting soliton-modelocked femtosecond Cr(4+):YAG laser using an antiresonant Fabry-Pérot saturable absorber", Appl. Phys. B 65, 335-338, 1997.

[92] Walter Koechner, *Solid-State Laser Engineering*, Springer Verlag, 1992.

[93] M. Haiml, R. Grange, U. Keller, "Optical characterization of semiconductor saturable absorbers", Appl. Phys. B 79, 331-339, 2004.

[94] G. Paunescu, J. Hein, R. Sauerbrey, W. Richter, "*In situ* characterization of semiconductor saturable absorber mirrors in an operating Yb:KGW mode-locked laser", Opt. Lett. 30, 1799-1781, 2005.

[95] website of HighQ Laser GmbH: $http://www.highQlaser.com$.

[96] L. R. Brovelli, U. Keller and T. H. Chiu, "Design and operation of antiresonant Fabry-Perot saturable semiconductor absorbers for mode-locked solid-state lasers", J. Opt. Soc. Am. B 12, 311-322, 1995.

[97] M. J. Lederer, V. Kolev, B. Luther-Davies, H. H. Tan, C. Jagadish, "Ion-implanted InGaAs single quantum well semiconductor saturable absorber mirrors for passive mode-locking," J. Phys. D 34, 2455-2464, 2001.